INFORMATION TO USERS

This manuscript has been reproduced from the microfilm master. UMI films the text directly from the original or copy submitted. Thus, some thesis and dissertation copies are in typewriter face, while others may be from any type of computer printer.

The quality of this reproduction is dependent upon the quality of the copy submitted. Broken or indistinct print, colored or poor quality illustrations and photographs, print bleedthrough, substandard margins, and improper alignment can adversely affect reproduction.

In the unlikely event that the author did not send UMI a complete manuscript and there are missing pages, these will be noted. Also, if unauthorized copyright material had to be removed, a note will indicate the deletion.

Oversize materials (e.g., maps, drawings, charts) are reproduced by sectioning the original, beginning at the upper left-hand corner and continuing from left to right in equal sections with small overlaps. Each original is also photographed in one exposure and is included in reduced form at the back of the book.

Photographs included in the original manuscript have been reproduced xerographically in this copy. Higher quality 6" x 9" black and white photographic prints are available for any photographs or illustrations appearing in this copy for an additional charge. Contact UMI directly to order.

UMI

A Bell & Howell Information Company
300 North Zeeb Road, Ann Arbor MI 48106-1346 USA
313/761-4700 800/521-0600

Equilibrium Structure and Dynamics of Near-Earth Plasma Sheet During Magnetospheric Substorms

A

THESIS

Presented to the Faculty

of the University of Alaska Fairbanks

in Partial Fulfillment of the Requirements

for the Degree of

DOCTOR OF PHILOSOPHY

By

Lin Zhang, B.S., M.S.

Fairbanks, Alaska

August 1997

Equilibrium Structure and Dynamics of Near-Earth Plasma Sheet During Magnetospheric Substorms

by

Lin Zhang

RECOMMENDED:

Dr. Davis Sentman

Dr. Roger Smith

Dr. Brenton Watkins

Dr. Antonius Otto, Chairman, Advisory Committee

Dr. Brenton Watkins, Head, Physics Department

APPROVED:

Dr. Paul Reichardt, Dean, College of Natural Sciences

Dr. Joseph Kan, Dean of the Graduate School

7-30-97

Date

Abstract

A magnetofrictional method and MHD simulation are used to study MHD equilibria and dynamic evolution of the Earth's magnetosphere during a substorm growth phase. I suggest that the new "entropy anti-diffusion instability" associated with plasma transport across field lines leads to an enhanced entropy gradient and accelerates the formation of a thin current sheet during the final substorm growth phase. Based upon the MHD simulations with a pressure diffusion term, I confirm that entropy anti-diffusion instability can lead to a very thin current sheet with $B_z < 0.5nT$ and thickness $< 1000km$ in the near-earth magnetotail ($x \sim -8$ to $-20R_e$) during the growth phase of substorm. The formation of the thin current sheet can explain the observed explosive growth phase of substorms. In the study of magnetotail equilibrium configurations, it is found that the profile of the magnetic field strength B_z component in the equatorial plane is mainly determined by the entropy $S(A)$ ($S = pV^{\gamma}$) on magnetic flux tubes. I obtain self-consistent equilibria of the Earth's magnetosphere with very strong lobe fields and a monotonically increasing B_z component towards the Earth. It is also confirmed that an enhancement of the lobe flux favors the formation of a current sheet during the early substorm growth phase. However, my results do not support the notion that a critical amount of the lobe flux is required for a collapse of the tail current sheet.

Contents

List of Figures

Acknowledgments

I would like to thank Dr. Antonius Otto and Dr. Lou-Chuang Lee, my thesis advisors in the University of Alaska, Fairbanks. Their continuous advice and encouragement made the completion of this thesis possible. I am grateful for this opportunity to work with them. My sincere appreciation also goes to other members of my graduate advisory committee: Professors Dave Sentman, Roger Smith, Brenton Watkins. Their concerns and helpful suggestions improved my research work and the quality of my thesis.

I would like to thank Dr. G. S. Choe for his help and discussions to develop the simulation codes. I would like to thank Dr H. J. Ca for his helpful discussions. I would also like to thank everybody in our group (M. Yan, Q. X. Cheng, H. Zhu, Hall, ...) for helpful discussions;

Finally, I would like to thank my parents Mr. Yong-Hei Zhang and Ms. Qing-Yun Cheng, my wife Yan-Jun Cheng, my brother Mr. Yi Zhang and all other my relatives. Their love, support and expectation encouraged me to finish this thesis with my greatest effort.

This thesis work was supported by the grant DE-FG06-91ER 13530 from the Department of Energy and SPTP grant NAG5-1504 from the National Aeronautics and Space Administration to the University of Alaska. The computing work was supported by the Arctic Region Supercomputer Center, the Pittsburgh Supercomputer Center and the San Diego Supercomputer Center.

Chapter 1

Introduction

There is abundant evidence that the near-earth magnetotail plays a crucial role in magnetospheric physics. It is widely regarded as the "heart" of magnetospheric substorm phenomena. In the most popular observation-based picture of the magnetospheric substorm, the classic substorm sequence begins with a southward turning of the interplanetary magnetic field, a subsequent increase in the reconnection rate at the dayside magnetopause, and a transfer of magnetic flux to the tail lobes [e.g., *Russell and McPherron*, 1973; *McPherron et al.*, 1973]; this initial substorm phase (growth phase) terminates at the onset of the expansion phase, when an X-type neutral line forms in the central plasma sheet, and a plasmoid forms tailward of that neutral line [e.g., *Schindler*, 1974; *Hones*, 1979, 1984; *Lyon et al.*, 1981]. Competing substorm models exist [e.g., *Smith et al.* ,1986], but in most cases, these models also depend crucially on the physics of the near-tail region.

Because of the intrinsic complexity of the near-magnetotail region, and its subtle coupling to the inner magnetosphere and the far tail, there are difficulties in

developing a perfect analytical theory. In this region, the magnetic field configuration and magnetospheric flows must be computed in a self-consistent manner, because they strongly affect each other. In this thesis numerical methods have been developed to describe the magnetotail equilibrium configurations and their evolution during a magnetospheric substorm.

1.1 Types of Magnetic Field Models

Several studies have produced quantitative magnetic field models for the Earth's average or quiet magnetosphere. The observation-based models [e.g. *Olson and Pfitzer*, 1974; *Tsyganenko and Usmanov*, 1982; *Stern*, 1985] include several major current systems and are approximately consistent with quiet time or average magnetic field measurements. However, these models are only magnetic field models and do not constitute global equilibrium, i.e., they do not enforce force balance between the magnetic field and the plasma.

Theoretically, global time-dependent magnetohydrodynamic (MHD) simulations [e.g., *Wu*, 1983; *Lyon et al.*, 1981; *Ogino et al.*, 1986] can generate self-consistent magnetic field configurations. However, they have not been applied to detailed studies of the inner magnetosphere. On the other hand, quasi-static MHD (inertial term of the momentum equation neglected) provides a convenient computational basis for a self-consistent theory for the magnetotail and two-dimensional magnetosphere. Birn et al. [1975] and Birn [1979] have calculated magnetic field models for the magnetotail self-consistently in two and three dimensions, respectively. Their conceptually simple analytic solutions satisfy the force balance equa-

tion within the asymptotic limit $L_x >> L_z$ but do not connect to the Earth's dipolar field (i.e., a weak dependence of the magnetotail configuration on the tailward coordinate). Fuchs and Voig [1979] extended the self-consistent theory to a two-dimensional model of the whole magnetosphere (dipole included) for the case of a rectangular magnetopause, and they found a set of linear analytic solutions that satisfy the static MHD force balance equation; however, that set lacks the generality required for a realistic representation of the magnetosphere.

In the chapter 2, a magnetofrictional method is used to construct two-dimensional MHD equilibria of the Earth's magnetosphere for a given distribution of entropy ($S = pV^{\gamma}$) on magnetic flux tubes, where p is the plasma pressure and V is the flux tube volume per unit magnetic flux. The purpose of this study is to determine typical properties of the earth's magnetospheric configurations during the growth phase and their dependence on the entropy function $S(A)$ and on the distribution of the lobe magnetic flux.

1.2 Magnetotail Dynamics

The formation and evolution of the current sheet is a crucial part of magnetotail dynamics. The evolution involves the storage and explosive release of magnetic energy and the energization of plasma. While these processes can be studied by direct measurements, theoretical and modeling tools are required to organize the diverse measurements into a comprehensive picture.

Theoretical studies of the magnetotail can be divided into three categories. The first and most widely used approach is one-fluid magnetohydrodynamic (MHD)

simulation where the plasma is treated as a fluid, usually with isotropic pressure [*Erickson and Wolf*, 1980; *Harel et al.*, 1981; *Notzel and Schindler*, 1985; *Erickson*, 1992; *Birn*, 1991; *Hesse and Birn* 1992a, b]. Because of its connection to basic conservation laws, MHD has been able to give us a reasonable large-scale description of the fluid parameters of the magnetotail system [*Erickson*, 1992; *Birn*, 1991] and has provided three-dimensional distributions of fluid parameters such as pressure and current.

Modeling of the magnetotail on local spatial scales has also been attempted with a method that has evolved from the test particle approach [*Speiser*, 1965; *Pudovkin and Tsyganenko*, 1973; *Hill*, 1975]. These models assume a very simple magnetic field geometry in which cold beams [*Francfort and Pellat*, 1976; *Burkhart*, 1992; *Pritchett and Coroniti*, 1992] that are launched from the edges of the system support the assumed one-dimensional plasma configuration self-consistently. While this is a more realistic approach that does not assume pressure isotropy the simulation geometry is too simple to yield a realistic description of the magnetotail, where particles convect through regions in which local conditions vary either gradually or abruptly. Because x and y dependencies are neglected, the model is relatively simple, but it cannot take convection into account properly: the convection electric field E_y is transformed away by moving into the deHoffman-Teller frame. This approach has demonstrated that thin current sheets can form embedded in the broader plasma sheet.

The third method of modeling the magnetotail is a compromise between the first two; it is a semifluid model that allows anisotropic pressures, $P_{parallel} \neq P_{perp}$, in a gyrotropic but diagonal pressure tensor[*Tsyganenko*, 1982; *Horton*, 1993]. This

approach is not valid within the central current sheet because guiding center approximation cannot be used there, especially in thin current sheets, and equations for $P_{parallel}$ and P_{perp} become inadequate, at least for the ions, which are the main cross-tail current carriers.

1.3 Basic Concept of a Geomagnetic Substorm

1.3.1 Magnetosphere

Figure 1.1 illustrates the various plasma domains within the earth's magnetotail. The solar-wind flow is obstructed and becomes deflected by the earth's magnetic field, resulting in the formation of a cavity, known as the earth's magnetosphere, carved out in the solar-wind stream. The magnetotail is the cylindrically-shaped portion of the nightside magnetosphere. Because of the high speed of the solar wind, exceeding the local sound or Alfven speed, a shock front called the bow shock is formed ahead of the magnetosphere. Behind the bow shock is a region known as the magnetosheath where the solar-wind flow is reduced and the particle population of the solar wind is thermalized. Adjacent to the magnetosheath is the magnetopause which defines the outer surface of the magnetosphere. As illustrated in Figure 1.1, on the dayside at high latitudes, there is an abrupt transition between magnetic field lines that permeate only the dayside magnetosphere and adjacent field lines at higher latitudes that extend downstream toward the magnetotail. This demarcation gives rise to an indentation region on the dayside magnetopause called the cleft or the polar cusp.

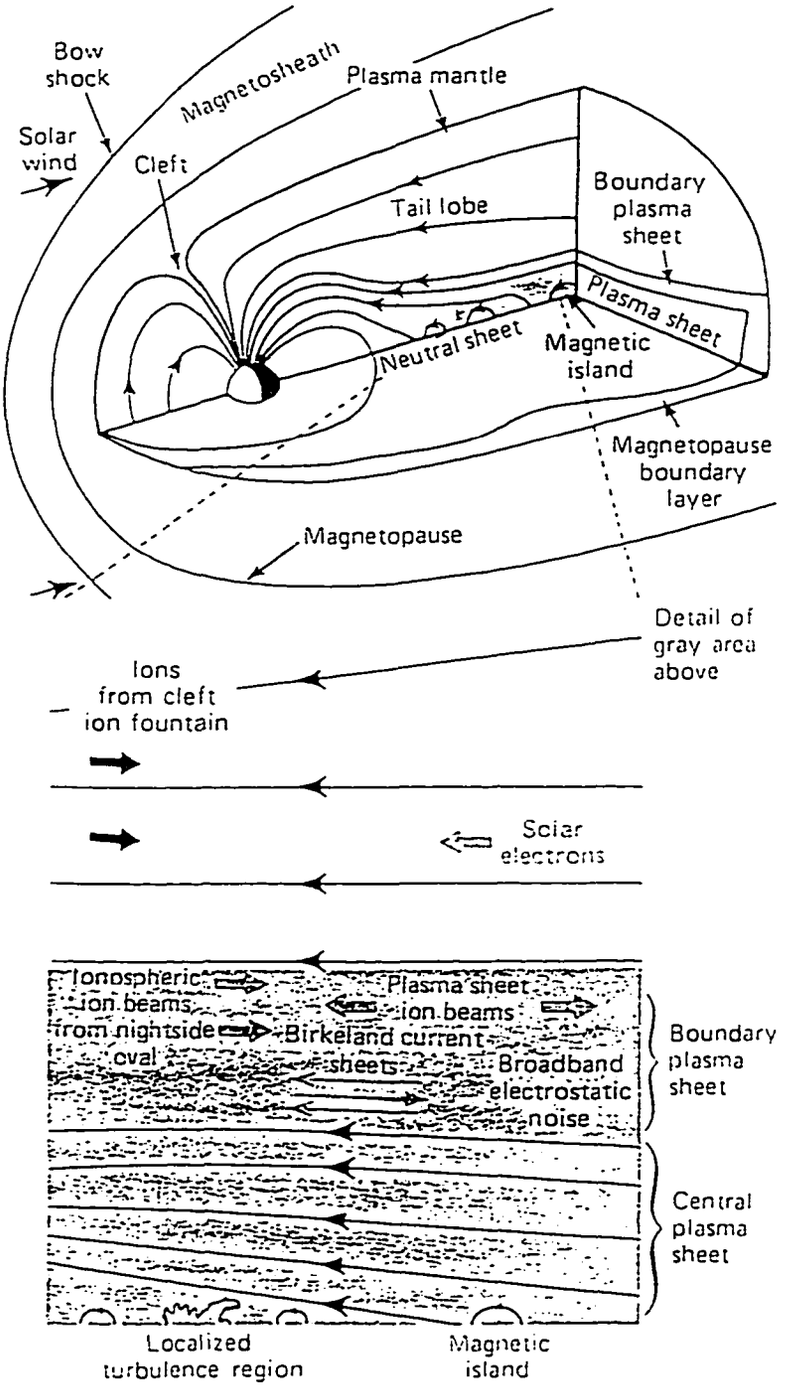

Figure 1.1 A three-dimensional drawing of the magnetotail, exhibiting the plasma domain within.

1.3.2 Tail Lobe and Neutral Sheet

A large portion of the magnetotail consists of two low-density regions known as the tail lobes, one in the northern half of the magnetotail and the other in the southern half. The field lines threading through the tail lobes are also open. Particles populating this region include ions from the polar region at low altitudes, and electrons from the solar wind entered into the tail lobe on open field lines. The energy density in the tail lobe is dominated by the magnetic field.

The neutral sheet, a sheet-like distribution of plasma, centers around the equatorial plane of the magnetotail. In the neutral sheet, the magnetic field is weak (a few nanoteslas). The field reverses direction from pointing sunward to pointing tail-ward or vice versa as the neutral sheet is crossed.

1.3.3 Substorm Growth Phase

The substorm growth phase is the interval during which the solar wind energy is stored in the magnetosphere. Based on the observations [*McPherron*, 1970; *Nagai*, 1982], the growth phase effects appear as the development of currents within the polar cap ionosphere approximately when an observed southward-directed component of the interplanetary magnetic field (IMF) impinged upon the dayside magnetosphere. The enhanced currents result from enhanced magnetospheric electric fields that map to the polar caps, and such enhanced electric fields during a period of southward IMF are generally believed to be a prerequisite for substorms. Enhanced electric fields immediately extend into the closed field line region of the magnetosphere. Enhanced growth phase electric fields strongly modify the

nightside magnetic field at synchronous orbit. Relative to the trend in the field components due to satellite motion, the northward-directed component (H) begins to decrease, and the magnitude of the radial-directed component (V) begins to increase shortly after the southward turning of the IMF. These changes are typical of the substorm growth phase and are generally believed to be due to an increase in the cross-tail current near synchronous orbit [e.g., *Kaufmann*, 1987]. An enhanced plasma pressure P, with P monotonically increasing with decreasing r, has been observed during the substorm growth phase at $r \sim 7 - 10R_e$ by Kistler et al. [1992], and these pressures are sufficient to account for the enhanced cross-tail current during the growth phase [*Lyons and Samson*, 1992]. Here, some of the major substorm features during the growth phase are listed below

(i) Thinning plasma sheet

(ii) Increase of the tail magnetic field

(iii) Earthward motion of inner edge of the neutral sheet

(iv) Equatorward motion of the auroral arcs

1.4 Summary of Magnetotail Observations

In order to formulate and test a substorm theory it is necessary to identify the fundamental observational features of a substorm. While individual substorms can vary in many ways, there are a number of general features that characterize the substorm event considered here. The phenomenon described here happens often and generally is agreed to be a substorm. The major features of the magnetospheric substorm in the magnetotail are listed below.

1.4.1 Plasma Sheet Thinning

(i) A plasma sheet thinning begins during the substorm growth phase.

(ii) At $X < -15R_e$, the thinning proceeds until the poleward expanding auroral bulge (or the electrojet) reaches about dipole latitude 75^o.

(iii) In general, plasma flow is weak during thinning. At $X > -15R_e$, when plasma flow is observable, it is directed sunward, while at $X \simeq -30R_e$, an anti-sunward flow is sometimes observed.

(iv) The plasma sheet becomes thinnest in the midnight sector. There is no indication of compression of the plasma sheet toward its midplane, since thinning occurs in the vicinity of the midplane.

1.4.2 Plasma Sheet Expansion

(i) At $X \simeq -15R_e$, the plasma sheet begins to reappear or expand at about the maximum epoch of substorms.

(ii) Plasma particles in the expanding plasma sheet are much hotter than in a quiet time plasma sheet. The proton energy increases from about 1 KeV (a quiet time value) to 20 keV.

(iii) Despite the high particle energy, the plasma pressure does not show a notable increase, indicating that the density is appreciably lower in the expanding plasma sheet than in the quiet time plasma sheet.

(iv) The expanding plasma sheet is almost always associated with a high speed ($\sim 500km/s$) sunward flow of plasma.

1.4.3 Magnetic Field Variations

(i) There is no strong indication of the formation of a new magnetic neutral line in the near-Earth plasma sheet, which leads to a large-scale change of the magnetic field configuration.

(ii) Most of the reported B_z component reversals are possibly a slight dipping of the **B** vector. The B_z component is predominantly positive in the midplane of the plasma sheet during substorms.

(iii) Small-scale loops appear to be common in the vicinity of the midplane during substorms.

(iv) Tailward plasma flows can be associated with both a negative B_z component (the dipping of the **B** vector) and a positive B_z component.

(v) The enhanced B_z component is much larger than the dipole value.

(vi) The magnetic field configuration becomes tail-like again during a late epoch of the recovery phase.

Figure 1.2 illustrates schematically the configuration of the plasma sheet and of the magnetic field at about the maximum epoch of a substorm [*Akasofu*, 1977].

1.4.4 Outline of the Thesis

Using the MHD simulations, the objective of this thesis is to study the two-dimensional equilibrium structure and dynamic evolution of the Earth's magnetosphere during the substorm growth phase.

In chapter 2, first a magnetofrictional method and related algorithms are developed. Based upon the magnetofrictional code, I construct two-dimensional

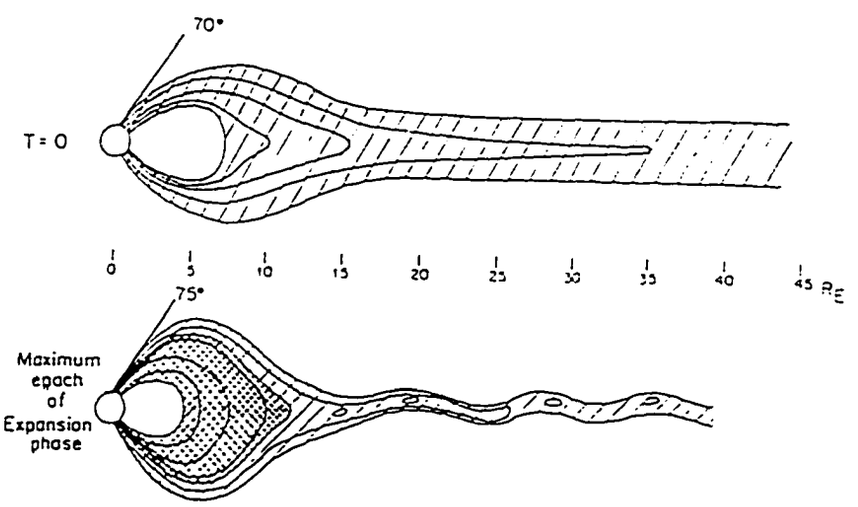

Figure 1.2 Schematic diagram showing the configuration of the plasma sheet and of the magnetic field at $T = 0$ and at the the maximum epoch of the magnetospheric substorm.

MHD equilibria of the Earth's magnetosphere for a given distribution of entropy ($S = pV^{\gamma}$) on magnetic flux tubes, where p is the plasma pressure and V is the flux tube volume per unit magnetic flux. I have found typical properties of the earth's magnetospheric configurations during the growth phase and their dependence on the entropy function $S(A)$ and on the distribution of the lobe magnetic flux.

In chapter 3, based on 2-D MHD simulations, I study the dynamic evolution of the magnetotail in the presence of a dawn-to-dusk electrostatic field. It is implied that the enhanced ionospheric convection electric field may be the main driving force of the near-earth magnetotail evolution during the substorm growth phase, which enhances the entropy and highly stretches the geomagnetic field lines tailward in the near-earth region.

A new entropy anti-diffusion instability, which leads to a further thinning of the near-earth current sheet and the onset of dipolarization of near-earth geomagnetic field lines, is reported in chapter 4. The dependence of the growth rate of the instability on the diffusion coefficient is also presented.

In the last chapter, I briefly summarize the results.

Chapter 2

Two-Dimensional Equilibrium Structure and Evolution of the Earth's Magnetosphere During the Substorm Growth Phase

The major sequence of a magnetospheric substorm consists of a growth phase, an expansion phase and a recovery phase [*Akasofu*, 1977]. Based on satellite observations in the equatorial magnetotail, the growth phase is characterized by an increase of the lobe field strength, a highly stretched geomagnetic field and thinning of the plasma sheet within $\sim 15R_e$ [e.g.. *Kokubun and McPherron*, 1981; *Kaufmann*, 1987; *Fairfield et al.*, 1987; *Lui et al.*, 1992]. The current sheet thinning starts before the onset of the expansion phase and the observed thickness of current sheets can be as small as 300-1000 km [*Mitchell et al.*, 1990; *Sergeev et al.*,

1990].

At the onset of the expansion phase, the stretched geomagnetic field lines in the near-earth region ($x \sim -6$ to $-12R_e$) are suddenly dipolarized [e.g., *Lui et al.*, 1992]. Recently Ohtani et al. [1992] found that an explosive growth phase, which is characterized by the presence of a thinner current sheet with a larger current density, can precede the full onset of substorms.

The onset of substorms is believed to be related to the evolution and stability of the current sheet in the near-earth ($-6\,R_e > x > -20\,R_e$) magnetotail. The formation of thin current sheets in the magnetotail was widely investigated based on MHD and particle simulations. Two-dimensional MHD simulations of current sheet formation and rapid reconnection in the near-Earth magnetotail driven by an external electric field were carried out by Lee et al., 1985; Birn et al., 1986, 1991; and Ma et al., 1995. Global three-dimensional MHD studies were done by Usadi et al., 1993, Ogino et al., 1994, and Fedder et al., 1995. Full particle simulations [*Pritchett and Coroniti*, 1995] and hybrid simulation [*Hesse et al.*, 1996] qualitatively confirm MHD results. All simulations indicate that a thin current sheet can form in an initially smooth magnetospheric equilibrium if a driving boundary condition consistent with a southward IMF is turned on. The ideal MHD evolution of the geomagnetic tail in response to an applied field with inward flow is characterized essentially by a quasi-static compression of the tail configuration. The electric field applied at the boundary propagates inward in the form of a fast MHD wave, becomes reflected at the plasma sheet boundary, and settles eventually after some wave traveling back and forth and interference of waves at an approximately linear decrease from the boundary toward has much smaller values within the plasma

sheet [*Birn et al.*, 1986]. The stretching and energization of the tail by the adiabatic lossless convection has been studied analytically [*Schindler and Birn*, 1982] and numerically [*Hau et al.*, 1989; *Erickson*, 1992]. These studies showed that the tail configuration can be stretched as convection proceeds and that a B_z-minimum can form in the plasma sheet. Birn and other [*Birn, J. and K. Schindler*, 1986; *Birn et al.*, 1994; *Schindler, K and J. Birn*, 1993] demonstrated that a thin current sheet can be formed under adiabatic conditions (when $S(A)$ is conserved) with the steep gradient of $P(A)$. The conservation of $S(A)$ requires a steep gradient of the flux tube volume $V(A)$ to compensate for the steep gradient of $P(A)$. The stretching in the presence of an enhanced ionospheric convection electric field has been studied analytically [*Cai et al.*, 1995]. This model implies that the enhanced ionospheric convection electric field is the main driving force of the near-earth magnetotail evolution during the substorm growth phase. Here, the formation of highly stretched field line configuration and the enhancement of entropy function in the near-earth region is a consequence of the enhanced ionospheric convection. Satellite observations [*Lui et al.*, 1992] indicated that the substorm onset may not be initiated by magnetic reconnection. Recent theoretical studies tried to explain the onset without resorting to reconnection [*Kan et al.*, 1988; *Roux et al.*, 1991; *Lui et al.*, 1992; *Birn et al.*, 1994].

When the interplanetary magnetic field turns southward, dayside reconnection leads to an increase of open magnetic flux, which is convected antisunward. As a result, the magnetic flux in the lobes increases. Based on force balance Siscoe and Cummings [1969] predicted the earthward displacement of the cross-tail current sheet for an increasing amount of the lobe flux. During the growth phase, the field

configuration in the near-earth plasma sheet becomes increasingly stressed and the cross-tail current sheet is displaced earthward with the buildup of a strong current density mostly in the near-earth region ($x \sim -6$ to $-20R_e$). Now the concept is widely accepted that the earthward displacement of the cross-tail sheet must cease at some point due to the dominant geomagnetic field near Earth. This provides a theoretical reason for a limit on the open magnetic flux allowed in the magnetotail. Open magnetic flux beyond this limit should lead to catastrophic changes which are possibly related to the substorm expansion phase.

Since the fast-mode transit time ($\sim$ a few minutes) across the magnetotail is much shorter than the growth phase time, the magnetotail in the growth phase can be approximated by a series of quasi-equilibrium configurations. In my recent study [*Lee et al.*, 1995], I use a magnetofrictional method to construct global MHD equilibria, in which the entropy per flux tube is imposed as a constraint. It is found that a very thin current sheet can be formed in the near-earth magnetotail during the growth phase of substorm. In this chapter, I study, in detail, conditions for and the formation of a thin current sheet during the growth phase, and construct the tail configuration corresponding to the conditions. I also discuss quantitatively the amount of open magnetic flux, its relation to the cross-tail current sheet, and the earthward displacement of this current sheet.

The present study of current sheet formation is based on a MHD formulation. The results provide a framework for further studies of the current sheet, including kinetic effects and instabilities. Based on my equilibrium results, the dynamic evolution of the tail configuration is studied in other chapters.

The next section introduces the equations for the magnetofrictional method.

It also presents boundary and initial conditions and I describe the model for the entropy function. The equilibrium field configurations corresponding to the entropy profiles are given in section 2.2, which shows favorable conditions to form a thin current sheet in near-earth magnetotail. I also discuss the relationship between the lobe flux and a current sheet. Finally a discussion and summary are given in section 2.3.

2.1 Numerical Model

2.1.1 Magnetofrictional Equations

A 2-D MHD equilibrium in the noon-midnight meridian plane (x-z plane in the geomagnetic solar magnetospheric (GSM) coordinates) is characterized by force balance, which is described by

$$\mathbf{J} \times \mathbf{B} - \nabla p = 0, \tag{2.1a}$$

$$\mathbf{B} = \nabla \times (A\hat{y}), \tag{2.1b}$$

$$\mathbf{J} = \nabla \times \mathbf{B}, \tag{2.1c}$$

where A is the y-component of vector potential and p is plasma pressure. Solutions of (2.1) can be obtained by specifying $S(A) = pV^{\gamma}$ as well as a boundary condition on A. Here $V(A) = \int ds/B$ is the flux tube volume per unit flux, and $S(A)$ is called the *entropy function* in this thesis [*Lee et al.*, 1995]. The equilibrium solution obtained by specifying $S(A)$ and boundary conditions on A is more relevant to the tail dynamics if the in- and outflow of plasma through the end of flux tubes are

ignorable. In this case, the magnetospheric field configuration is controlled by the boundary flux distribution and the entropy content in each flux tube. Since there are no significant material flows from and to the ionosphere observed before the substorm onset, the adiabatic, lossless picture is close to the real magnetosphere.

When the system is force balance, it is in a state of minimum energy. In the chapter, a state of minimum energy is approached in terms of using the magnetofrictional method [*Chodura and Schlüter*, 1981; *Lee et al.*, 1995], in which an arbitrary initial field configuration satisfying the boundary condition and containing no X line is loaded with $S(A)$ and the whole system is allowed to evolve according to the following equations.

$$\mathbf{v} = \alpha(\mathbf{J} \times \mathbf{B} - \nabla p), \tag{2.2}$$

$$\frac{\partial A}{\partial t} = -\mathbf{v} \cdot \nabla A, \tag{2.3}$$

$$\frac{\partial h}{\partial t} = -\nabla \cdot (h\mathbf{v}), \tag{2.4}$$

where t is a time-like parameter, α is a positive function of space and t, whose magnitude is less than one and limited by a numerical stability condition, and $h = p^{1/\gamma}$ with $\gamma = 5/3$. Eq.(2.2) is equivalent to a usual momentum equation without the inertia term. The kinetic energy converted from the excessive potential energy is removed after each time-step, so that all the oscillatory modes are damped and the system moves toward the lowest energy state. Eq.(2.4) is obtained from the conservation of mass ($\partial\rho/\partial t = -\nabla \cdot (\rho\mathbf{v})$) and the Lagrangian invariance of specific entropy ($(d/dt)(p/\rho^\gamma) = 0$). Eq.(2.4) guarantees that $I_v = \int_V p^{1/\gamma} dV$ is conserved for any volume V enclosing certain fluid elements in every relaxation step. For an infinitesimal fluid element, we can define $s \equiv p(\delta V)^\gamma$. Since $s^{1/\gamma} =$

$p^{1/\gamma}(\delta V)$ is conserved, s is also conserved, which means the entropy conservation for a fixed fluid element. During the relaxation of the magnetofrictional scheme, we cannot define the quantity $S(A) = p(A)V^{\gamma}$ before we reach the equilibrium because p is not necessarily constant along the field line, But I_v is defined and conserved for each differential flux volume labeled by A. In the equilibrium, $I_A = p^{1/\gamma}V(A) = S(A)^{1/\gamma}$. It is to be reminded that the entropy constraint expressed as $S(A) = pV^{\gamma}$ instead of I_V is based on the assumption of the equilibrium. In the magnetofrictional method, only the final equilibrium is a valid solution. Equation (2.1) for MHD equilibrium is of elliptic type, whereas (2.2)-(2.4) form a parabolic system. The solution of the latter thus asymptotically approaches the solution of the former. Since the initial condition can be chosen quite arbitrarily, only the final solution is significant. The parameter t tells us the direction of relaxation sequence. In this chapter, equations (2.2)-(2.4) are solved numerically. Every time step, I first solve equation (2.2) to obtain the velocity $\mathbf{v}$, where $\alpha = dt/(\mathbf{B}^2 + \gamma p)$. Then the magnetic field A and h evolve according to the equations (2.3) and (2.4) respectively. I repeat the procedure until the net force is smaller than 10^{-4} to 10^{-5}, which implies a typical time-scale for plasma acceleration of 10^5 to 10^6 seconds. The relaxation method requires 10^4 to 10^5 iteration steps (the large value applies to cases with very thin current sheets).

To compare my results with observations, I normalize the length scales to one Earth radius (R_e), the magnetic field to $B_0 = 30\,\mathrm{nT}$, which would be the Earth's dipole field strength at $r = 10\,R_e$ in the equatorial plane, magnetic flux to $A_o = B_o R_e = 30 nT R_e$; and the pressure to $p_0 = B_0^2/\mu_0 = 0.71\,\mathrm{nPa}$.

2.1.2 Boundary conditions and Initial Field Configuration

My simulation domain is bound by a circle of radius of $3\,R_e$ concentric with the Earth ($\partial\Omega_1$), a mimicked magnetopause ($\partial\Omega_2$) composed of a parabola, which is described by $x = -[15(10 - z)]^{1/2}$, extending from the subsolar point $(10, 0)$ to $(-5, \pm 15)$ and abutting straight lines extending to $(-70, \pm 28)$, and a straight tailside boundary at $x = -70$ ($\partial\Omega_3$). At all boundaries, the flux function A is set constant in time. At $\partial\Omega_1$, the magnetic flux is matched to a 2-D dipole field described by $A_D = -100x/(x^2+z^2)$. The computation domain is shown in Fig.2.1.

Following the southward turning of the IMF, the dayside reconnection creates the open magnetic flux, which is then convected antisunward. The distance traveled by the first open flux tube in about 30 minutes (growth phase time scale) can be estimated as $\Delta x \simeq 250\text{kms}^{-1} \times 1800\text{s} \simeq 72R_e$. The newly open flux is expected to be distributed over the region $x > -70R_e$ of the tail magnetopause. Since the open flux along the dayside magnetopause ($x > 0$) affects mainly the dayside field configuration, I simply set the open flux to zero along the dayside magnetopause. Therefore, A is set to a constant value A_1 along the dayside magnetopause ($x \geq 0$), and the open flux ($A_2 - A_1$) is uniformly distributed along the nightside magnetopause ($x < 0$). Here A_2 is the value of A at corner of the two boundaries $\partial\Omega_2$ and $\partial\Omega_3$. These are shown in Fig.2.1.

Along the tailside boundary $\partial\Omega_3$, I simply choose $B_x(z) \propto z/(z^2+a^2)^{1/2}$, which leads to $A(x = -70, z) = A_3 - (A_3 - A_2)[(a^2+z^2)^{\frac{1}{2}} - a]/[(a^2+28^2)^{\frac{1}{2}} - a]$. Here A_3 is the value of A at the intersection of the x-axis and $\partial\Omega_3$, and a is a parameter controlling the distribution of flux along the tailside boundary. For $a \ll z_w$, where

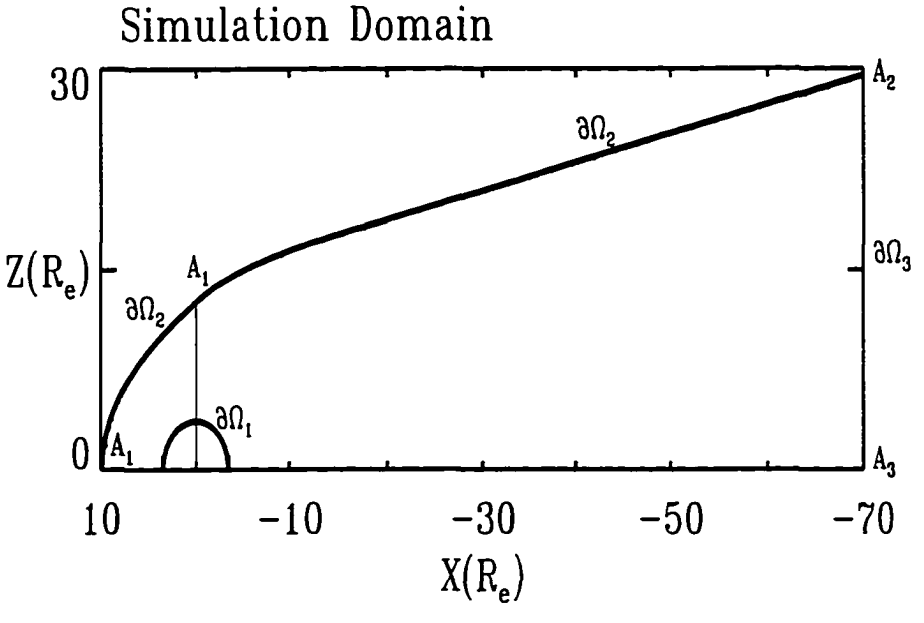

Figure 2.1 Sketch of the simulation domain in the noon midnight meridian plane. $\partial\Omega_1$, $\partial\Omega_2$ and $\partial\Omega_2$ are the simulation boundaries.

z_w is the half-width of the magnetotail and equal to $28R_e$, a sharp current layer appears near the central part($z \simeq 0$) of this boundary and the flux is rather uniformly distributed across the tail boundary. For $a \gg z_w$, the current layer is broadened and more flux is concentrated in the region near the magnetopause. The latter is thought to be more realistic and I tested a number of values of a ($10 \leq a \leq 300$). The inflated magnetic field lines in the region $x \leq -20R_e$ are mainly caused by the presence of open flux along the magnetopause. The results are not sensitive to the boundary condition imposed at the tailside boundary. The detailed results and discussion are given later. In the following cases, a is simply set to 200. The flux $(A_3 - A_2)$ is defined as the lobe flux and the flux $(A_c - A_3)$ as the closed flux.

The initial field profile is set up by interpolating the flux function A between inside and outside boundaries and contains no neutral point in the domain. The method I use in the chapter is described as follows. For any inside point (x, z) a straight line is determined by this point and the origin. This line intersects inside and outside boundaries at two points respectively. Then initial flux function $A(x, z)$ is given by the flux values of these two points in terms of interpolation. During the relaxation of the magnetofrictional scheme, the magnetic field evolves according to the ideal MHD, i.e., field lines cannot be reconnected or diffused. The field line topology of the final equilibrium configuration is fixed by the topology of the initial field.

2.1.3 Entropy Function Profile of $S(A)$

As pointed out in earlier studies [*Lee et al.*, 1995], the evolution of geomagnetotail during the substorm growth phase can be described as a series of quasi-equilibrium configurations, which is defined by the entropy function $S(A)$.

Once an initial field profile is given, the differential flux volume $V(A)$ can be calculated, and one can obtain the initial pressure $p(A) = S(A)/V(A)^{\gamma}$ for a given entropy profile $S(A)$. I have calculated the entropy function and the plasma pressure along the x-axis based on Tsyganenko empirical field models[1989]. The force balance between the lobes and the current sheet at $x = -60R_e$ is employed to determine the pressure at $x = -60R_e$ on the equatorial plane. Using this pressure constant and $\mathbf{J} \times \mathbf{B} = \nabla p$ along the x axis, I obtain the pressure distribution along the x axis. The results are presented for different K_p and the substorm growth phase in Fig.2.2. [*Zhang et al.*, 1994]

It is found that the modified entropy function S is very small near the earth, increases tailward and reaches a nearly constant value. The decrease of $S(A)$ towards the Earth is due to the fact that hot ions cannot penetrate into the strong dipole field region. In addition, there is one mathematical constraint in 2-D geometry: $S(A)$ should be zero at the point where the x-axis intersects the inner boundary, because the differential flux volume $V(A)$ is zero at these points unless they are O-type neutral points. Therefore, I choose the entropy profile in my model as

$$S(A) = \frac{1}{2} S_m \left[1 + \tanh\left(\frac{A_c - A}{\Delta A}\right) \right]. \tag{2.5}$$

Here S_m, A_c and ΔA are constant parameters. S_m controls the amplitude of the entropy function. The entropy gradient is presented by the transition width

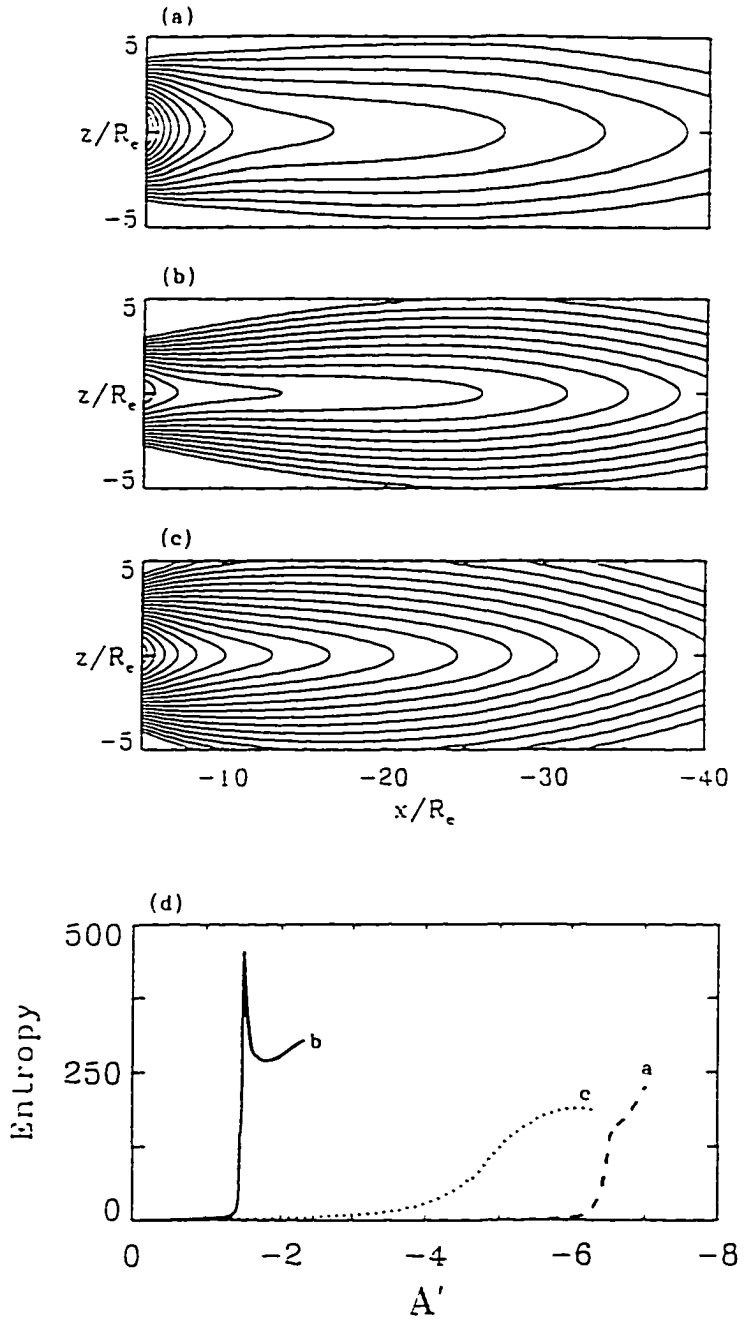

Figure 2.2 The configurations for different K_p in Tsyganenko empirical field models. (a) $K_p = 1$ for quiet time; (b)$K_p = 5$ and with an enhanced cross-tail current sheet for growth phase; (c) $K_p = 6$ for the configuration after a substorm onset; (d)corresponding entropy function $S = pV^{\gamma}$ versus flux $A' = A - A_{61^o}$.

ΔA. The constant A_c largely determines where the thin current sheet is formed in the A-space. In this chapter, I carry out systematic study of properties of how the $S(A)$ determine the configuration of magnetosphere and relate to the growth phase of substorms. This analysis will be done using parameter variations of A_c, ΔA, S_m and the distribution of the lobe flux. I will demonstrate that, for instance, the formation of a thin current sheet is highly related to the enhancement of the entropy gradient and magnitude S_m.

The pressure $p(A)$ in the lobe and dayside for the equilibrium solutions is determined by the following method: The region with $A \leq A_3$ is divided into two regions, one is $A \leq A_2$, another $A_2 \leq A \leq A_3$. Since the pressure in the lobe is almost constant and the dayside magnetosphere does not play an active role in the tail configuration. The pressure in the region where $A \leq A_2$ is simply set to a constant $b_1 p_L$, where p_L is the pressure for flux value A_3, i.e., it is the pressure in the edge of current sheet, and b_1 is a constant parameter and should be less than one. In my cases, p_L is a small constant, and equal to $p(A_3)$. The pressure for $A_2 \leq A \leq A_3$ increases with the increase of the flux A and is given by the function $p(A) = p_L exp[K\frac{(A_3-A)}{A_3-A_2}]$, where $K = lnb_1$ [*Fuchs and Voigt*, 1979]. I also set the pressure inside the inner edge is not less than $b_2 p_p$, where b_2 is a constant and less than one, p_p is the peak pressure. My results are not sensitive to choice of b_1 and b_2 to calculate lobe and dayside pressure. In this chapter, I simply set b_1 to 0.5 and b_2 to 0.2. In my computation, I employ a staggered mesh and need not specify pressure at the boundary points. At all the boundaries, I set $\mathbf{v} = 0$.

Thus, the equilibrium is totally determined by the entropy function profile and the open and lobe magnetic flux. In the following section, I will discuss in detail the

properties of the equilibrium configuration and how they depend on the parameter A_c, ΔA, S_m, and the magnetic flux in the lobe. This will determine conditions for the stretching of the magnetotail in the subsection 2.1, current sheet formation in the subsection 2.2, the effects of a large lobe magnetic flux in the subsection 2.3, and I will justify the tailward boundary condition in the subsection 2.4.

2.2 2-D Equilibrium Structure

2.2.1 Tailward stretching of magnetic field lines

During the growth phase, the field configuration in the near-Earth region becomes tail-like and a current sheet is displaced earthward. Based on the Tsyganenko empirical field models [1989], the entropy function $S(A)$ shifts earthward in A-space, which resulting in transition point A_c moving earthward and an increase of the lobe flux $(A_3 - A_2)$.

Here, I obtain the equilibrium field configurations with different transition points A_c, and fixed open flux $(A_2 - A_1)$, closed flux $(A_c - A_3)$, transition width ΔA and S_m. The transition point A_c shifts earthward from 17.75 to 21, and corresponding lobe flux $(A_3 - A_2)$ enhances from 7.3 to 10.55. The results shown in Figure 2.3. In this case, $S_m = 500$ in units of $S_0 = B_0^{1/3} R_e^{5/3}/\mu_0$, $A_1 = -14.$, $A_2 = 1.5$, and $\Delta A = 0.1$. In run 1, shown in Figure 2.3a, $A_3 = 8.8$, $A_c = 17.75$. In run 2, shown in Figure 2.3b, $A_3 = 9.8$, $A_c = 18.75$. In run 3, shown in Figure 2.3c, $A_3 = 10.8$, $A_c = 19.75$. In run 4, shown in Figure 2.3d, $A_3 = 12.05$, $A_c = 21$.

As shown in Fig.2.3a and 2.3c, a shift of $S(A)$ in A-space causes the following

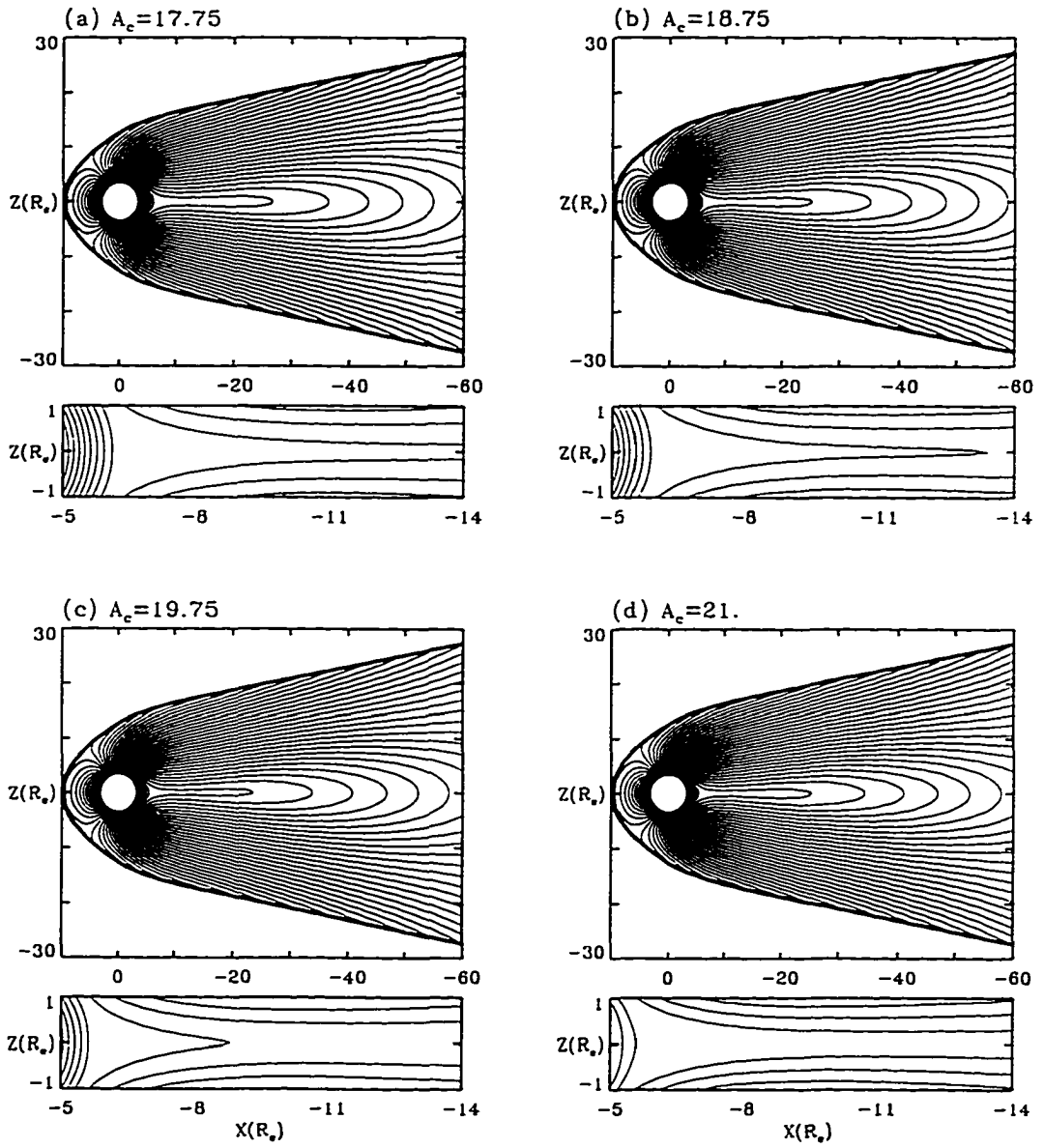

Figure 2.3 The evolution of the equilibrium configuration if the entropy function $S = pV^{\gamma}$ is shifting in A-space from $A_c = 17.75$ to $A_c = 21$. The shift generates a more stretched field configuration.

changes: Dipole field lines in the near-earth region $-5.5\,R_e \geq x \geq -7\,R_e$ are stretched tailward, the lobe flux increases, and the inner edge of the plasma sheet moves toward the earth about 1 R_e, which is consistent with previous studies [*Siscoe and Cummings*, 1969; *Coroniti and Kennel*, 1972]. The location X_e of the inner edge of the plasma sheet as a function of A_c is shown in Fig.2.4a. The tailward displacement of geomagnetic field lines can also be seen in Fig.2.4b, which shows the flux function A in the equatorial plane (z=0) as a function of x. For example, the magnetic field line with $A = 20$ is located at $x \simeq -5.3R_e$ as $A_c = 17.75$ and stretches to $x \simeq -30.R_e$ as $A_c = 21$. But the current sheet properties and the minimum B_z almost do not change during $S(A)$ shifting in A-space.

2.2.2 Formation of a very thin current sheet

Our previous results [*Lee et al.*, 1995] show that the current sheet thickness is mainly determined by the transition width ΔA and the magnitude S_m of the entropy function. Using MHD simulations with a pressure diffusion [*Lee et al.*, 1995], I demonstrated that the entropy anti-diffusion instability results in a steepening of the entropy profile in A-space, which finally leads to an enhanced current density and a thining current sheet in the near-earth region. For the empirical Tsyganeko field model [1989], the flux tube volume V and plasma pressure p are calculated for different K_p and for the substorm growth phase. It is found that the specific entropy and its gradient in the near-earth flux tube, which are connected to the ionosphere in the latitudinal range of $62^o \sim 64^o$, is highly enhanced as compared to the quite time values [*Zhang et al.*, 1994].

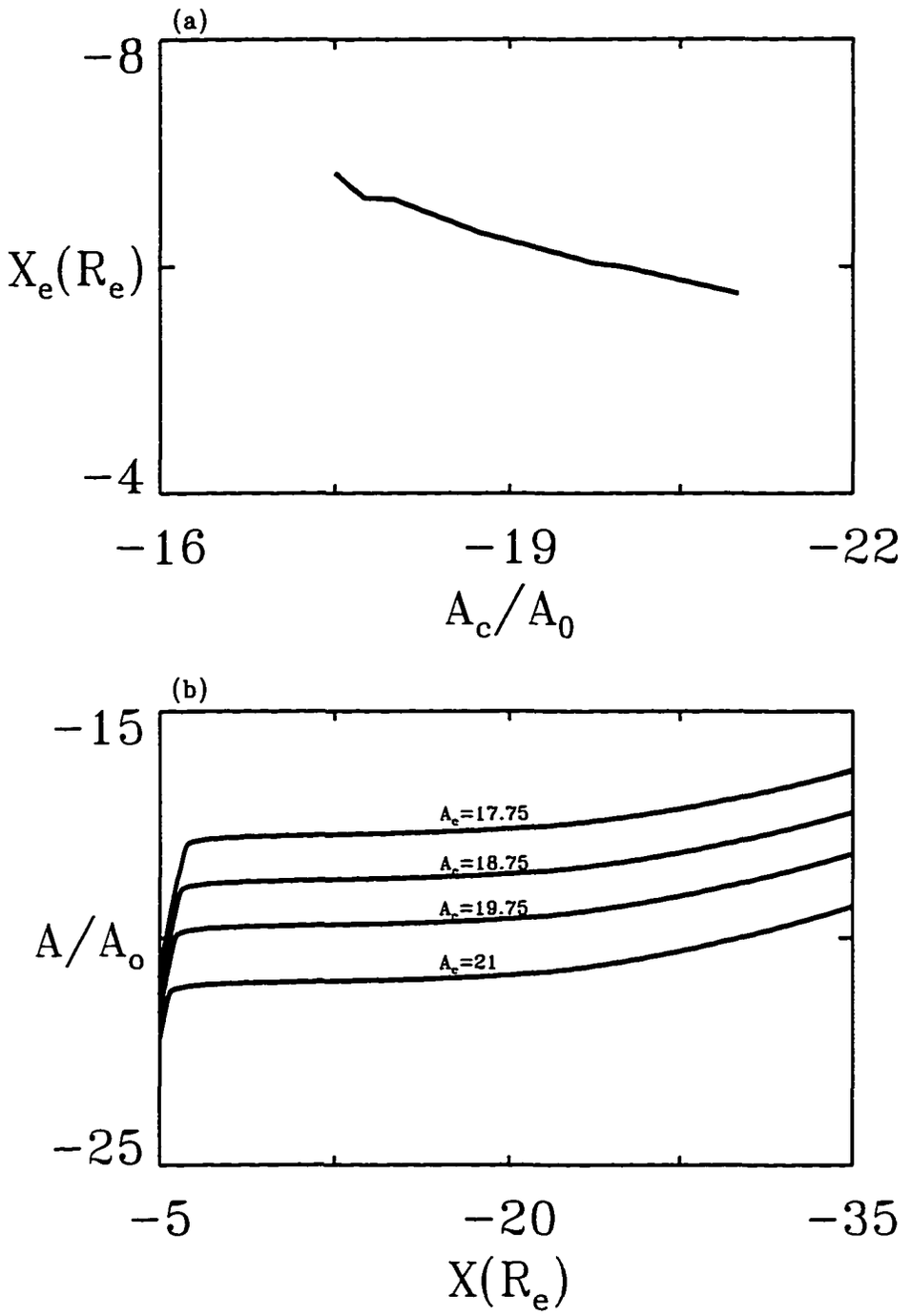

Figure 2.4 (a) The inner edge X_e of the plasma sheet moves toward the earth about 1 R_e as $S(A)$ shifts to the earth about $3.25A_0$ in A-space; (b) The magnetic flux A in the equatorial plane versus the distance $X(R_e)$ for A_c=17.75, 18.75, 19.75 and 21. The dipole field is stretched tailward when $S(A)$ shifts to the earth.

The results shown in Fig.2.5, give equilibrium field configurations that have same parameters except for transition width ΔA, in which ΔA decreases from $\Delta A = 1.0$ to $\Delta A = 0.05$, and finally a very thin current sheet is formed in the near-Earth region. In this case, $S_m = 500$, $A_1 = -14.$, $A_2 = 1.5$, $A_3 = 9.8$ and $A_c = 18.75$. Figure 2.5a, 2.5b, 2.5c and 2.5d have $\Delta A = 0.05$, 0.3, 0.5 and 1.0 respectively. As shown in Fig.2.5a, the magnetic field lines in the region $-6.5\,R_e \geq x \geq -25\,R_e$ are very tail-like. The field lines are cusp-shaped, i.e., the angle between the field line in $z > 0$ and that in $z < 0$ is nearly zero. Note that the cusp-shaped magnetic field configuration is stable to the interchange or ballooning instability.

Fig.2.6 shows the entropy function S, p, B_z, and the current density J_y, which corresponds to Fig.2.6a ($\Delta A = 0.05$), in the equatorial plane as a function of x. The magnetic field B_z is very small in the region $-8\,R_e \geq x \geq -16\,R_e$ and the minimum value of B_z is found to be $B_{z\min} \simeq 0.007\,B_0 \simeq 0.21\,\mathrm{nT}$. The half-thickness of the obtained thin current sheet measures $d \simeq 0.08 R_e \simeq 500\,\mathrm{km}$, which corresponds to three grid spacings, and the peak pressure reaches $1.96\,p_0 \simeq 1.39\mathrm{nPa}$, which is consistent with observations by Spence et al. [1989] and Lui et al. [1992]. As ΔA gradually decreases magnetic field lines in the region $-6\,R_e \geq x \geq -15\,R_e$ are highly dipolarized and field lines in the far tail region $x < -20 R_e$ is stretched tailward. The distances of field line's moving earthward vary.

When ΔA decreases from 1 to 0.05, the flux function A and the distance $D(X_{Aref}) = X_A(A) - X_{Aref}$ of field line displacement in the equatorial plane (z=0) as a function of X_{Aref} are shown in Fig.2.7. $X_A(A)$ is the location of the flux A in the equatorial plane for $\Delta A = 0.05$ and X_{Aref} is for $\Delta A = 1.0$ as a reference

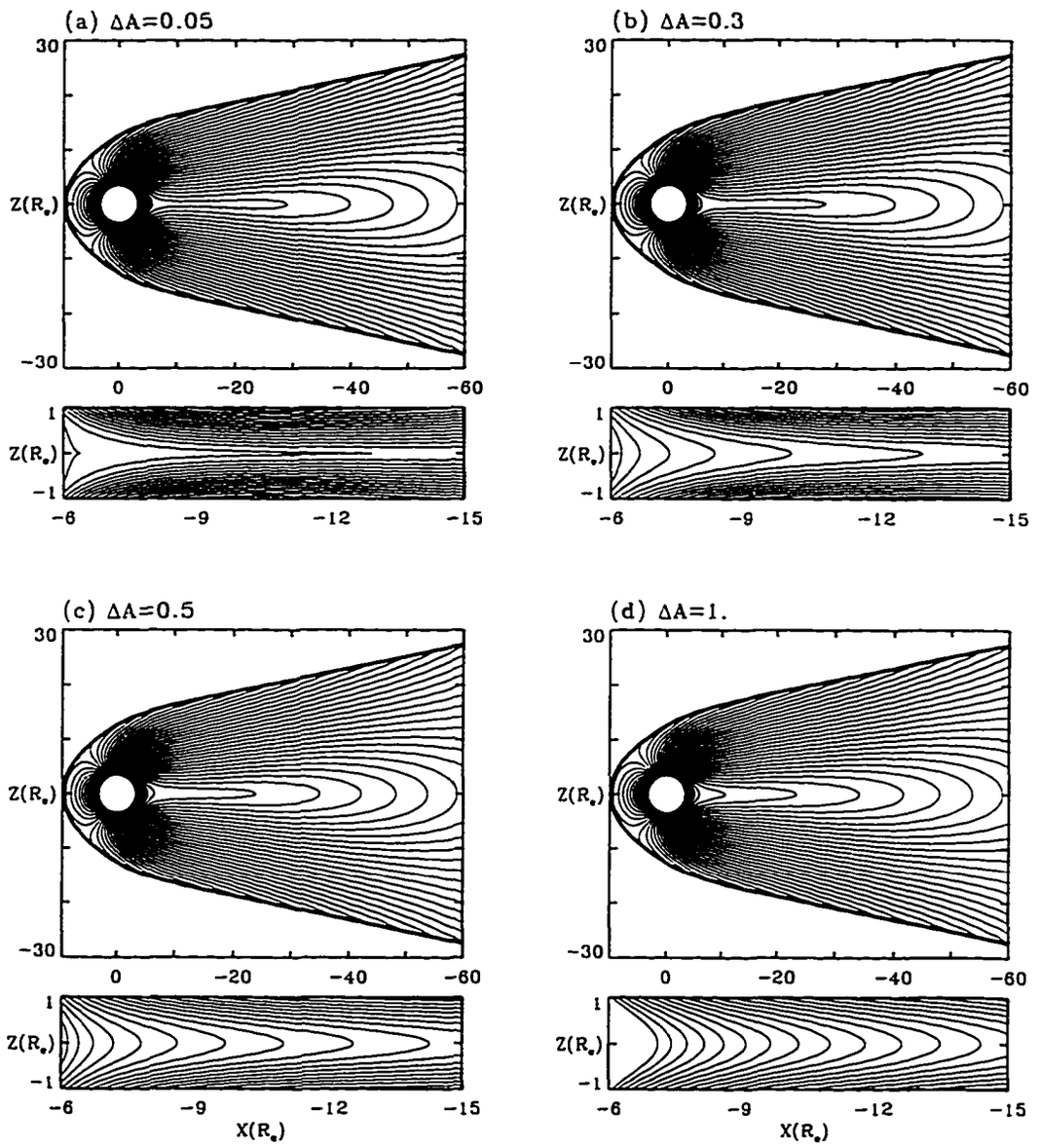

Figure 2.5 Sequence of equilibrium configurations showing the effect of increasing ΔA with (a) $\Delta A = 0.05$, (b) $\Delta A = 0.3$, (c) $\Delta A = 0.5$, (d) $\Delta A = 1.0$. The equilibrium field configuration for $\Delta A = 0.05$ contains a very thin current sheet ($d \sim 0.08 R_e$) and a minimum B_z of $\sim 0.007 B_o \sim 0.21 nT$. The magnified view below the main plot shows a cusp-like field lines for the $-6R_e \leq x \leq -15R_e$. For $\Delta A = 1.0$, the magnetic field is more dipolar in the region $-6R_e \leq x \leq -15R_e$. The current sheet is very thick ($d \sim 1.47 R_e$).

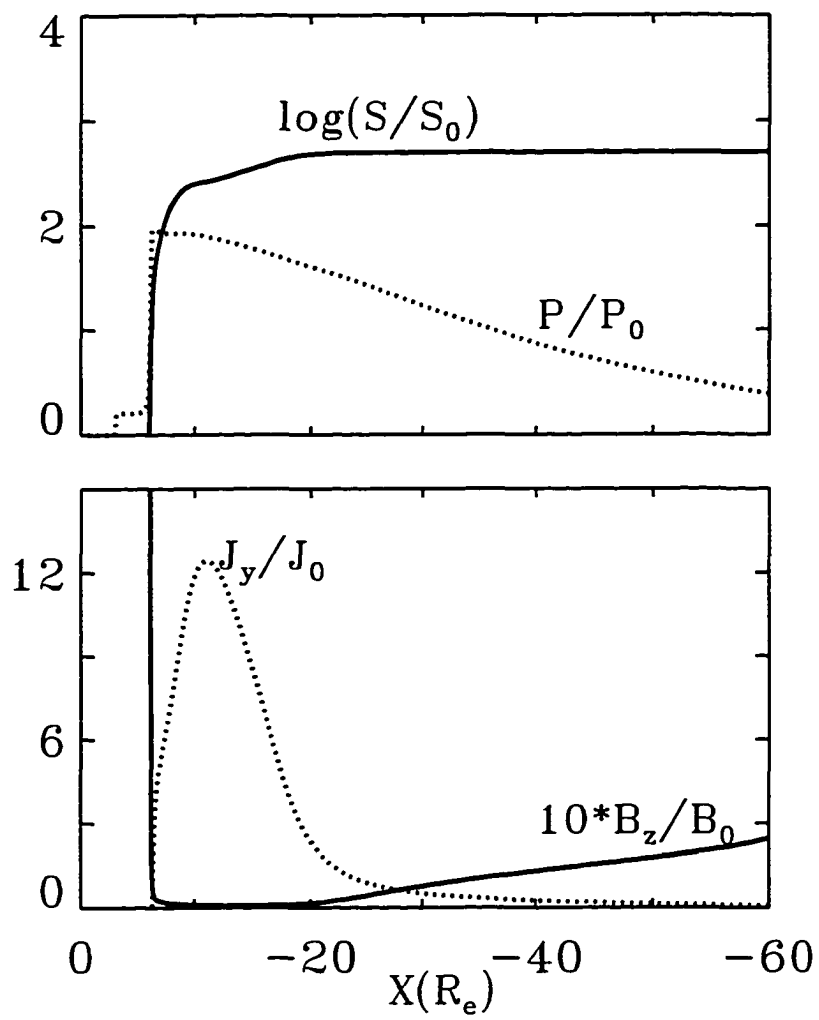

Figure 2.6 Entropy function $S = pV^{\gamma}$ and pressure p (upper plot), and magnetic field B_z and current density J_y (lower plot) in the equatorial plane as a function of x for $\Delta A = 0.05$.

case. So magnetic field strength B_z in $-8\,R_e \geq x \geq -16\,R_e$ sharply decreases as ΔA gradually decreases. Finally shapes cusp field lines is shaped. Simultaneously, the current sheet density sharply increases and the thickness of the current dramatically decreases. The maximum value of the current sheet density increases from $1.25J_o$ to $12.43J_o$. The half-thickness $d(R_e)$ and maximum density J_{max} of a current sheet and the minimum value B_{zmin} of B_z as a function of ΔA are shown in Fig.2.8.

The two cases shown in Fig.2.9, give equilibrium field configurations that have same parameters except for S_m. Here, $A_1 = -14.$, $A_2 = 1.5$, $A_3 = 9.8$, $\Delta A = 0.3$ and $A_c = 18.75$. Fig.2.9a and 2.9b have $S_m = 250$ and 750 respectively. As shown in Fig.2.9b, the magnetic field lines in the region $-6\,R_e \geq x \geq -35\,R_e$ are highly stretched tailward. The flux function A and the tailward displacement $D(X_{Aref}) = X_A(A) - X_{Aref}(A)$ of field line in the equatorial plane (z=0) as a function of X_{Aref}, when S_m increases from 250 t0 750, are shown in Fig.2.10. Here, $X_A(A)$ is for $S_m = 750$ and X_{Aref} is for $S_m = 250$ as reference. In the region $-6\,R_e \geq x \geq -20\,R_e$, the tailward displacement of field line is proportional to x. Field line's stretching tailward result in a sharp decrease of magnetic field strength B_z. Finally, a current sheet is formed in the near-earth region. The half-thickness $d(R_e)$ and maximum density J_{max} of a current sheet and the minimum value B_{zmin} of B_z as a function of S_m are shown in Fig.2.11.

It is shown that a larger entropy or a higher entropy gradient is required to form a thin current sheet in the near-earth region. But the enhancement of the entropy or the entropy gradient produces a different process in the near-earth magnetotail. A thin current sheet is formed in the near-earth region due to field line's stretching

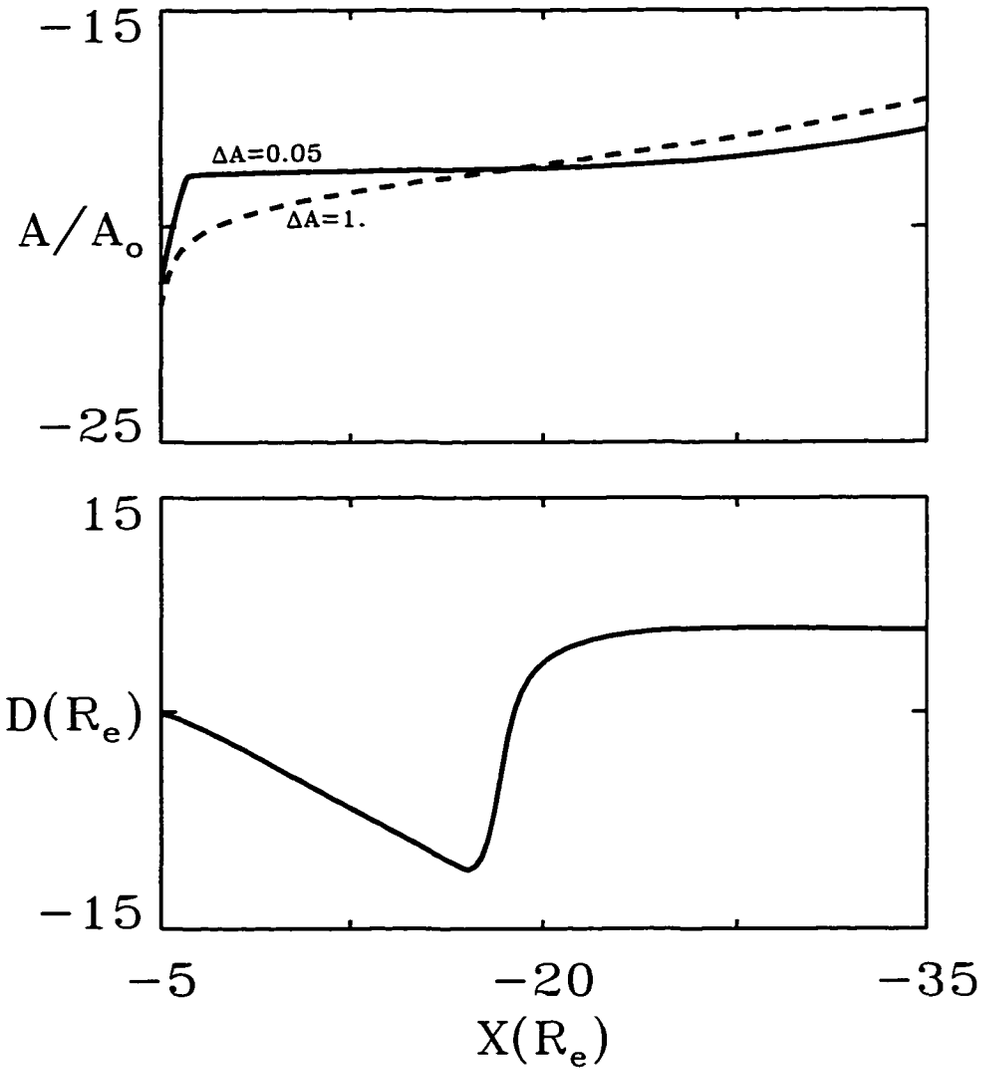

Figure 2.7 The magnetic flux A in the equatorial plane versus the distance $X(R_e)$ for $\Delta A = 0.05$ and $\Delta A = 1.0$ (upper plot). The separation $D(X_{Aref})$ of magnetic field lines with the same value of A along the equatorial plane for the configuration with $\Delta A = 0.05$ compared to the reference case with $\Delta A = 1.0$ (lower plot).

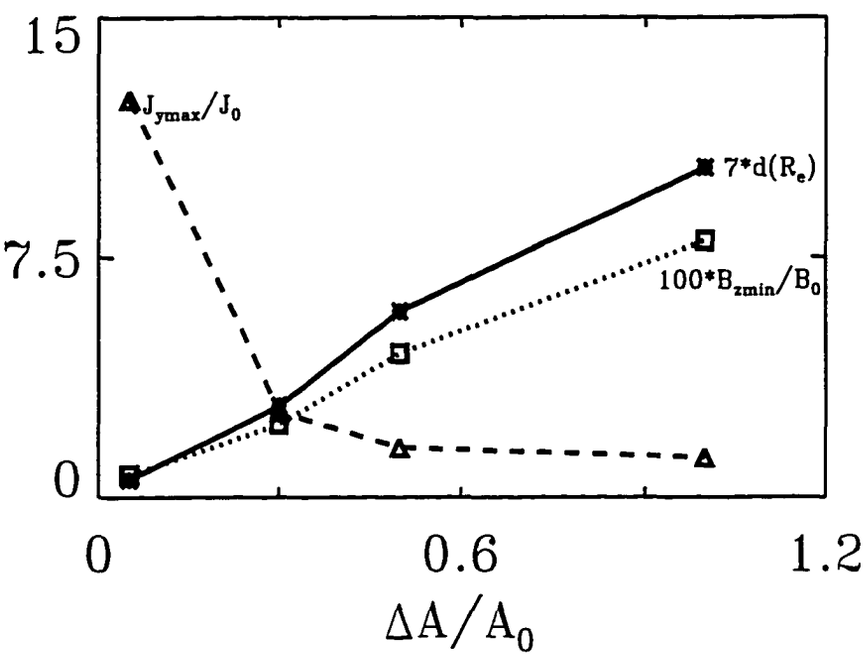

Figure 2.8 The half-thickness $d(R_e)$ $(7 * d(R_e))$ of the current sheet, maximum current density J_{ymax} and minimum B_z $(100 * B_{zmin})$ versus ΔA.

tailward as the entropy S_m enhances. The dipolarization resulting from increasing entropy gradient leads to a very thin current sheet in the near-earth region.

2.2.3 Relationship between lobe flux and a current sheet

During the substorm growth phase the interplanetary magnetic field (IMF) turns southward, and the solar wind transports open magnetic flux to the magnetotail. Consequently the lobe field strength increases. It is believed that the lobe flux has an important effect on the thickness and the earthward displacement. Siscoe and Cummings [1969] suggested that in a three-dimensional tail sheet model the inner edge of the cross-tail sheet must move earthward to accommodate an increasing lobe flux in the tail, as a consequence of force balance between the Earth and the solar wind. In the chapter, the effects of lobe flux on a current sheet in two-dimensional tail current model is discussed.

For comparison with previous studies [*Siscoe and Cummings*, 1969; *Cao and Vasyliunas*, 1995], the open magnetic flux is set to zero, i.e., $A_2 = A_1$. I obtain an approximate constant lobe field strength B_t. In following discussion, I supposed that tail-lobe does not expand and the magnetopause boundary ($\partial\Omega_2$) is fixed. So the lobe field strength B_t increases proportionally with the lobe flux enhancement. In our original model, a current sheet is formed in the tail boundary center ($\partial\Omega_3$, $z = 0$) if the lobe flux is too large. To obtain a equilibrium configuration ($x \geq -60$) without a current sheet in the tail boundary. I prolong the computer domain tailward to $-100R_e$. After force balance, I obtain equilibrium configurations ($x \geq -60$).

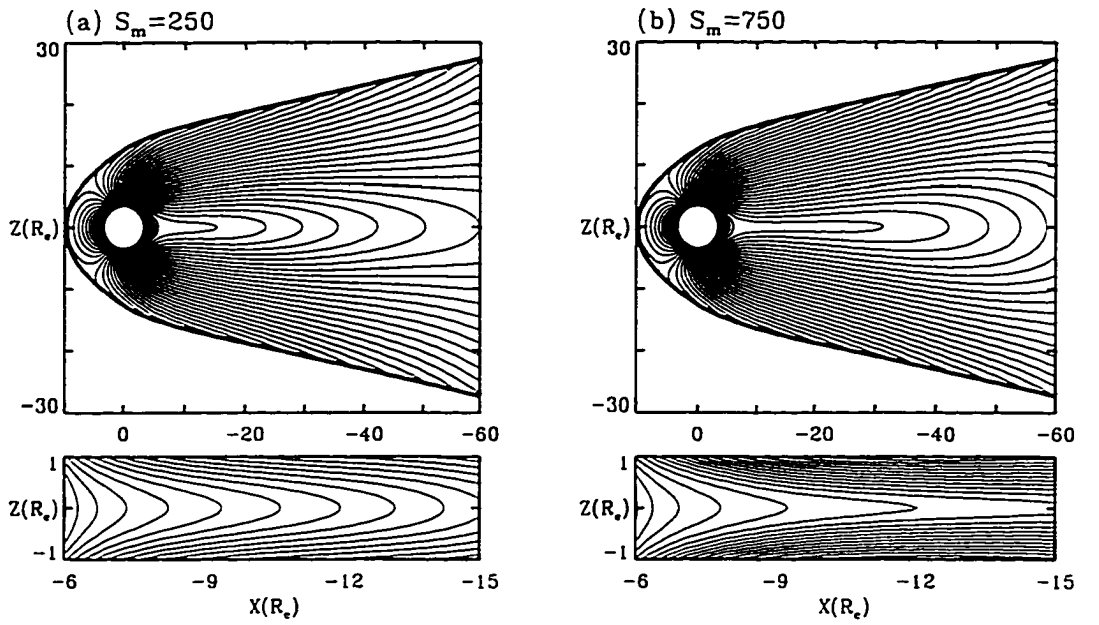

Figure 2.9 The dependence of the equilibrium configuration on the magnitude S_m of the entropy function. For $S_m = 250$ (a), the magnetic field is more dipolar field in the region $-6R_e \leq x \leq -15R_e$, while $S_m = 750$ leads to a thinner current sheet and a more stretched magnetotail configuration.

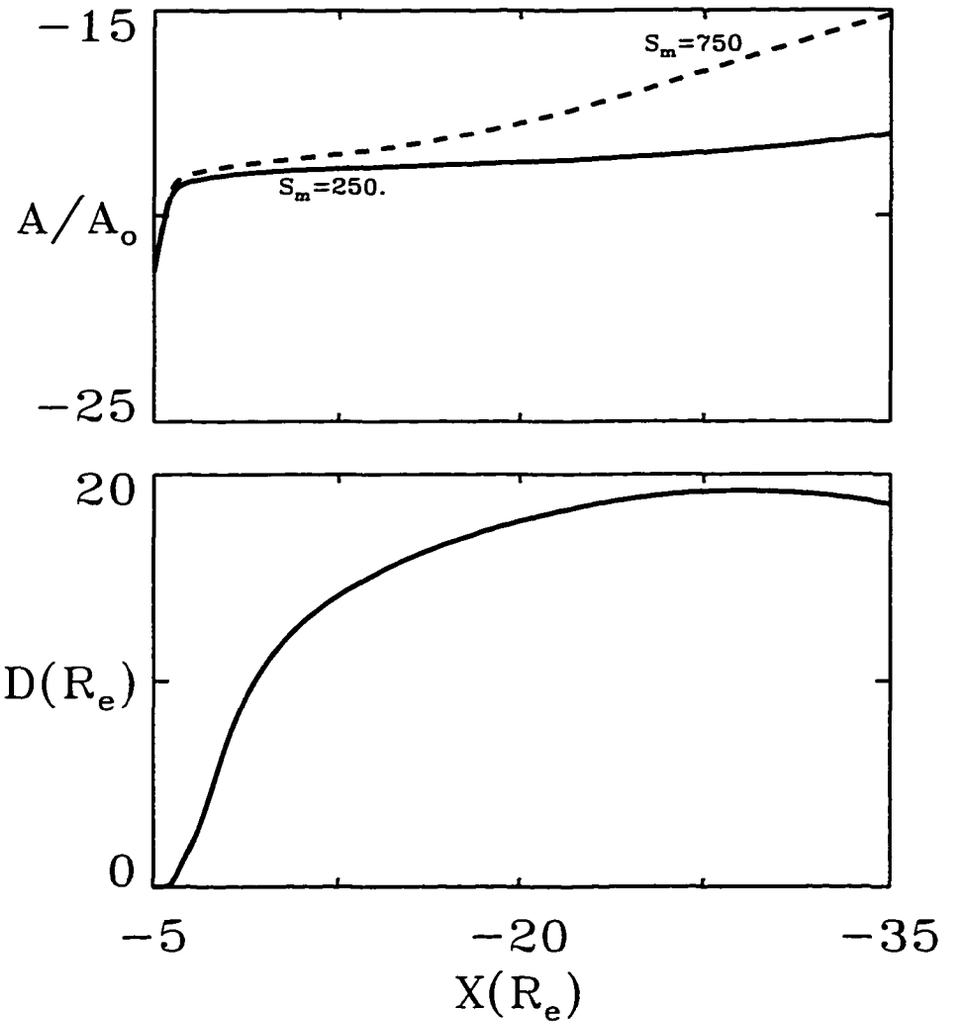

Figure 2.10 The distribution of magnetic flux A in the equatorial plane versus the distance $X(R_e)$ for $S_m = 750$ and $S_m = 250$ (upper plot). The bottom plot shows the separation $D(X_{Aref})$ of field lines in the equatorial plane as a function of X_{Aref} for $S_m = 750$ and 250.

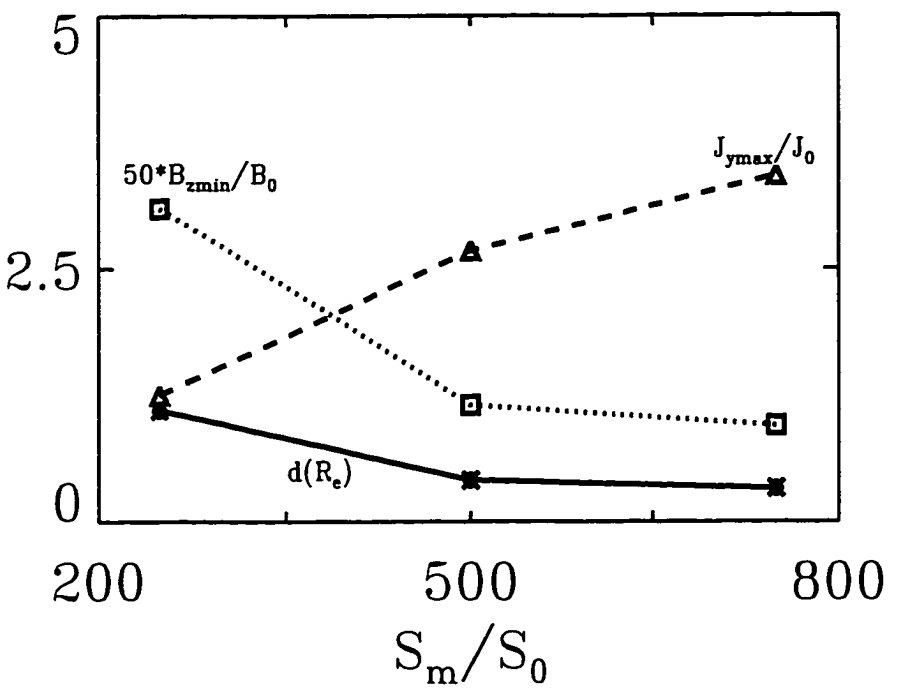

Figure 2.11 The half-thickness of the current sheet $d(R_e)$, maximum current density J_{ymax} and minimum B_z $(50 * B_{zmin})$ versus S_m.

My results confirm that a current sheet moves earthward continuously as the lobe flux enhances. But the thickness of a current sheet does not decreases much and the current density hardly increases with the enhancement of the lobe flux A_{lob}. Fig.2.12 shows the inner edge X_e, maximum current density J_{max} and thickness $d(R_e)$ as a function of the lobe flux A_{lob}. Here the lobe flux is defined as $A_{lob} = A(x = -60, z = 0) - A_2$. But total cross-tail current $\int J_y dz$ enhances significantly, as shown in Fig.2.13. It is consistent with a significant enhancement of the lobe flux.

My result show there are equilibrium configurations even if the lobe field strength B_t is very large. It does not support the existence of a critical amount of the lobe flux, over which the tail current sheet supposedly collapses. Fig.2.14a shows an example with a large lobe field strength. Here, $S_m = 500$, $A_1 = A_2 = -20$, $A_3 = 8.05$, $\Delta A = 2.$ and $A_c = 18.75$. The lobe magnetic field strength down tail $-20R_e$ is about $B_t = 1.71B_0 \simeq 51nT$, and corresponding B_z and J_y as a function of x is shown in Fig.2.14a. In this case the equatorial B_z has a B_z minimum. An enhancement of the lobe flux results in a B_z minimum in the equatorial plane when $S(A)$ does not change. But I also find that increasing lobe field strength B_t does not always causes a B_z minimum. The B_z profile in the equatorial plane is mainly determined by the entropy function $S(A)$. The higher entropy gradient favors the formation of a B_z minimum in the equatorial plane. An equilibrium configuration with a large lobe field strength and B_z decreasing monotonically down the tail is shown in Fig.2.14b. The lobe magnetic field strength B_t down the tail $-20R_e$ is about $B_t = 1.7B_0 = 51nT$. Corresponding B_z and J_y as a function of x is shown in Fig.2.14b. In this case, all parameters are as same as in the previous case

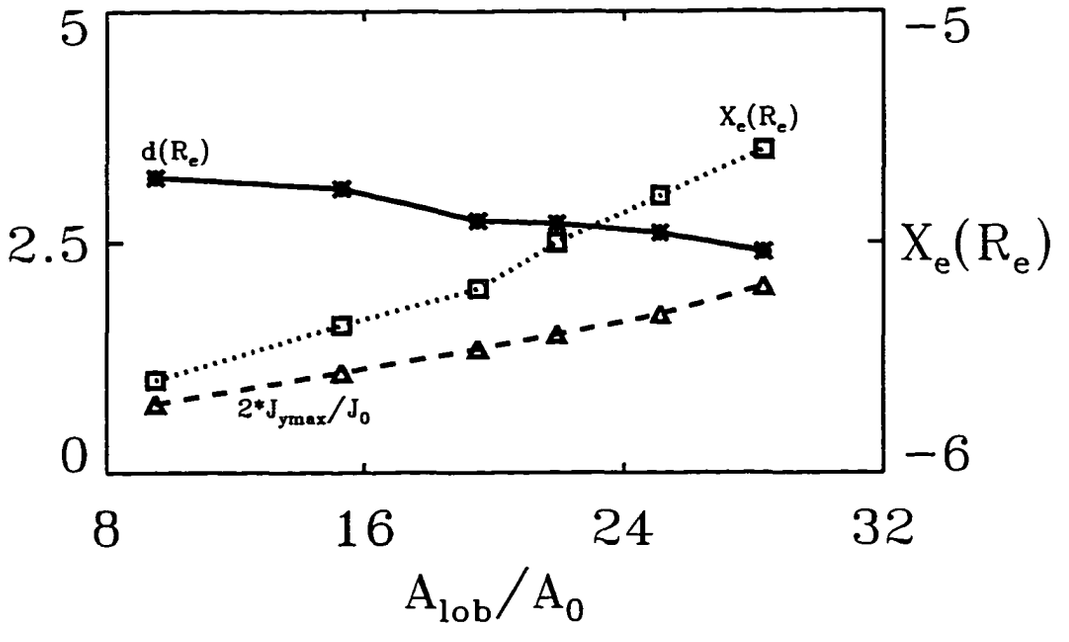

Figure 2.12 The half-thickness of the current sheet $d(R_e)$, maximum current density J_{ymax} and inner edge X_e versus $A_{lob} = A(x = -60, z = 0) - A_2$, for fixed $S_m = 500$ and $\Delta A = 2$.

(Fig.2.14a), except for $\Delta A = 4$. It is shown that during an early phase of substorm, the enhancement of the lobe magnetic field strength B_t results in increasing and thining an current sheet. But continuous enhancement of the lobe field does not thin an current sheet further. There must be other mechanisms such as entropy anti-diffusion instability to thin an current sheet during a final substorm growth phase.

2.2.4 lobe and tail (parameter a) boundary conditions

In the previous sections I have explored the influence of the amount of magnetic flux in the lobes (for open and closed lobe boundaries) and of the gradient of the entropy function (ΔA and S_m) on the tail configuration and on the thickness of the near Earth current sheet. So far unresolved for the presented model is the effect of a varying distributions of open magnetic flux at the tail magnetopause. Another important aspect is the potential influence of the magnetic flux distribution through the tailward boundary $\partial\Omega_3$ which is controlled by the parameter for B_x at this boundary.

First I consider the influence of the lobeward boundary using 4 cases with different boundary conditions. Here I include also basic cases with a nonuniform distribution of open magnetic flux. Such a nonuniform distribution of open flux could be generated for instance by a variation of the IMF B_z component such as a short northward turning which has been recently suggested by Lyons [*Lyons*, 1995] as a possible trigger for magnetic substorms. A nonuniform flux distribution is also relevant to time dependent simulation studies which sometimes assumed a

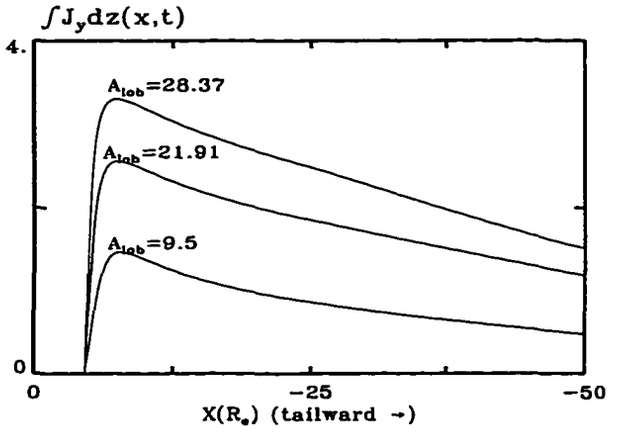

Figure 2.13 The total current $\int J_y dz$ for different lobe flux A_{lob} as a function of x.

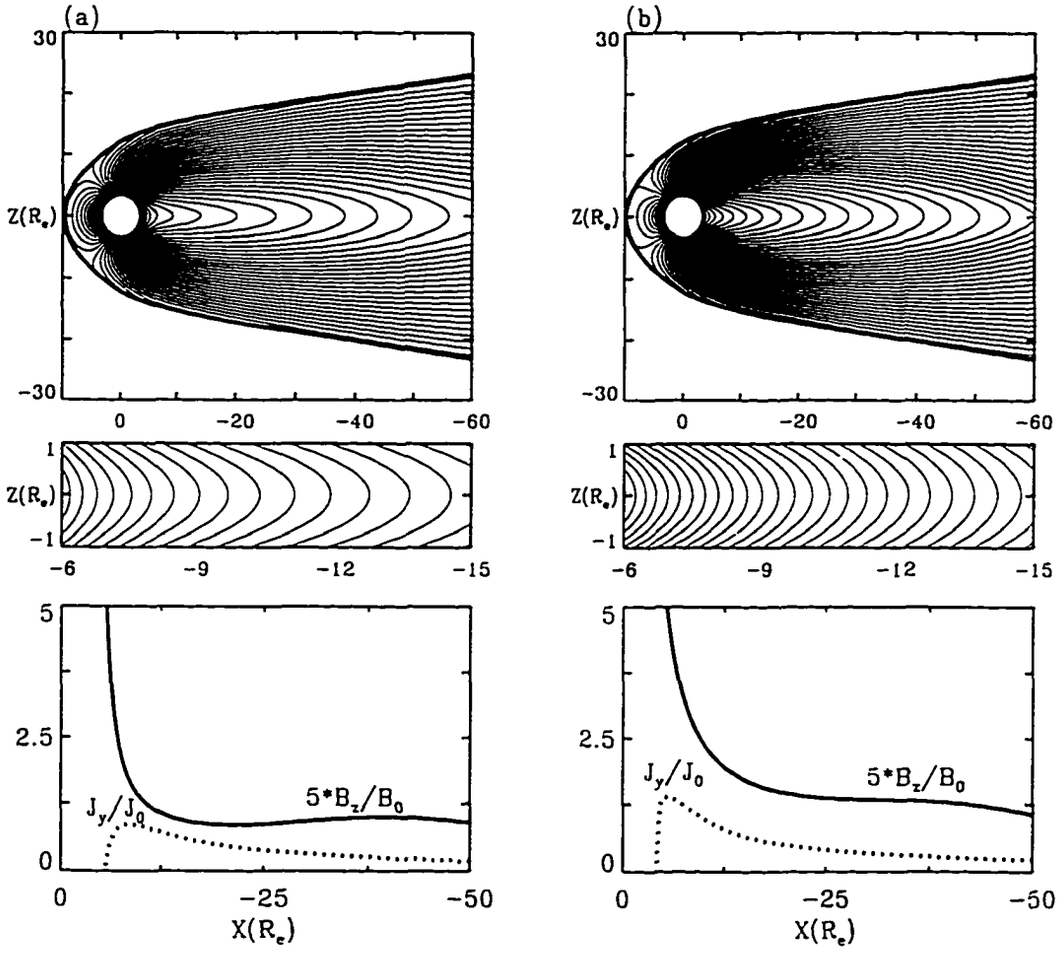

Figure 2.14 (a) An equilibrium field configuration with the lobe flux $A_{lobe} = A(x = -60, z = 0) - A_1 = 28.07A_o$, and a transition width $\Delta A = 2.0$; magnified view in the $-6R_e \leq x \leq -15R_e$; the magnetic field component B_z $(5 * B_z)$, and the current density J_y in the equatorial plane as a function of x. (b) An equilibrium field configuration with the lobe flux $A_{lobe} = A(x = -60, z = 0) - A_1 = 28.08A_o$, and a transition width $\Delta A = 4$; B_z decreases monotonically down the tail.

non constant electric field at the lobe boundary [*Birn et al.*, 1986].

To relate to the results of section I choose the same parameters as for the first series of runs in section 3.2 (Figures 2.4 to 2.8) with $\Delta A = 0.3$. Thus my reference case here is the one shown in Figure 2.6b with a uniform distribution of open flux at the lobe magnetopause. The second case has the same amount of lobe flux, however, with an entirely closed magnetopause as shown in Fig.2.15a. To study the influence of a nonuniform distribution of open lobe flux I have selected the cases shown in Figure 2.15b and c. For both cases (b) and (c) the total amount of open flux is the same as for the reference in Figure 2.6b. The run in Figure 2.15b has a closed magnetopause close to the Earth (between $x = 0$ and $x = -20$) and all open flux is located at larger distances from the Earth. The result in Figure 2.15c uses an open magnetopause close to the Earth (between $x = 0$ and $x = -25$) and a closed magnetopause at larger distances.

The results in Figure 2.6b and Figure 2.15a to c show that all cases except for the one with the fully closed magnetopause show a very thin current sheet close to the Earth. A closed magnetopause implies a larger amount of flux in the more distant lobes and thus requires a larger crosstail current in the more distant magnetotail. This is in fact seen in Figure 2.15a which shows a larger current density and a thicker current sheet in the more distant tail.

Comparing the cases with an open flux distribution the result in Figure 2.15c with the open flux boundary close to the Earth shows the largest maximum and the thinnest current density (about 50% larger and 50% thinner than in Figure 2.6b). Although this increase is moderate compared to the influence of ΔA, it is interesting to see the maximum current density for this particular case (Figure

2.15c) because it is has the smallest lobe flux at $x = -13R_e$ consistent with the open magnetic boundary. In terms of a slow quasi-static evolution of the magnetotail a nonuniform open flux would be caused by a nonuniform convection (and electric field) at the boundary. I note that a stronger local thinning of the current sheet has also been found in time-dependent studies with a localized electric field applied to the boundary [*Birn et al.*, 1986]. Regarding a possible trigger of magnetic substorms the results show that the thinning of the current sheet is stronger for an open flux distribution at the tail magnetopause. An additional variation of the open flux distribution can contribute to some moderate further thinning and could possibly trigger a substorm if the configuration is already in a marginal state. It appears that such further thinning can be expected for an increase of open flux in the near Earth region.

In my model, the distribution of magnetic flux along the tailside boundary is controlled by parameter a. As $a >> z_w$, the results are not sensitive to a. Fig.2.16 gives equilibrium configurations with same parameters except for a. In the case, $S_m = 500$, $A_1 = -14$, $A_2 = 1.5$, $A_3 = 9.8$, $A_c = 18.75$ and $\Delta A = 0.3$. Fig.2.16a and 2.15b have $a = 200$, 5 respectively. Corresponding p, B_z and J_z are shown in Fig.2.16. It is shown that an equilibrium configuration is independent of parameter a ($a >> z_w$).

2.3 Discussion and Summary

As mentioned earlier, three conditions are needed for the formation of very thin current sheets: (1) the entropy function S is enhanced, in the near-earth region

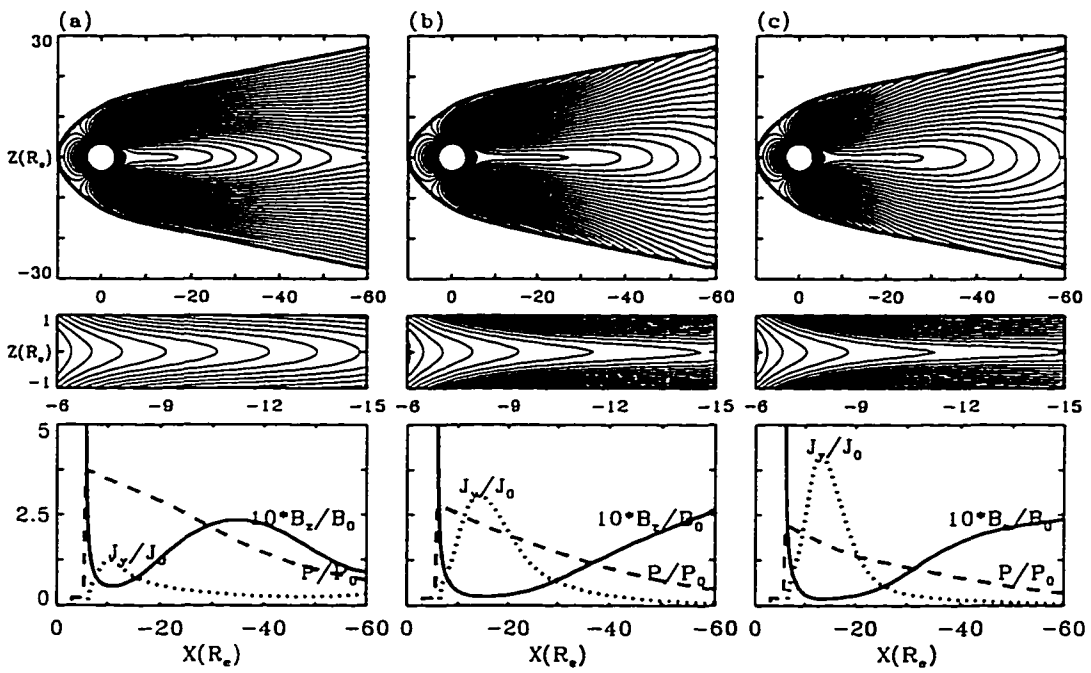

Figure 2.15 Equilibrium field configurations for different flux distribution in the magnetopause boundary; The magnified view in the $-6R_e \leq x \leq -15R_e$; B_z, J_y and p in the equatorial plane as a function of x. (a) An entirely closed magnetopause. (b) Open flux is located at far-tail. (c) Open flux is close to the Earth.

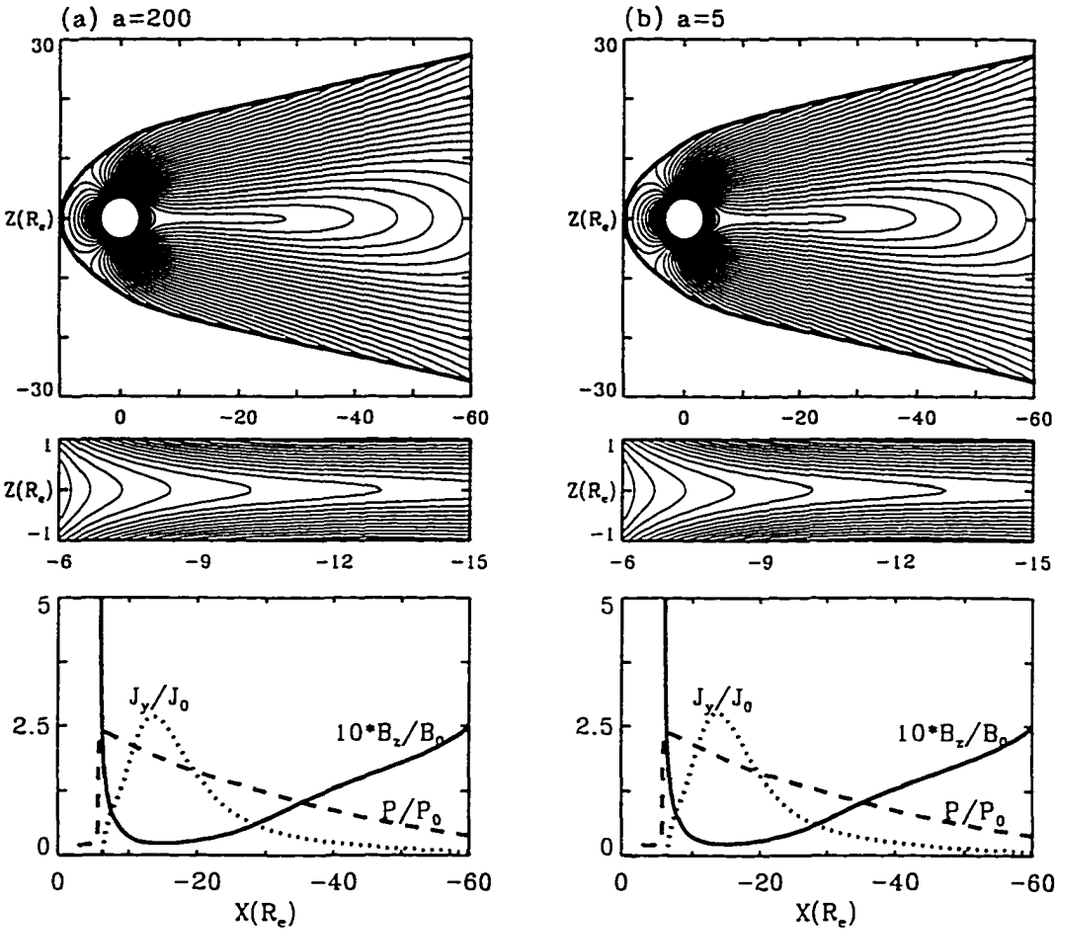

Figure 2.16 Equilibrium field configurations with (a) $a = 200$, (b) $a = 5$.

($-15R_e < x < -6R_e$), (2) the entropy gradient is steepened in A-space and (3) the lobe flux enhances. Satellite observations show that the plasma pressure in the region $-6R_e > x > -10R_e$ increases during the growth phase to about ten times the value in the quiet time [*Kistler et al.*, 1992]. At the same time, the magnetic field in the equatorial plane (B_z) may decrease to about 1/7 of the dipole field strength [*Lui et al.*, 1992]. As a rough estimate, the differential flux volume thus increases to seven times and the entropy function to about 250 times the quiet time value at a fixed point. The decrease of B_z also indicates the decrease of the entropy transition width ΔA.

As the interplanetary magnetic field (IMF) turns southward, dayside magnetic reconnection leads to an increase of open magnetic flux in the polar cap. This in turn leads to an increase of electric potential drop across the polar cap, and hence an increase of dawn-to-dusk electrostatic electric field [e.g., *Reiff et al.*, 1981]. Through the penetration of electric field in the conducting ionosphere, the electric field in the auroral oval region is also enhanced [*Swift*, 1967; *Vasyliunas*, 1970; *Wolf*, 1970]. This enhanced electric field can be transmitted by Alfven waves from the ionosphere to the closed field region of magnetotail along magnetic field lines. This would contribute to a dawn-to-dusk electrostatic component E_s of electric field in the plasma sheet. The enhanced convection electric field in the growth phase results in an adiabatic evolution of the plasma sheet in the A-space and enhances the entropy in the near-earth region. Simultaneously, the entropy transition region shifts toward the earth. Under the assumption of adiabatic evolution, the entropy

function satisfies the following conservation equation in A-space,

$$\frac{\partial H(A,t)}{\partial t} + E_s(t)\frac{\partial H(A,t)}{\partial A} = 0, \tag{2.6}$$

where $H(A,t) \equiv S^{1/\gamma} = p^{1/\gamma}V$, Note that (2.6) is consistent with the particle conservation and entropy conservation. $E_s(t)$ is assumed to change slowly with time[*Cai et al.*, 1995]. If a dawn-dusk electrostatic field is $E \sim 0.3mV/m$ (80kV over $40R_e$) and a growth phase lasts about Δt~$0.5 - 1$ hour. So the entropy function shifts about

$$\Delta A = E_s \Delta t \sim 85 - 175 nTR_e = 2.8 - 5.8A_0, \tag{2.7}$$

where A_0 is a flux unit of $A_0 = 30nTR_e$. It is implied that the enhanced ionospheric convection electric field is the main driving force of enhancing the entropy in the near-earth magnetotail during the substorm growth phase. Non-adiabatic particle heating, such as the damping of fast mode waves and drift instabilities [e.g., *Lui et al.*, 1992], also contributes to the observed enhancement of entropy in the near-earth region. Further a localized non-adiabatic heating in the entropy transition region can lead to the steepening of the entropy profile in A-space. In the chapter 3, I use MHD simulations with a dawn-to-dusk electrostatic field E_y to confirm the conclusion. An enhanced ionospheric convection electric field can enhance the entropy and highly stretch geomagnetic field lines tailward in the near-earth region.

When open magnetic flux is convected from the dayside to the magnetotail, the enhancement of the lobe magnetic flux is accompanied by a gradual thining, and inward motion of the plasma sheet during early substorm growth phase. It is found that it is unlikely to form a very thin current sheet in the near-earth region

only by an enhancement of the lobe flux. We are confronted with the problem of finding a new mechanism for the plasma sheet thining without invoking an enhanced reconnection in the near-earth region.

I suggest there are two approaches to form a thin current sheet. First, during the formation of thin current sheet, the lower-hybrid drift instability may occur in the region where there exists a sharp pressure gradient and $\beta < 2$ [*Huba et al.*, 1977]. The regions with high density gradient favor the lower-hybrid-drift instability, leading to the transport of particles across magnetic field lines. The diffusion of pressure associated with the particle transport can further steepen the entropy profile, corresponding to an effective "anti-diffusion" of entropy function. In Fig.2.6, I can obtain some physical insights to this process. From the pressure maximum outward, the pressure decreases monotonically, but the entropy increases. This pressure diffusion will result in a sharper gradient in entropy and hence a thinner current sheet which also means a steeper pressure gradient. The process is thus further accelerated in itself and also leads to a dipolarization where pressure is decreased and formation of a very thin current sheet. During the process, the evolution of the entropy function is approximatively described as

$$\frac{\partial H(A,t)}{\partial t} + E_s(t)\frac{\partial H(A,t)}{\partial A} = -D\frac{\partial^2 H(A,t)}{\partial A^2}, \tag{2.8}$$

where D is anti-diffusion coefficient of the entropy function. This instability is seen in my MHD simulation of the dynamic magnetotail evolution and the results are presented in Chapter 4. This "entropy anti-diffusion instability" leads to the onset of dipolarization of near-earth geomagnetic field lines and a very thin current sheet in the near-earth region. The growth time is proportional to the diffusion

coefficient and ~ 1 minute. The instability may correspond to the explosive growth phase observed before the full onset of substorms [*Ohtani et al.*, 1992].

Another mechanics to form and thin a current sheet may be provided by the nonuniform of electrostatic field E_s, especially y-component. In two dimension, the electrostatic field E_y is strictly a constant. But in three dimensions, the electrostatic y-component E_y could be nonuniform. Jaggi and Wolf [1973, 1975] suggested that there is 'the Alfven layer' at $\sim -7R_e$ region. The electric field becomes much weaker in the near-earth region $x > -7R_e$ and Eq(2.6) becomes a nonlinear convection equation. The plasma sheet convects with different convection velocities at different location. The plasma further from the earth, convects faster toward the Earth. In the 'Alfven layer', the convection velocity is almost zero. The entropy function steepens during the current sheet convection, and finally, a very thin current sheet is formed in the near-earth region $x \simeq -7R_e$.

In summary for this chapter, I have constructed 2-D MHD equilibria with the entropy function $S(A)$ as a constraint and found that the larger entropy or the higher entropy gradient favors the formation of very thin current sheets. It is also shown that the enhanced ionospheric convection electric field may be the main driving force to form highly stretched field line configuration and enhance the entropy function in the near-earth region during the substorm growth phase. In the final substorm growth phase, the "entropy anti-diffusion instability" associated with pressure diffusion or with a nonuniform y-component of the electrostatic field leads to the dipolarization of near-earth field lines and accelerates the formation of a very thin current sheet, which may explain the observed explosive growth phase of substorms. Corresponding dynamic simulations will be presented in Chapter 4.

In the next chapter, I present MHD simulations with a dawn-to-dusk electrostatic field to confirm my equilibrium results: An enhanced ionospheric convection electric field may be the main driving force to form highly stretched field line configuration and enhance the entropy function in the near-earth region during the substorm growth phase.

Chapter 3

Dynamic Evolution of the Earth's Magnetosphere During Substorm Growth Phase

One of the most important topics in magnetospheric physics is the study of magnetospheric dynamics during substorm growth phase. A typical observed feature of the growth phase is highly stretched geomagnetic field lines just before the onset of substorms [e.g., *Kokubun and McPherron*, 1981; *Kaufmann*, 1987; *Fairfield et al.*, 1987; *Lui et al.*, 1992]. This phenomenon can be modeled using an intense thin current sheet in the near-earth magnetotail [e.g., *Kaufmann*, 1987]. An outstanding problem in the substorm study is to identify particles which constitute the current [*Akasofu*, 1994] and to understand how the near-earth magnetic field lines are distributed in that extraordinary way(highly stretched) during the substorm growth phase [*Vasyliunas*, 1994]

The stretching and energization of the tail by the adiabatic lossless convection has been studied analytically [*Schindler and Birn*, 1982] and numerically [*Hau et al.*, 1989; *Erickson*, 1992; *Wiegelmann and Schindle*, 1995]. These studies showed that the tail can be stretched as convection proceeds and a B_z-minimum can be formed in the plasma sheet region. The magnetohydrodynamic(MHD) simulations [*Lee et al.*,1985; *Birn and Hesse*, 1991; *Ma et al.*, 1995] shown that, based on rapid reconnection, geomagnetic dipole field can be stretched out and a current sheet forms and is thining in the near-earth magnetotail driven by an external electric field that induces an equatorward boundary flow, in which the X or Y lines and plasmoids form during the period when the driving force is being applied. The hybrid [*Hesse et al.*, 1996] and full particle simulations [*Pritchett and Coroniti*, 1995] qualitatively confirm MHD results. In these simulations, the current sheet formation and thining rely on reconnection and the formation of X or Y line in the near-earth region. Satellite observations [*Lui et al.*, 1992] indicated that the substorm onset may not be initiated by magnetic reconnection. Recent theoretical studies tried to explain the onset without resorting to reconnection [*Kan et al.*, 1988; *Roux et al.*, 1991; *Lui et al.*, 1992; *Birn et al.*, 1994].

I studied the evolution of the earth's magnetosphere during growth phase analytically[*Cai et al.*, 1995] and numerically [*Lee et al.*, 1995; *L.Zhang et al.*, 1997] in Chapter 2. The magnetotail in the growth phase can be approximated by a series of quasi-equilibrium configurations. The equilibria of the earth's magnetosphere were determined by the distribution of entropy function ($S = pV^{\gamma}$). So the evolution of the earth's magnetosphere can be shown in term of the evolution of the entropy function profile. It is found that the formation of highly stretched

field lines is mainly due to enhancement of the entropy function S in the near-earth region. Satellite observations show that the plasma pressure in the region $-6R_e > x > -10R_e$ increases during the growth phase to about ten times the value in the quiet time [*Kistler et al.*, 1992]. At the same time, the magnetic field in the equatorial plane (B_z) may decrease to about 1/7 of the dipole field strength [*Lui et al.*, 1992]. As a rough estimate, the differential flux volume thus increases to seven times and the entropy function to about 250 times the quiet time value at a fixed point. I study the evolution of the entropy profile in presence of the enhanced ionospheric convection electric field and construct the tail configurations corresponding to the entropy function profiles. It is shown that the enhanced ionospheric convection electric field is the main driving force of the near-earth magnetotail evolution during the substorm growth phase. The enhancement of entropy function, the formation of highly stretched field line configuration in the near-earth region and the earthward movement of the plasma sheet inner edge are consequences of the enhanced ionospheric convection.

It should be shown that my scenario of substorm growth comes from the steady state evolution presented in Chapter 2, in which the magnetotail in the growth phase can be approximated by a series of quasi-equilibrium configurations. In this chapter, I use MHD simulation to study substorm growth phase. My results in Chapter 2 can actually be reached physically in a dynamic evolution. It is shown that the enhanced ionospheric convection electric field causes that the flux tubes in the outer plasma sheet are convecting adiabatically toward the inner plasma sheet, and the lobe flux and entropy function in near-earth region enhances. Simultaneously, in the A-space, entropy function S shifts to the Earth and the

plasma sheet inner edge moves earthward in the real space.

In the next section the MHD equations with static electric field are presented. Boundaries and initial configuration are explained. The simulation results is presented in section 3.2. In the section two simulation runs, in detail, is shown for different initial equilibrium configurations. It is shown that a driving dawn-to-dusk electrostatic field cause the enhancement of entropy in the near-earth region and the earthward moving of plasma sheet inner edge. Finally a discussion and summary are given in section 3.3.

3.1 Simulation Model

In this chapter, I study the magnetotail dynamics based on the two-dimensional magnetohydrodynamic equations with a dawn-to-dusk electrostatic field $E_s(t)$. The simulation space is in the noon-midnight meridian plane (x-z plane in the GSM coordinates). The MHD equations are described by

$$\frac{\partial \rho}{\partial t} + \nabla \cdot (\rho \mathbf{v}) = 0, \tag{3.1}$$

$$\rho \left(\frac{\partial \mathbf{v}}{\partial t} + \mathbf{v} \cdot \nabla \mathbf{v} \right) = \mathbf{J} \times \mathbf{B} - \nabla p, \tag{3.2}$$

$$\frac{\partial A}{\partial t} + \mathbf{v} \cdot \nabla A = E_s(t), \tag{3.3a}$$

$$B_x = -\frac{\partial A}{\partial z}, \quad B_z = \frac{\partial A}{\partial x}, \tag{3.3b}$$

$$\frac{\partial h}{\partial t} + \nabla \cdot (h\mathbf{v}) = 0, \tag{3.4a}$$

$$h = p^{1/\gamma}. \tag{3.4b}$$

where $E_s(t)$ is dawn-to-dusk electrostatic field. $E_s(t)$ should be constant in a pure two-dimension plane. In the chapter, dawn-to-dusk electrostatic field is constant and $\sim 0.33mV/m$ (80kV over $40R_e$). To compare my results with observations, I normalize the length by the Earth's radius (R_e), the magnetic field by $B_0 = 30\,\mathrm{nT}$, which would be the Earth's dipole field strength at $r = 10\,R_e$ in the equatorial plane, and the pressure by $p_0 = B_0^2/\mu_0 = 0.71\,\mathrm{nPa}$ and average plasma density $n \simeq 0.5cm^{-3}$. Thus I have $V_A \simeq 1100km/s$, $t_A \simeq 5.7s$ and electric field unit $E_o = V_A B_0 \simeq 33mV/m$.

My computational domain is surrounded by a circle of radius of $3\,R_e$ concentric with the Earth ($\partial\Omega_1$), a mimicked magnetopause ($\partial\Omega_2$) composed of a parabola extending from the subsolar point $(10, 0)$ to $(-5, \pm 15)$ and abutting straight lines extending to $(-70, \pm 28)$, and a straight tailside boundary at $x = -70$ ($\partial\Omega_3$). The initial equilibrium is given by previous results in Chapter 2 [*Zhang et al.*, 1997], in which a magnetofrictional method is used to construct two-dimensional MHD equilibria of the Earth's magnetosphere for a given distribution of entropy function ($S(A) = pV(A)^\gamma$) and distribution of flux A in the boundaries, where p is the plasma pressure and V is the tube volume per unit magnetic flux and equal to $\int ds/B$. In the initial equilibrium, the flux distribution in the boundaries are explained as follows. At $\partial\Omega_1$, the magnetic flux is matched to a 2-D dipole field described by $A_D = -100x/(x^2 + z^2)$. Since the open flux along the dayside

magnetopause ($x > 0$) affects mainly the dayside field configuration, I simply set the open flux to zero along the dayside magnetopause. Therefore, A is set to a constant value A_1 along the dayside magnetopause ($x \geq 0$) and the open flux ($A_2 - A_1$) is uniformly distributed along the nightside magnetopause ($x < 0$). Along the tailside boundary $\partial\Omega_3$, I simply choose $B_x(z) \propto z/(z^2 + a^2)^{1/2}$, which leads to $A(x = -70, z) = A_3 - (A_3 - A_2)[(a^2 + z^2)^{\frac{1}{2}} - a]/[(a^2 + 28^2)^{\frac{1}{2}} - a]$. Here A_2 is the value of A at the corner of the two boundaries $\partial\Omega_2$ and $\partial\Omega_3$, and A_3 at the intersection of the x-axis and $\partial\Omega_3$. In the presented cases, a is simply set to 200, since the final equilibrium configuration is not sensitive to the choice of a [*Zhang et al.*, 1997]. The simulation domain is shown in Fig.2.1.

The entropy profile in each initial equilibrium configuration is given by

$$S(A) = \frac{1}{2}S_m\Big[1 + \tanh(\frac{A_c - A}{\Delta A})\Big]. \tag{3.5}$$

The pressure in the dayside magnetosphere and lobe is set to small constant p_L.The initial density ρ is loaded by

$$\rho = C_\rho h, \tag{3.6}$$

where C_ρ is a constant. An initial global configuration of the magnetotail is shown in Figure 3.1a.

I point out that (i) plasma always moves in real space with $\mathbf{v} = \mathbf{E} \times \mathbf{B}/B^2$, where $\mathbf{E}$ is the total electric field and includes both electrostatic and inductive electric field, and (ii) the motion of magnetic field lines is only associated with the inductive electric field. Since the decomposition of electric field depends on the choice of "gauge", field line motion also depends on the "gauge". In this chapter, I choose a gauge in which a field line is identified by its ionospheric footprint and

assume that the field line labeled A does not move at the ionosphere. Note, that this is different from the identification of field lines using the frozen-in concept if here is ionospheric convection (as is implied the presence of an electrostatic field). The boundary condition is specified as follows. Along the Earth and magnetopause boundaries ($\partial\Omega_1$ and $\partial\Omega_2$), the magnetic flux is maintained at the initial value. the velocities are set to be $v_z = E_s B_x/B^2$, $v_x = -E_s B_z/B^2$. The boundary conditions imposed at the tailside boundary ($\partial\Omega_3$) are $\frac{\partial \mathbf{v}}{\partial x} = 0$ and $\frac{\partial A}{\partial t} + \mathbf{v}\cdot\nabla A = E_s$. However, in the region with an inward plasma flow ($v_x > 0$), I set $v_x = 0$ to reduce the wave reflection at the boundary. At $z = 0$ a symmetric boundary condition is imposed. For the density ρ and h, continuous condition is imposed in all boundaries.

The governing equations are finite differenced in space-centered form and integrated in time using semi-implicit scheme[*Harned and Schnack*, 1986; *Choe and Lee*, 1991]. My algorithm is free from the Courant-Friedrichs-Lewy (CFL) condition. Due to the symmetry property of each variable across the x-axis, I carry out the numerical simulation in half of the physical domain in the x-z plane, with $x \in (10, -70)R_e$ and $z \in (-30, 0)R_e$. With a 251 $\times$ 111 array and a nonuniform mesh, I are able to resolve $0.08R_e$ in x and $0.06R_e$ in z.

3.2 Simulation Results

The dynamical evolution of magnetotail in response to a dawn-to-dusk electrostatic field E_s is presented. I simulate many cases for different initial equilibria and present two case in detail. Figure 1 shows Case A, in which the initial equilibrium configuration is obtained in Chapter 2 with $A_1 = -14.$, $A_2 = 1.5$, $A_3 = 8.55$,

$A_c = 17.5$, $\Delta A = 0.1$, $p_L = 0.127$ and $S_m = 500$ in units of $S_o = B_o^{1/3} R_e^{5/3}/\mu_o$. The dawn-to-dusk electrostatic field is set to $E_s = 0.01$

The initial equilibrium of magnetic field is shown in Figure 3.1a. The field configuration at $t = 300t_0$ is shown in Figure 3.1b. It can be seen that due to the dawn-to-dusk electrostatic field E_s the dipolar magnetic field lines in the near-earth region ($-5R_e \geq x \geq -8R_e$) are stretched tailward and the lobe flux A_{lobe} increases from $6.36A_0$ to $8.28A_0$, where $A_{lobe} = A(z = 0, x = -70) - A(z = 28, x = -70)$. The increase is about 30% of total lobe magnetic flux. The tailward movement of geomagnetic field lines can also be seen in Figure 3.2c, which shows the location $X_e(A, t)$ of the flux function A in the equatorial plane ($z = 0$) as a function of A. For example, the magnetic field line with $A = 20.07$ is initially ($t = 0$) located at $x \simeq -5.3R_e$ and moves to $x \simeq -14.6R_e$ at $t = 300t_o$. Figure 3.2c shows the location $X_e(A, t)$ of $A(z = 0, x)$ at different simulation times $t = 0$, 165 and $300t_0$.

Figure 3.2a shows the entropy function, as a function of A at different simulation times $t = 0$, 165 and $300t_0$. As time increase, the entropy function $S(A, t)$ shifts $3A_0$ units earthward during $\Delta t = 300t_0 \sim 0.5$ hour. The transition point A_c of the entropy function $S(A, t)$ shifts from $17.50A_0$ to $20.50A_0$. It is consistent with $E_s \Delta t = 3A_0$. In the presence of the driving electrostatic field E_s, the plasma drifts earthward. It can be seen that the inner edge move to the earth about $\sim 1R_e$ in Figure 3.2b and 3.2d. It is also found that, only driven by the electrostatic field E_s, the current thickness is almost constant and only total current sheet $\int J_y dz$ increases slightly. It is consistent with our previous equilibrium results and observations[*Zhang et al.*, 1997]. I have calculated the modified entropy function along the x-axis based on Tsyganenko empirical field models[1989]. It is found

that the modified entropy function $S(A,t)$ shifts about $3A_0$ during the substorm growth phase in Fig.2.2.

Figure 3.3 shows the magnetic field lines and flow patterns at different simulation times, $t = 75$, 165, 235 and $300t_0$ for case A. Only the region with $-5R_e \geq x \geq -45R_e$ and $5R_e \geq z \geq -5R_e$ is shown. The plasma flows earthward driven by the driving electrostatic field $\mathbf{E}_s$. As time increases, earthward flows in the center part of plasma sheet decreases. Because the plasma can not cross dipolar field lines and piles up just behind the inner edge. It causes the enhance of the pressure in the region and stops plasma convection. At same time, the flux convects as the velocity $\mathbf{v} + \mathbf{v}'$, where $\mathbf{v}'$ is related to the dawn-to-dusk electrostatic E_s and is given by $v'_z = -E_s B_x/B^2$, $v'_x = E_s B_z/B^2$. So the field lines are stretched tailward as the plasma flows earthward.

The tailward stretching of geomagnetic field lines and the earthward moving of the plasma sheet due to the driving electrostatic field E_s can be understood as follows. If $E_s = 0$ and hence $dA/dt = 0$, magnetic field lines move with plasma. In other words, the plasma, which stays on the field line labeled A, will stay on the field line with the same label A. If $E_s \neq 0$, a plasma element located in the flux tube labeled A at time t will move to the flux tube labeled $A = A + E_s\delta t$. Therefore, the plasma drift velocity in A-space is

$$u_s(t) = \frac{A' - A}{\delta t} = E_s. \tag{3.7}$$

For $E_s \neq 0$, the plasma stays the flux tube while the flux tube labeled A at time t move to the flux tube labeled $A = A + E_s\delta t$. Here I supposed that the magnetotail is balanced at time t. Relabeling field lines is equal to moving footprints of field

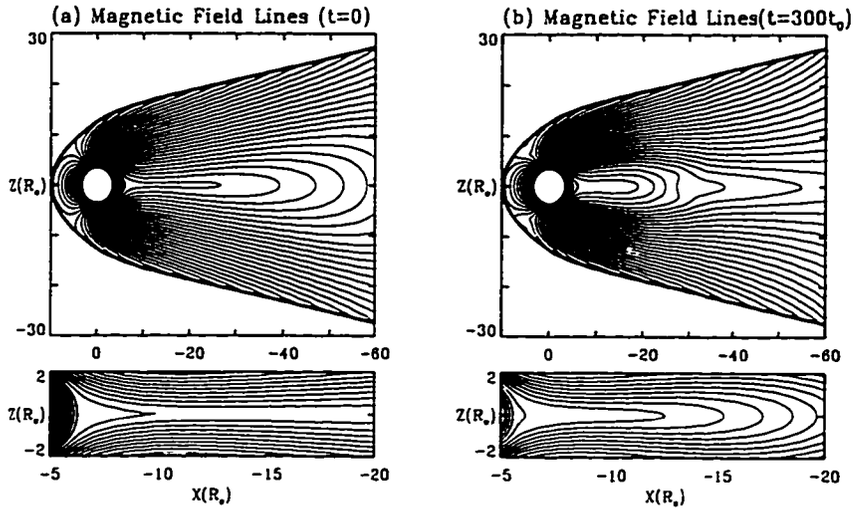

Figure 3.1 (a) The initial field configuration (t=0) and (b) the final configuration (t=300) for Case A.

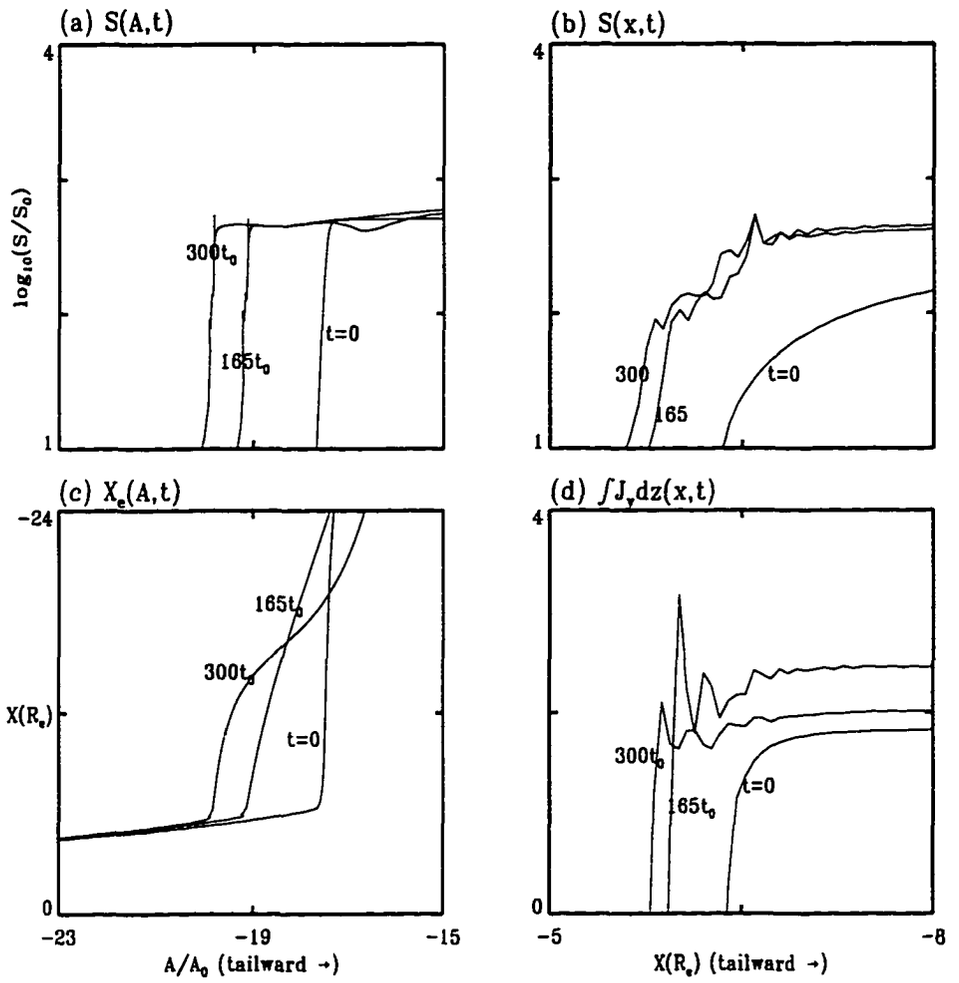

Figure 3.2 (a) The evolution of $S = pV^{\gamma}$ in A-space from $t = 0$ to $t = 300$. (b) The evolution of S in real-space. (c) The change of the field line position in the equatorial plane, $\Delta x_e = x_e(A, t_1) - x_e(A, 0)$, shows the tailward stretching of a field line labeled A. (d) The evolution of $\int j_y dz$ along x axis for Case A.

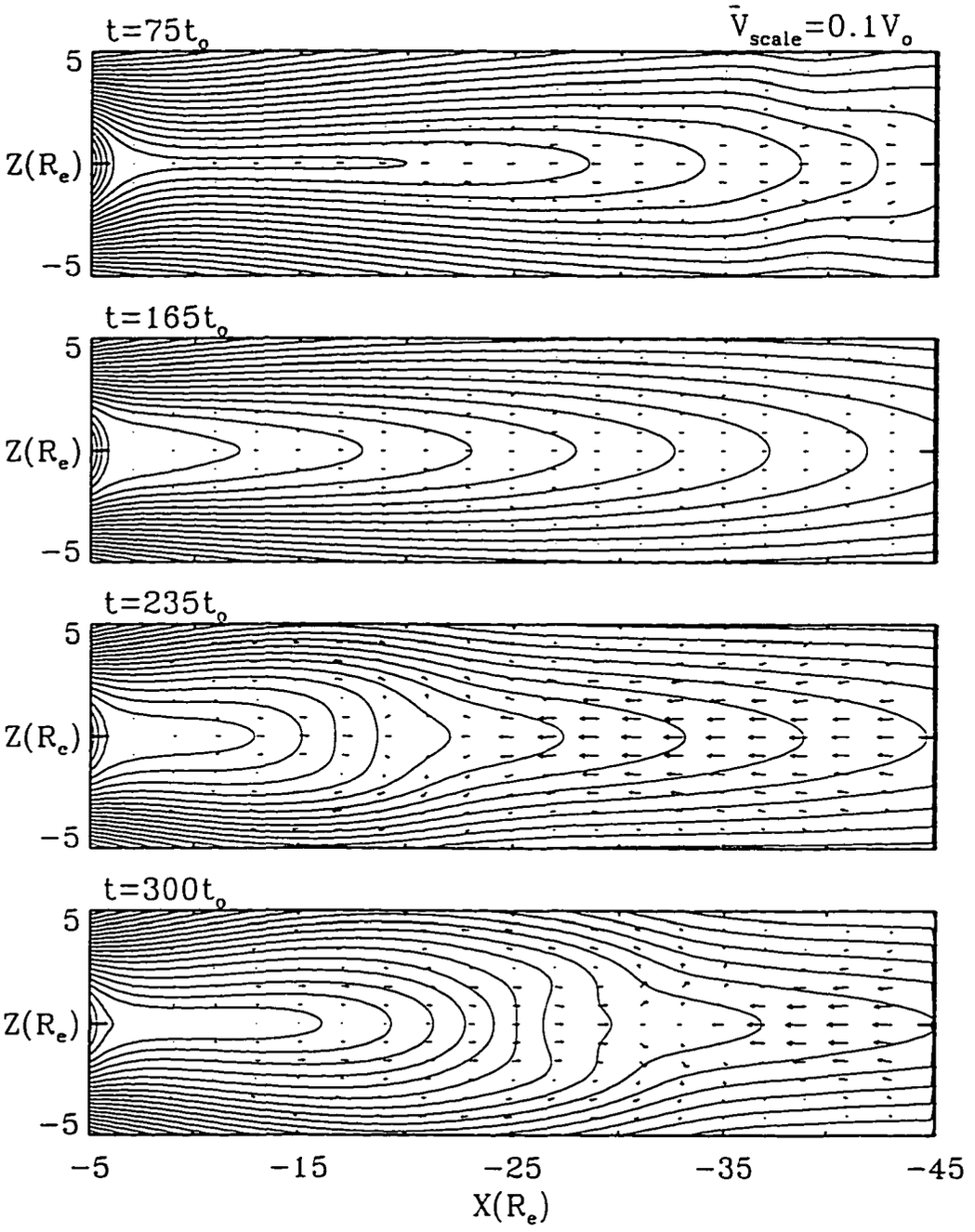

Figure 3.3 Plasma flow patterns at t=75, 165, 235, and 300t_o for Case A. Earthward flows are present in the central part of plasma sheet.

lines in ionosphere equatorward and turning dayside magnetic field lines to nightside. The force balance of the magnetotail is destroyed by both the equatorward movement of the footprints of magnetic field lines in the ionosphere and the increase of the lobe flux. The unbalanced force causes that the plasma and the flux A convect earthward. But from the "gauge" that field lines are identified by the value A in the ionosphere, total convection of the flux must include the convection velocity v' relative to the driving electrostatic field E_s. The location $X_e(A,t)$ of the flux at equatorial plane ($z=0$) is [*Cai et al.*, 1995]

$$X_e(A,t) \simeq \int_0^t v(A'(t'), z=0, t')dt' + X_e(A'(t), t=0), \tag{3.8}$$

where $A'(t) = A - \int_0^t E_s(t")dt"$. So under the chosen "gauge", the magnetic field lines in the near-earth region are stretched tailward during the driving process.

Figure 3.4a and 4b show the field configurations at t=0 and $t = 340t_0$ for Case B. The parameters used in Case B are the same as in Case A, except that $\triangle A = 1.$ in Case B. The entropy profile $S(A,t)$,S(x,t), the location $X_e(A,t)$ of $A(z=0,x)$ and the total current sheet $\int J_y dz$ at $t = 0$, 155 and $340t_0$ are shown in Figure 3.5. The entropy profile $S(A,t)$ shifts $3.4A_0$ units in A-space and the inner edge moves earthward $\sim 1R_e$ during $\triangle t = 340t_0$. The magnetic field lines and flow patterns at different simulation times, $t = 80$, 155, 250 and $340t_0$ for case B are shown in Figure 3.6. The dynamic evolution of the magnetotail is qualitative similar to Case A. The driving electrostatic field E_s causes that the current sheet moves earthward and the field lines in the near-earth region are stretched tailward. But the current sheet thickness remains almost constant during the dynamic evolution.

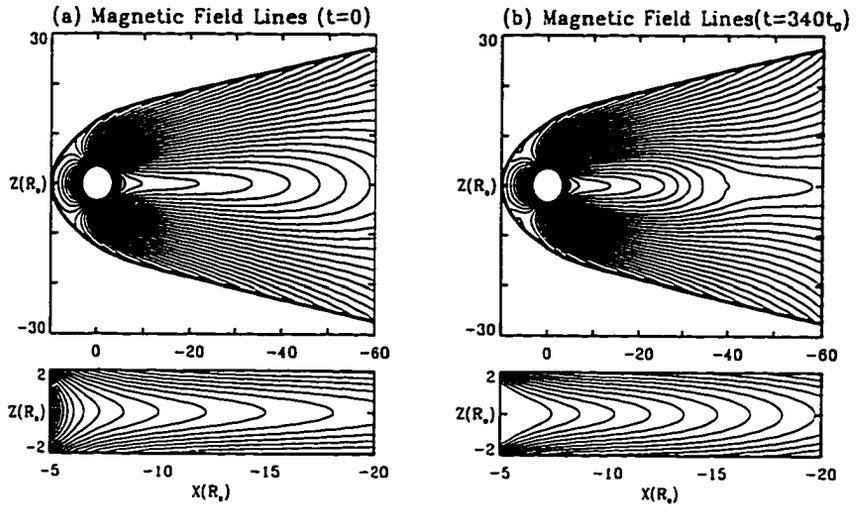

Figure 3.4 (a) The initial field configuration (t=0) and (b) the final configuration (t=340) for Case B.

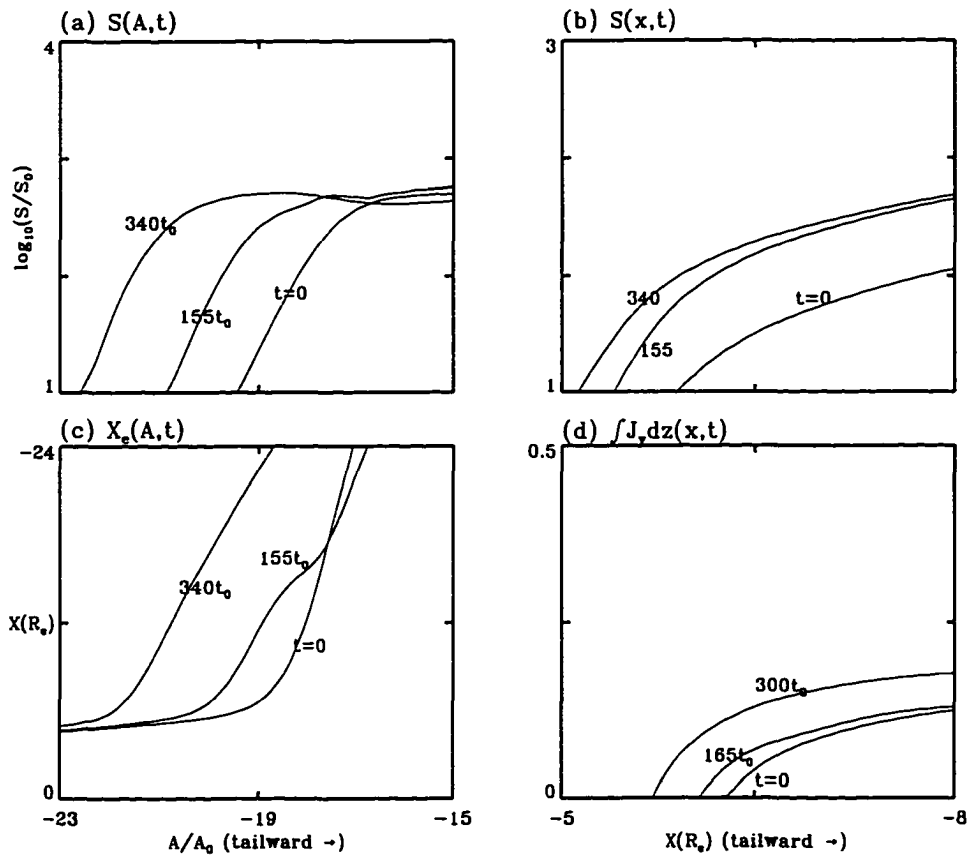

Figure 3.5 (a) The evolution of $S = pV^{\gamma}$ in A-space from $t = 0$ to $t = 300$. (b) The evolution of S in real-space. (c) The change of the field line position in the equatorial plane, $\Delta x_e = x_e(A, t_1) - x_e(A, 0)$, shows the tailward stretching of a field line labeled A. (d) The evolution of $\int j_y dz$ along x axis for Case B.

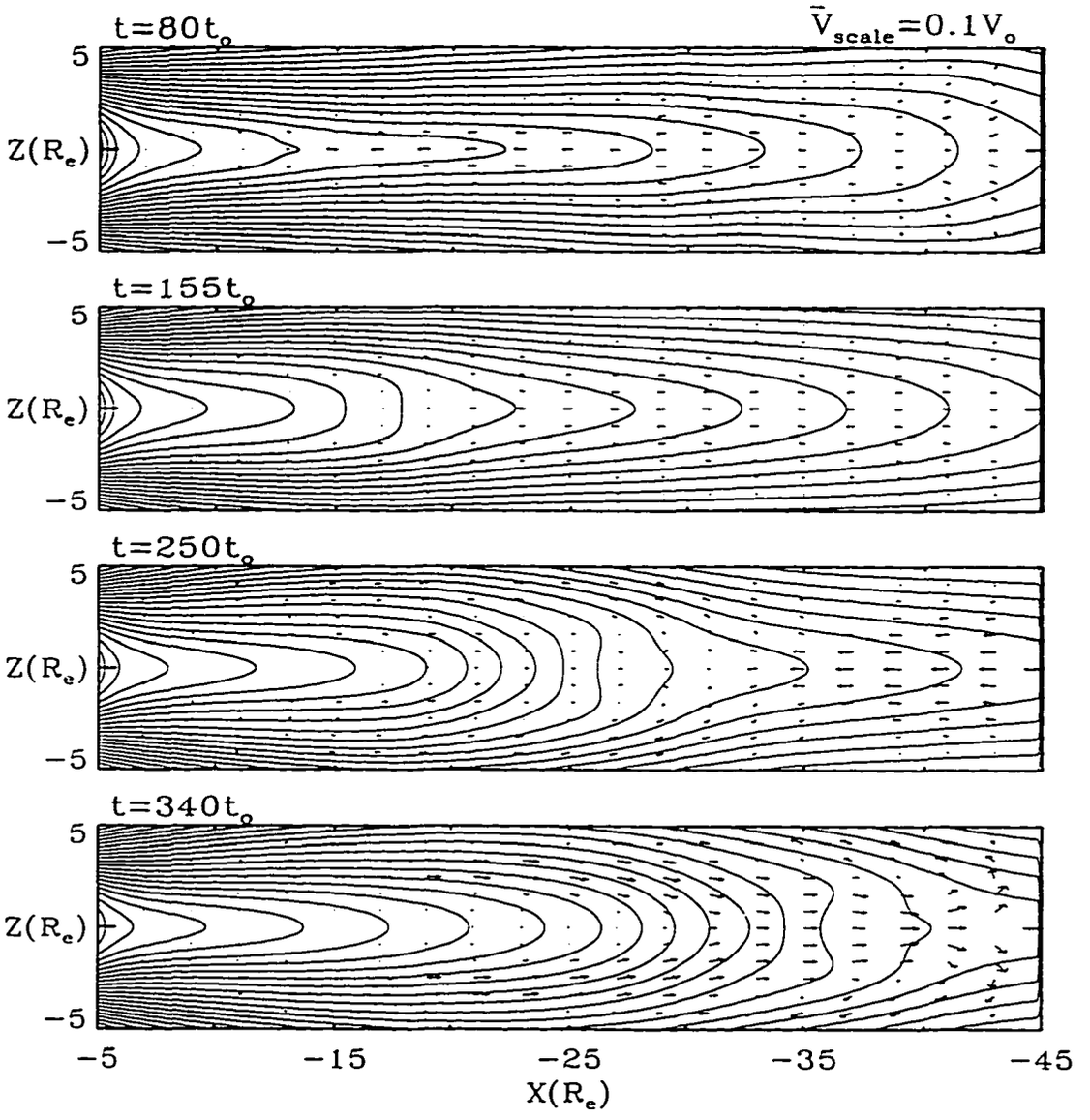

Figure 3.6 Plasma flow patterns at t=80, 155, 250, and 340t_o for Case B. Earthward flows are present in the central part of plasma sheet.

3.3 Discussion and Summary

The simulation results indicate that in the "gauge" in which a field line is identified by its ionospheric footprint and assume that the field line labeled A does not move at the ionosphere, a dawn-to-dusk electrostatic field can drive a current sheet to move earthward and simultaneously stretch the dipolar magnetic field lines tailward. During the driving process, it is also found that the thickness of the current sheet is almost constant. It is consistent with equilibrium results in Chapter 2 [*Zhang et al.*, 1997]. It also is confirmed that in the presence of a dawn-to-dusk electrostatic field E_s, under the adiabatic evolution, the entropy function $S(A,t)$ satisfies the following conservation equation in A-space,

$$\frac{\partial S(A,t)}{\partial t} + E_s(t)\frac{\partial S(A,t)}{\partial A} = 0. \tag{3.9}$$

As the interplanetary magnetic field (IMF) turns southward, dayside magnetic reconnection leads to an increase of open magnetic flux in the polar cap. This in turn leads to an increase of electric potential drop across the polar cap, and hence an increase of dawn-to-dusk electrostatic electric field [e.g., *Reiff et al.*, 1981]. Through the penetration of electric field in the conducting ionosphere, the electric field in the auroral oval region is also enhanced [*Swift*, 1967; *Vasyliunas*, 1970; *Wolf*, 1970]. This enhanced electric field can be transmitted by Alfven waves from the ionosphere to the closed field region of magnetotail along magnetic field lines. This would contribute to a dawn-to-dusk electrostatic component E_s of electric field in the plasma sheet. My simulation results show that the enhanced convection electric field E_s in the growth phase enhances the entropy in the near-earth region. Simultaneously, the entropy transition region shifts toward the earth. It is implied

that the enhanced ionospheric convection electric field is the main driving force of enhancing the entropy and highly stretching magnetic field lines in the near-earth magnetotail during the substorm growth phase.

It is found that only from a constant driving electrostatic field E_s, a thin current sheet can not formed in the near-earth region, which is shown by Wiegelmann and Schindler[1995]. But I can obtain some physical insights from my simulation results. If there is a driving electrostatic field E_s, the evolution of the entropy function $S(A,t)$ satisfies eq.(3.9). My equilibrium results [*Lee et al.*, 1995; *Zhang et al.*, 1997] show that the high entropy gradient in A-space results in forming of a very thin current in the near-earth region. One mechanics to form and thin a current sheet may be provided by the nonuniform of electrostatic field E_s, especially y-component. In two dimension, the electrostatic field E_y is strictly a constant. But in three dimensions, the electrostatic y-component E_y could be nonuniform. Jaggi and Wolf [1973, 1975] suggested that there is 'the Alfven layer' at $\sim -7R_e$ region. The electric field becomes much weaker in the near-earth region $x > -7R_e$ and Eq(3.9) becomes a nonlinear convection equation. The plasma sheet convects with different convection velocities at different location. The plasma further from the earth, convects faster toward the Earth. In the 'Alfven layer', the convection velocity is almost zero. The entropy function steepens during the current sheet convection, and finally, a very thin current sheet is formed in the near-earth region $x \simeq -7R_e$.

In summary, I have examined the dynamic evolution of the magnetotail in the presence of a dawn-to-dusk electrostatic field E_s. It is implied that the enhanced ionospheric convection electric field may be the main driving force of the near-earth

magnetotail evolution during the substorm growth phase. I demonstrate that the formation of highly stretched field line configuration, the enhancement of entropy function in the near-earth region and the earthward movement of the plasma sheet inner edge are consequences of the enhanced ionospheric convection. In my 2-D model, the earthward moving of plasma sheet inner edge, the enhancement of cross-tail current, the increase of tail lobe magnetic fields, and the plasma convection in the equatorial plane during substorm growth phase are found to be consistent with observations. It is also shown that it is impossible to form a very thin current sheet whose thickness is about $0.1R_e$. I still need some theory to explain how to form a very thin current sheet in the last stage of a substorm growth phase.

In the next chapter, I report a new instability, called as "entropy anti-diffusion instability", produced by a pressure diffusion in the current sheet region, which can leads a very thin current sheet with about $0.1R_e$ thickness during a substorm growth phase.

Chapter 4

Entropy Anti-Diffusion Instability and Formation of a Thin Current Sheet During Magnetospheric Substorms

During the substorm growth phase, an increase of the lobe field strength, highly stretched geomagnetic field lines and formation of a thin current sheet are observed at a radial distance $\sim 7-15R_e$ from the Earth[e.g., *Kokubun and McPherron*, 1981; *Kaufmann* 1987; *Lui et al.*, 1992]. After the onset of substorms, the stretched field lines are suddenly dipolarized and earthward plasma flows are observed. Ohtani et al.(1992) reported that an explosive growth phase, which is characterized by the presence of a thinner current sheet with a large current density, proceeds the full onset of substorm. Satellite observations [e.g., *Lui et al.*, 1992] indicated that the

substorm onset and dipolarization of geomagnetic field lines may not be initiated by magnetic reconnection.

Two approaches have been used to understand the formation of a thin current sheet in the magnetotail. In the first approach, a driving or perturbed electric field is applied at the boundary of simulation domain to obtain the formation of a thin current sheet inside the plasma sheet of a magnetotail-like configuration. In both MHD simulations [*Lee et al.*, 1985; *Wiegelmann and Schindler*, 1995; *Ma et al.*, 1995] and particle simulations[*Prictchett and Coroniti*, 1995; *Hesse et al.*, 1996], it was found that the presence of driving electric field can lead to formation of a thin current sheet.

In the second approach, the global MHD equilibrium configuration of the Earth's magnetosphere is constructed and conditions for the formation of a thin current sheet are obtained [*Hau et al.*, 1989; *Erickson* 1992; *Lee et al.*, 1995; *Cai et al.*, 1995]. In addition, Birn et al. (1994) found that a thin current sheet can be formed under isobaric dynamic conditions, i.e., the plasma pressure in each flux tube is held constant in time during the dynamic evolution.

In my study presented in Chapter 2, it was found that as the profile of entropy function S becomes steeper, the current sheet in the near- earth magnetotail becomes thinner. Here the entropy function $S = pV^{\gamma}$, p is the plasma pressure and V is the volume of a unit magnetic flux tube and $\gamma = 5/3$. It was also found that in the equilibrium configuration the entropy function increases tailward , while the plasma pressure decreases tailward. Since S is proportional to p, the presence of particle transport or pressure diffusion across magnetic field lines leads to an effective anti-diffusion of the entropy function. This, in turn, leads to a sharper

gradient in the entropy profile and hence a thinner current sheet, which favors the pressure diffusion. Thus I have a positive feedback process, which accelerates the formation of a very thin current sheet. This process is called the "entropy anti-diffusion instability". In this chapter, I use MHD simulation to demonstrate that this instability can indeed occur and lead to the dipolarization of geomagnetic field lines and formation of a very thin current sheet. For this purpose, I will first use model equations to study the effect of only the pressure diffusion term. To complete the study, I test the influence of a resistive term which is a more realistic case of diffusion due to momentum exchange by electrons and ions. The growth rate and plasma flow pattern resulted from this instability are also obtained.

4.1 Formulation

In order to examine the plasma sheet dynamics in the presence of pressure diffusion, I start with a 2-D global equilibrium configuration in the x-z plane, which is obtained from the magnetofrictional method developed in Chapter 2 [*Lee et al.*, 1995]. The following 2-D MHD equations are then applied to study the dynamic evolution:

$$\frac{\partial \rho}{\partial t} + \nabla \cdot (\rho \mathbf{v}) = 0, \tag{4.1}$$

$$\frac{\partial \rho \mathbf{v}}{\partial t} = \nabla \left(\rho \mathbf{v}\mathbf{v} + (p + \frac{1}{2}B^2)\mathbf{I} - \mathbf{B}\mathbf{B} \right) + D\nabla^2 \rho \mathbf{v}, \tag{4.2}$$

$$\frac{\partial A}{\partial t} + \mathbf{v} \cdot \nabla A = \eta \nabla^2 A, \tag{4.3}$$

$$\frac{\partial p}{\partial t} = -\gamma p \nabla \cdot \mathbf{v} - \mathbf{v} \cdot \nabla p + \nabla \cdot (D \nabla p) + (\gamma - 1)\eta J^2 + (\gamma - 1)H, \tag{4.4}$$

$$H = \nabla \cdot (D\mathbf{v}) \nabla \cdot (\rho \mathbf{v}) + \nabla \times (D\mathbf{v}) \cdot \nabla \times (\rho \mathbf{v}), \tag{4.5}$$

Here ρ is the plasma density, $\mathbf{v}$ is the plasma velocity, D is the diffusion coefficient, η is the resistivity, $\mathbf{J}$ is the current density, A is the vector potential in the y direction and magnetic field $\mathbf{B} = \nabla \times (A\hat{y})$. I write (4.4) in the conservative form using the time-step splitting method[*Choe and Lee*, 1992]. Equation (4.1) through (4.4) can be rewritten and yield total conversation of mass, momentum and energy.

In (4.1)-(4.5), I normalize the length by the Earth's radius (R_e), the magnetic field by $B_0 = 40\,\mathrm{nT}$, which would be the Earth's dipole field strength at $r = 10\,R_e$ in the equatorial plane, the density by $n_o = 0.5cm^{-3}$, $\rho_o = m_p n_o$, the velocity by $V_o = B_o/(4\pi\rho_o)^{1/2} = 1200km/s$, the time by $t_o = R_e/V_o = 5s$, and the pressure by $p_0 = B_0^2/8\pi = 1.27\,\mathrm{nPa}$. m_p is proton mass. The dimensionless resistivity η is given by $\eta = \frac{\eta_{ph} c^2}{4\pi R_e V_0}$, where η_{ph} is the resistivity in Gaussian units (sec) and c is the speed of light. The dimensionless diffusion coefficient is given by $D = \frac{D_{ph}}{D_0}$ with D_{ph} in physical units and $D_o = R_e V_o = 7.4 \times 10^{12} m^2/s$.

My computational domain is surrounded by a circle of radius of $3\,R_e$ concentric with the Earth ($\partial\Omega_1$), a mimicked magnetopause ($\partial\Omega_2$) composed of a parabola extending from the subsolar point $(10, 0)$ to $(-5, \pm 15)$ and abutting straight lines extending to $(-70, \pm 28)$, and a straight tailside boundary at $x = -70$ ($\partial\Omega_3$). In the initial equilibrium configuration, the flux A in the boundaries are described

below. At $\partial\Omega_1$, the magnetic flux is matched to a 2-D dipole field described by $A_D = -100x/(x^2+z^2)$. Since the open flux along the dayside magnetopause ($x > 0$) effects mainly the dayside field configuration, I simply set the open flux to zero along the dayside magnetopause. Therefore, A is set to a constant value A_1 along the dayside magnetopause ($x \geq 0$) and the open flux ($A_2 - A_1$) is uniformly distributed along the nightside magnetopause ($x < 0$). Along the tailside boundary $\partial\Omega_3$, I simply choose $B_x(z) \propto z/(z^2+a^2)^{1/2}$, which leads to $A(x=-70,z) = A_3 - (A_3 - A_2)[(a^2+z^2)^{\frac{1}{2}} - a]/[(a^2+28^2)^{\frac{1}{2}} - a]$. Here A_2 is the value of A at the corner of the two boundaries $\partial\Omega_2$ and $\partial\Omega_3$, and A_3 at the intersection of the x-axis and $\partial\Omega_3$. In the presented cases, a is simply set to 200, since the final equilibrium configuration is not sensitive to the choice of a. The computation domain is shown in Fig.2.1.

The entropy profile in each initial equilibrium configuration is given by

$$S(A) = \frac{1}{2}S_m\left[1 + \tanh(\frac{A_c - A}{\Delta A})\right]. \tag{4.6}$$

The pressure in the dayside magnetosphere and lobe is set to p_L. An initial global configuration of the magnetotail is shown in Figure 4.1a. Detailed properties of equilibria for a given distribution of entropy function are discussed [*zhang et al.*, 1997; *Lee et al.*, 1995] in Chapter 2.

In the presence of a finite diffusion coefficient D in (4.2) and (4.5), the pressure profile will be re-distributed and the initial configuration will be no longer in equilibrium and will evolve with time. During the evolution, the following boundary conditions in the simulation domain are applied. In my computation, I employ a staggered mesh and need not specify pressure at the boundary points. At all

boundaries, I set $\mathbf{v} = 0$, and A remains constant with time.

Although the classical diffusion is expected to be very low in the collisionless space plasma, a sufficiently large anomalous diffusion may be provided by particles being scattered by plasma waves, probably lower hybrid waves [*Huba et al.*, 1977; *Gary et al.*, 1990; *Lee*, 1991]. The diffusion coefficient from the development of lower-hybrid drift (LHD) instability associated with pressure gradient can be estimated as

$$D_{LHD} \sim 0.085\rho_i^2\Omega_i = 0.17\frac{T_i c}{eB} = 0.02D_0, \tag{4.7}$$

where ρ_i, Ω_i, and T_i are respectively the ion gyroradius, gyrofreqrency and thermal energy. In (4.7), I set $T_i = 10keV$ and $B = 10nT$ in the central plasma sheet. For comparison, the Bohm diffusion coefficient can be estimated as

$$D_B = \frac{T_i c}{eB} = 8.63 \times 10^{11} m^2/s = 0.12D_0 \tag{4.8}$$

The Bohm diffusion coefficient D_B can be considered as the upper bound of D. Simultaneously, a anomalous resistivity is expected from the anomalous collisional frequency caused by lower-hybrid drift instability [*Gary et al.*, 1990; *Lee*, 1991]. The anomalous collisional frequency ν can be written as

$$\nu = \frac{D_{LHD}}{\rho_e^2(1 + T_i/T_e)}. \tag{4.9}$$

The corresponding anomalous resistivity η is

$$\eta_{ph} = \frac{D_{LHD} m_e}{\rho_e^2 e^2 n(1 + T_i/T_e)}. \tag{4.10}$$

The ratio of the dimensionless anomalous resistivity η to the diffusion coefficient D_{LHD} is given by

$$\frac{\eta}{D} = \frac{\eta}{D_{LHD}} = \frac{m_e c^2}{4\pi\rho_e^2 e^2 n(1 + T_i/T_e)} = 0.04, \tag{4.11}$$

where ρ_e is the electron gyroradius, T_e is the electron thermal energy, m_e is the electron mass, and n is the number density. In (4.9), (4.10) and (4.11), I set $T_e = 2keV$ and $n = 0.5cm^{-3}$

Note that the diffusion coefficient in (4.7) is obtained for a current sheet with a thickness of several ion gyroradii. For a thicker current sheet, the diffusion coefficient will be smaller. The MHD approximation is not valid for scales of the order of the ion gyroradius or smaller such that transport caused by very sharp gradients such as diffusion or resistivity with an influence on the large scale dynamics has to be incorporated into the MHD fluid model. MHD is limited to predict the "final" thickness and the structure of a current sheet to scale larger than the ion gyro-scale. However, MHD can demonstrate large scale mechanism which lead to the thining of an initially thick current layer.

4.2 Simulation Results

The pressure diffusion term is a crucial term in the entropy anti-diffusion instability. In the most basic models to study the entropy anti-diffusion instability, I only have a constant pressure diffusion term and ignore the anomalous resistivity ($\eta = 0$). In this chapter, I present case A, B, C only with a constant pressure diffusion. In addition, I discuss the effect of anomalous resistivity η on the formation of a thin current sheet resulted by the entropy anti-diffusion instability. Anomalous diffusion D_{LHD} and resistivity η caused by the lower-hybrid-drift instability is proportional to β^{-1}, where $\beta = 8\pi n_i kT_i/B^2$ [*Brackbill et al.*, 1984; *Birk and Otto*, 1991]. In the central plasma sheet region, the magnetic field is very weak and β

is very large, such that the anomalous diffusion coefficient D_{LHD} and resistivity η is very small in the central plasma sheet region ($|z| \sim 0$). I run more realistic cases in which D_{LHD} and η are proportional to the function of $g = 1 - exp(-2z^2)$ such that the corresponding transport is zero in the center of the current sheet in agreement with the high β stabilization of the lower hybird drift instability. This functional dependency is considered in the case D and E. To compare the effects of resistive or pressure diffusion I consider the case F with $\eta = 0$ and $D = D_{LHD}$ and the case G with $D = 0$ and η proportional to the function g.

I simulate many cases, which only have a constant pressure diffusion term, and present two cases in detail. Figure 4.1 shows Case A, in which the initial equilibrium configuration is obtained with $A_1 = -12.75$, $A_2 = 2.75$, $A_3 = 11.05$, $A_c = 20.0$, $\triangle A = 1.0$, $p_L = 0.127$ and $S_m = 500$ in units of $S_o = B_o^{1/3} R_e^{5/3}/\mu_o$. The diffusion coefficient is set to $D = 0.05 D_o$. The initial equilibrium configuration of the magnetic field is shown in Figure 4.1a. The field configuration at $t = 80$ is shown in Figure 4.1b. It can be seen that the magnetic field lines in the lobes collapse toward the center of plasma sheet and form a thin current sheet. As shown in the magnified figures of the field lines in the region $-6R_e \geq x \geq -17R_e$, magnetic field lines move earthward and become more dipolar in the region $x > -7R_e$. Field lines at $t = 80t_o$ are cusp-shaped. Figure 4.1c shows the entropy function $log_{10}(S/S_o)$, as a function of the flux function A at different simulation times, $t = 0$, 20, 50, and $80t_o$. In the evolution, the profile becomes steeper and the transition region moves toward the region with a large A due to the pressure diffusion across field lines. The entropy profile $S(A)$ indeed shows an effective anti-diffusion in A space.

The earthward motion or dipolarization of geomagnetic field lines can also be seen in Figure 4.1d, which shows the flux function A in the equatorial plane (z=0) as a function of x. For example, the magnetic field line with $A = 21.38$ is initially ($t = 0$) located at $x \simeq -12.5R_e$ and moves to $x \simeq -5.6R_e$ at $t = 50t_o$. The current sheet thickness d at the position with the maximum current density is plotted as a function of time in Figure 4.2. The thickness d decreases from $\sim 1.4R_e$ at $t = 0$ to $\sim 0.1R_e$ at $t = 10$.

Figure 4.3 shows the magnetic field lines and flow patterns at different simulation times, $t = 20$, 50 and $80t_o$, for Case A. Only the region with $-5R_e \geq x \geq -45R_e$ and $-5R_e \geq z \geq 5R_e$ is shown. The plasma flows earthward in the central part of plasma sheet, while plasma flows tailward on the outer parts. Notice that the initial pressure is high in the earthward region. The diffusion of pressure leads to a decrease of pressure in the inner flux tube. This results in a force imbalance and earthward flows. The pressure diffusion also leads to a pressure increase in the earthward part of outer flux tubes, which results in a tailward flow on the outer part of plasma sheet. The maximum flow velocity is $\sim 0.30V_o \simeq 350km/s$.

Figures 4.4a and 4.4b show the field configurations at $t = 0$ and $t = 80t_o$ for Case B. The parameters used in Case B are the same as in Case A, except that $\triangle A \simeq 0.5$ in Case B. Due to the smaller value of the transition width of the initial entropy profile, the initial current sheet in Case B is thinner with a thickness $\sim 0.3R_e$. At $t = 80t_o$, the current sheet becomes very thin with a thickness $\sim 0.06R_e$ as shown in Figure 4.2. The entropy profile $S(A)$ and the flux function $A(x)$ at $t = 0$, 20, 50, and $80t_o$ are shown in Figures 4.4c and 4.4d, respectively. The entropy profile becomes steeper at $t = 50$ and $80t_o$. The maximum value of

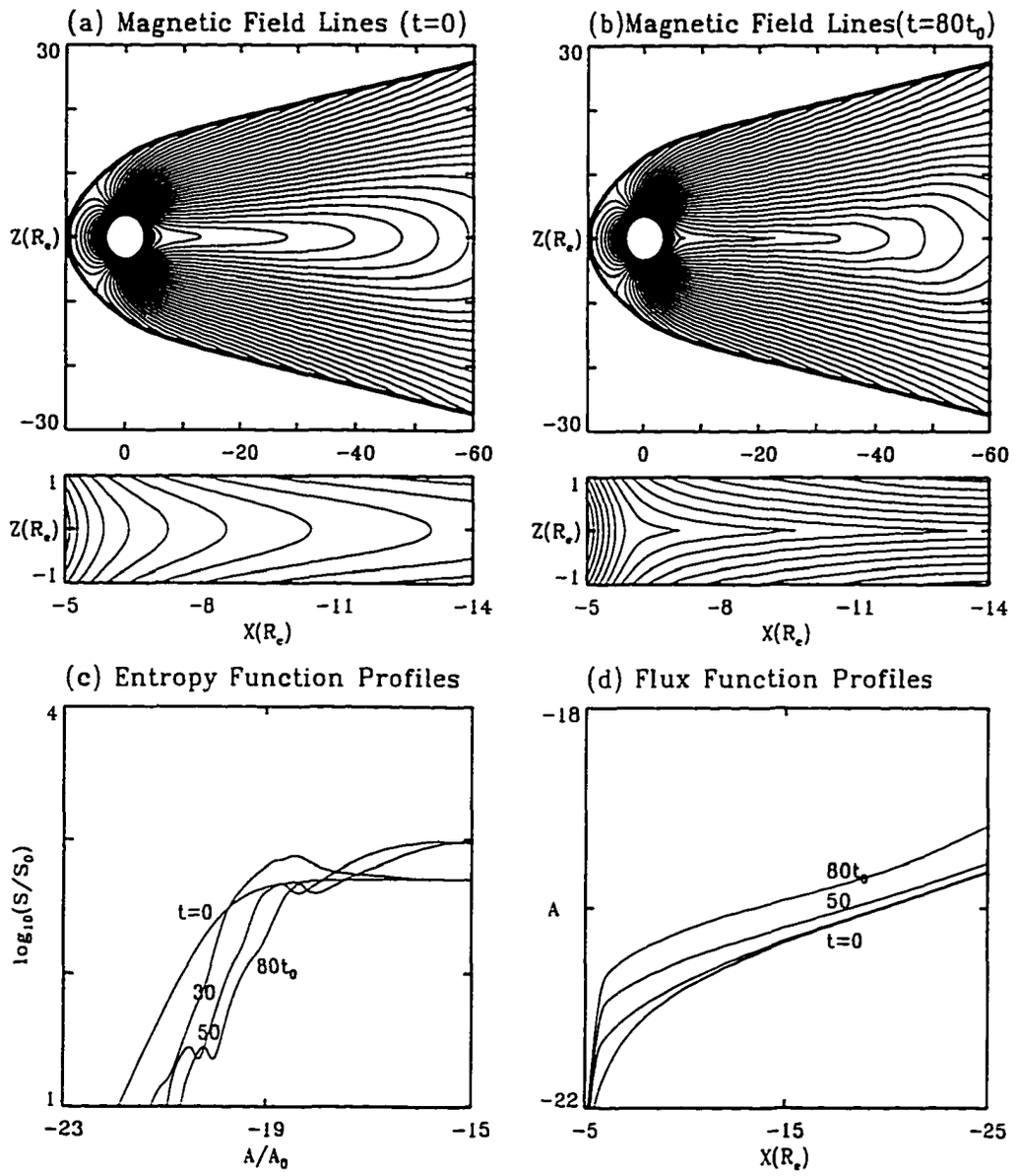

Figure 4.1 (a) The initial field configuration (t=0) and (b) the final configuration (t=80) for Case A ($\Delta A = 1.$). (c) The entropy function S as a function of A, and (d) the flux function A as a function of x at different simulation times.

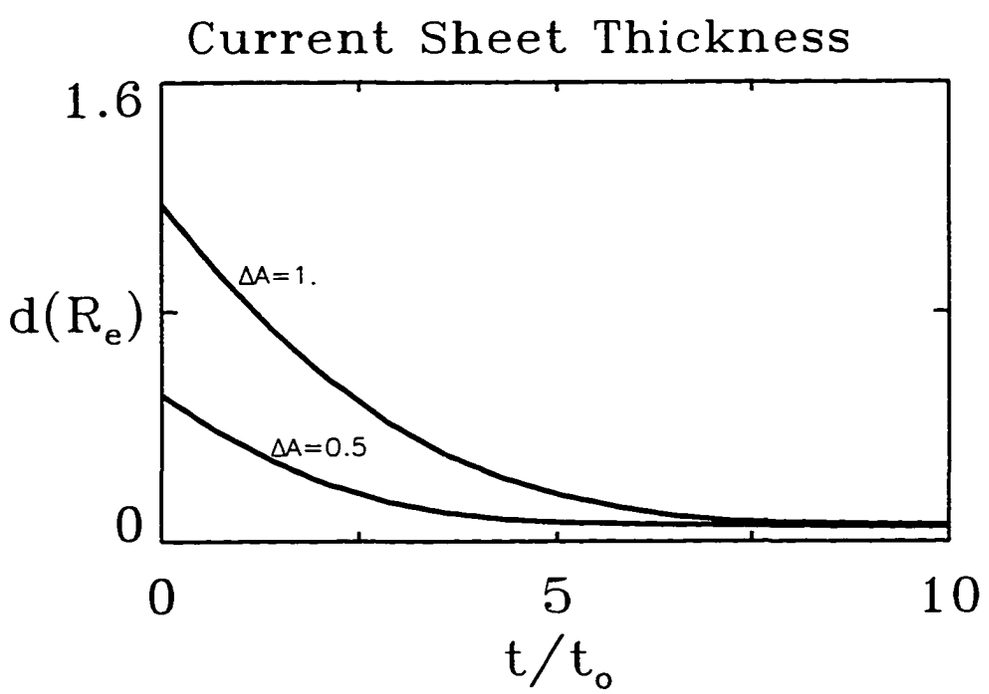

Figure 4.2 The current sheet thickness d at the position of maximum current density as a function of time for Case A and Case B.

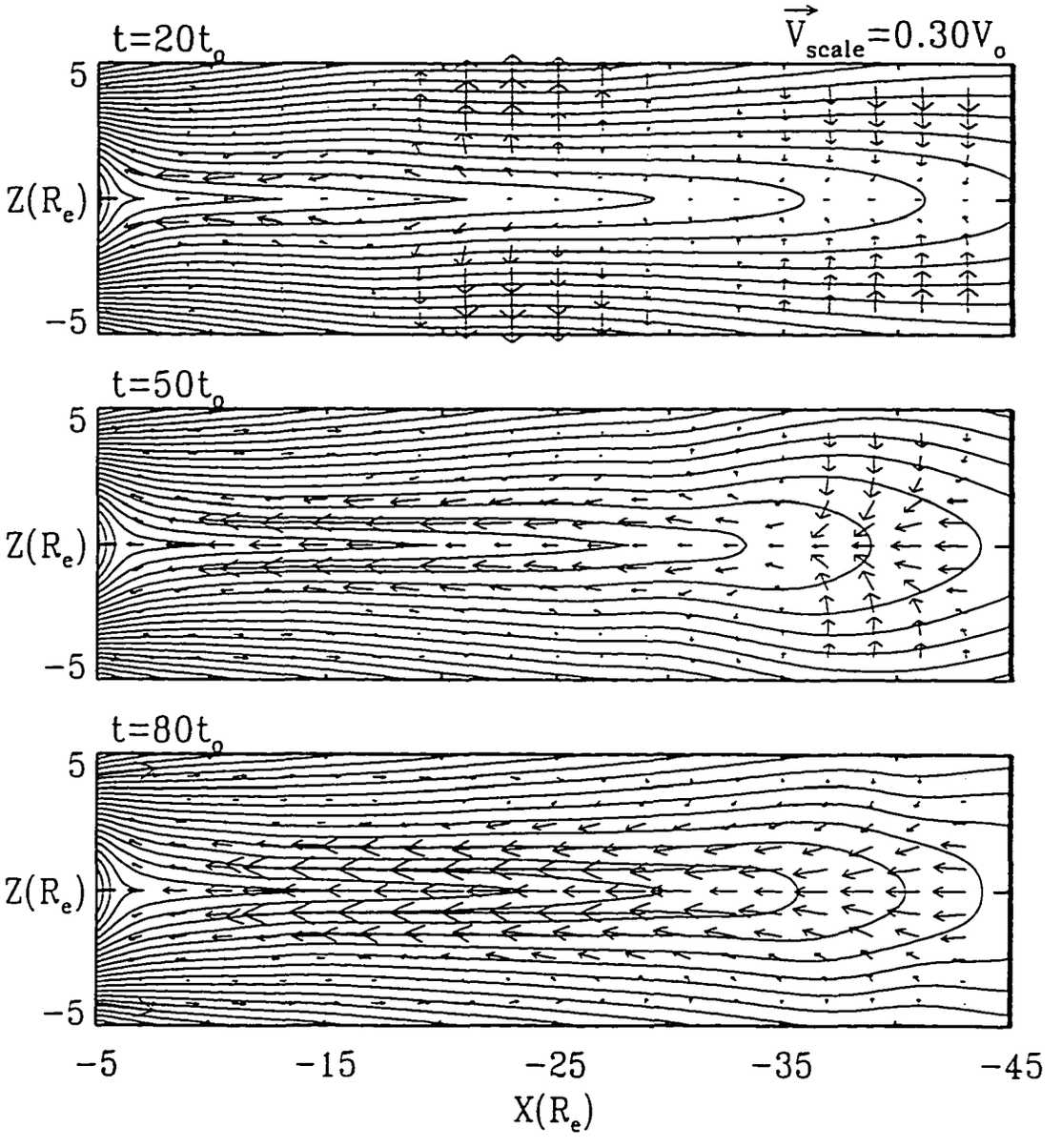

Figure 4.3 Plasma flow patterns at t=20, 50, and 80t_o for Case A. Earthward flows are present in the central part of plasma sheet.

current density, J_{max}, as a function of time is plotted in Figure 4.5a for Case A, B and C. In Case C, $\Delta A = 0.3$ and all other parameters are the same as those in Case A and Case B. In Case A, J_{max} reaches its saturation value at $t \simeq 20t_o$; in Case B, J_{max} reaches the saturation value at $t \simeq 10t_o$. The slopes (dashed lines) in Figure 4.5a can be used to calculate the growth rates. The growth rate in Case A is $\Upsilon = 0.351t_o^{-1}$; $\Upsilon = 0.415t_o^{-1}$ in Case B; $\Upsilon = 0.458t_o^{-1}$ in Case C.

The normalized growth rates for different values of ΔA and different values of diffusion coefficient D are plotted in Figure 4.5b. In all cases, the parameters used,except ΔA and D, are the same as those in Case A. For the same initial configuration (same ΔA), the growth rate increases linearly with diffusion coefficient D. The growth rate is higher for a thinner current sheet initially with a smaller value of ΔA.

If the diffusion coefficient is set to the value in (4.7), $D = 0.02$, which is associated with the lower hybrid drift instability, I would have the growth rate $\Upsilon = 0.407t_o^{-1}$, 0.340 and 0.293 for $\Delta A = 0.3$, 0.5 and 1.0 respectively. The e-folding time $\Upsilon^{-1} \simeq 2.3$, 2.8 and $3.5t_o$, corresponding to 13.6s, 16.2s and 18.8s.

I add the anomalous resistivity η to eq.(4.3) to study the effect of the anomalous resistivity η to the entropy anti-diffusion instability. First, based on the diffusion D and anomalous resistivity η produced by lower-hybird-drift instability being proportional to β^{-1}, D and η are expressed as

$$D = D_{LHD}(1 - exp(-2z^2)). \tag{4.12a}$$

$$\eta = \alpha D_{LHD}(1 - exp(-2z^2)), \tag{4.12b}$$

where α is a constant. The function form (4.12) is a simple representation of the

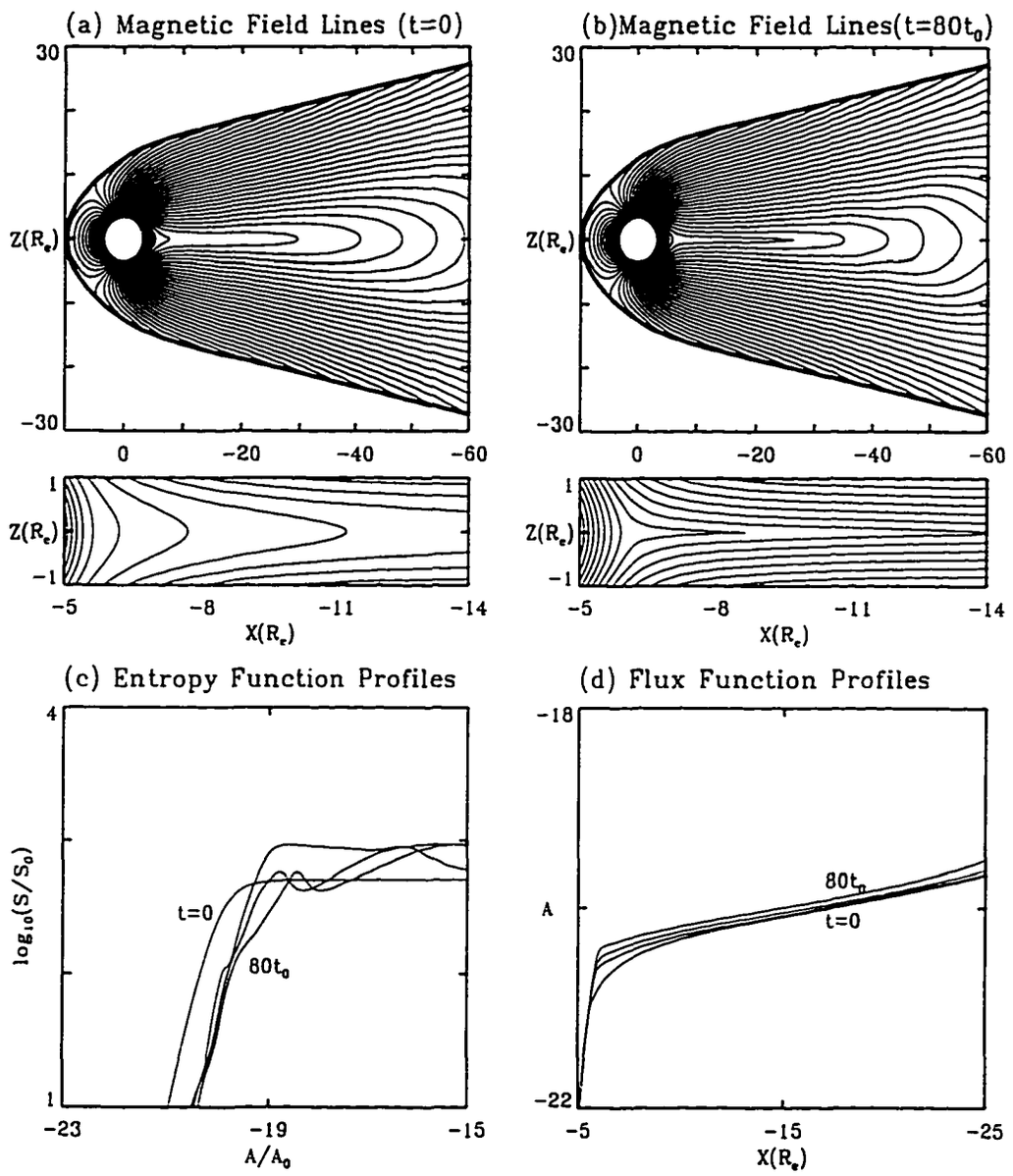

Figure 4.4 (a) The initial field configuration (t=0) and (b) the final configuration (t=80) for Case B ($\Delta A = 0.5$). (c) The entropy function S as a function of A, and (d) the flux function A as a function of x at different simulation times.

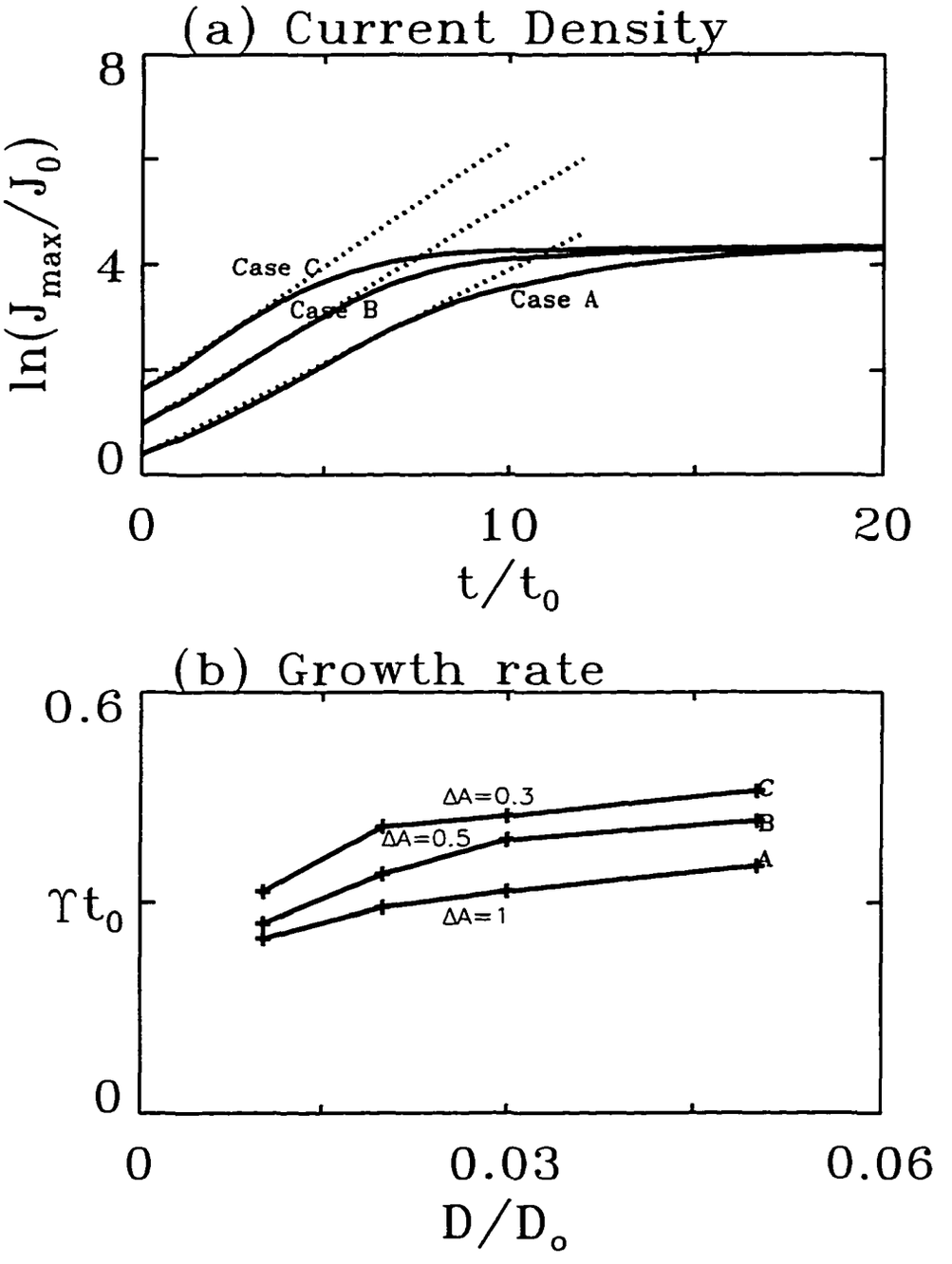

Figure 4.5 (a) The maximum current density J_{max} in plasma sheet as a function of simulation time for Case A ($\Delta A = 1.0$), Case B ($\Delta A = 0.5$) and Case C ($\Delta A = 0.3$); (b) The normalized growth rate Υt_o as a function of diffusion coefficient D for three different values of ΔA ($\Delta A = 0.3$, 0.5 and 1.0).

diffusion and resistivity that are zero at central line ($z = 0$), increases monotonically with increasing $|z|$ and has the maximum value D_{LHD}.

Two cases address the current sheet evolution if the resistivity is given by eq.(4.12b). The two cases have the same parameters and initial configuration as in case B except D and η. For case D, $\alpha = 1.$ and for case E, $\alpha = 0.04$. Figure 4.6 and 4.7 show the configurations at $t = 0$ and $t = 65t_0$ for case D and E respectively. The magnetic field lines and plasma flow at different simulation times are shown in Figure 4.8 (case D) and Figure 4.9 (case E). (case D). To show the influence of a resistivity η, I run case F, in which the parameters and initial configuration are same as in case D, except the resistivity η is zero. The corresponding configurations is shown in Figure 4.10. It is shown when the anomalous resistivity η is very small in the current sheet region ($|z| < 0.5R_e$) it accelerates the formation of a thin current sheet. The evolution of magnetosphere is qualitatively similar to case B. To compare with case F, the growth rate increases from $0.0838t_0^{-1}$ to $0.2855t_0^{-1}$(case D, $\alpha = 1.$) and $0.0888t_0^{-1}$(case E, $\alpha = 0.04$) respectively. The relative evolution of the maximum current density J_{ymax} for case D and E are plotted in Figure 4.12. This including a resistive diffusion which is zero in the center of the current sheet appears to accelerate the instability. Note that $\eta = 0$ at $z = 0$ (motivated by the stabilized LHD instability in high β plasma) excludes magnetic reconnection. I suspect that this acceleration of the instability is caused by the additional pressure diffusion from the resistive term. From Figure 4.12, when resistivity η is small (α is small), the linear stage of the growth phase is very longer than in the large resistivity cases. Final value of the maximum current density J_{ymax} is determined by the resistivity η.

This is indeed confirmed by the results shown in Fig.4.11 and 4.12 for case G which uses only a resistive term eq.(4.12) and no explicit pressure diffusion($D = 0$). Figure 4.12 demonstrates that resistive diffusion is in fact sufficient to lead to a significant growth of the maximum current density and a strong current sheet thinning. Fig.4.11a and 4.11b demonstrate the existence of a very thin current sheet and the evolution is very similar to the case B with zero resistivity and $D = 0.05$.

The final two cases address the current sheet evolution if the resistivity is non-zero at $z = 0$ and thus allow magnetic reconnection. The two cases have the same parameters and initial configuration as in case B except η is

$$\eta = \alpha D_{LHD}. \tag{4.13}$$

For case H, $\alpha = 0.04$ and for another run, $\alpha = 0.1$. Because of the present of the resistivity in the center region ($|z| \simeq 0$), the magnetic reconnection occurs in near-earth region ($x \sim 10R_e$) very soon after the current sheet begin to thin, as shown in Figure 4.12. After the magnetic reconnection, previous similar results [*Lee et al.*, 1985] can been seen in my simulations.

4.3 Discussion and Summary

The simulation results in the last section indicate that the growth rate is linearly proportional to the diffusion coefficient D and also decreases with increasing ΔA or initial current sheet thickness. Furthermore, the diffusion coefficient due to density/pressure gradient for a thick current sheet is expected to be much smaller

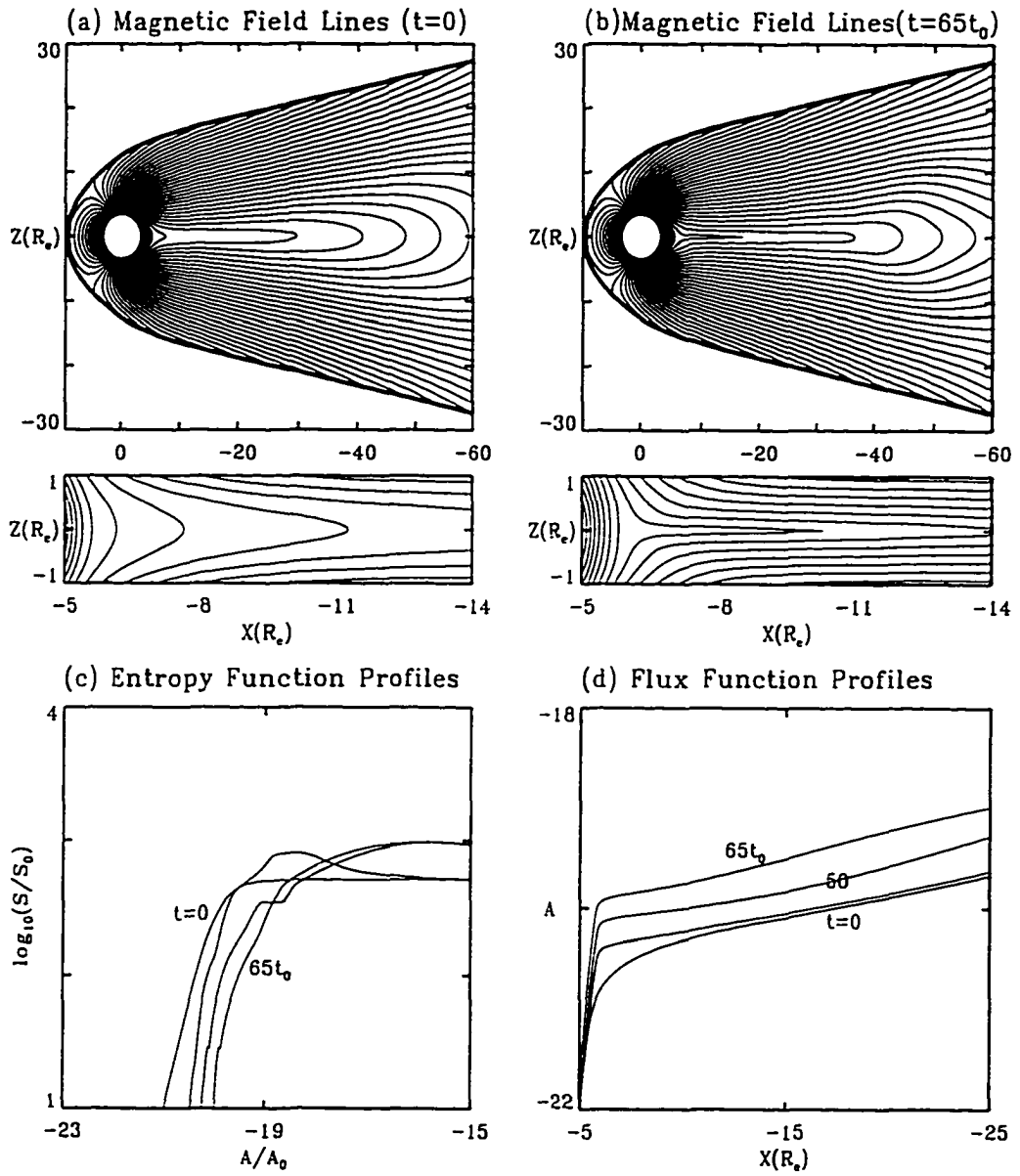

Figure 4.6 (a) The initial field configuration (t=0) and (b) the final configuration (t=65) for Case D ($\alpha = 1.$). (c) The entropy function S as a function of A, and (d) the flux function A as a function of x at different simulation times.

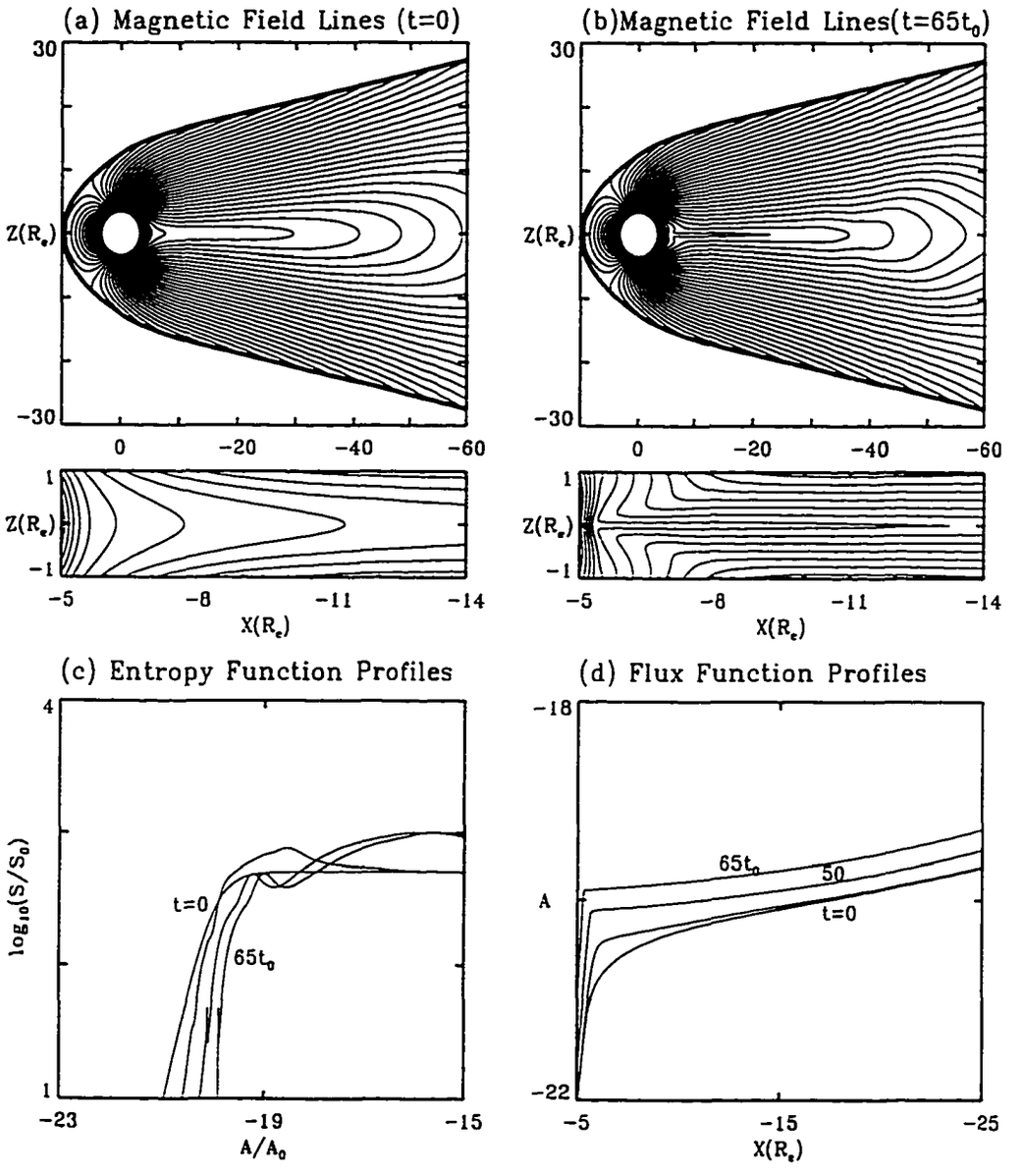

Figure 4.7 (a) The initial field configuration (t=0) and (b) the final configuration (t=65) for Case E ($\alpha = 0.04$). (c) The entropy function S as a function of A, and (d) the flux function A as a function of x at different simulation times.

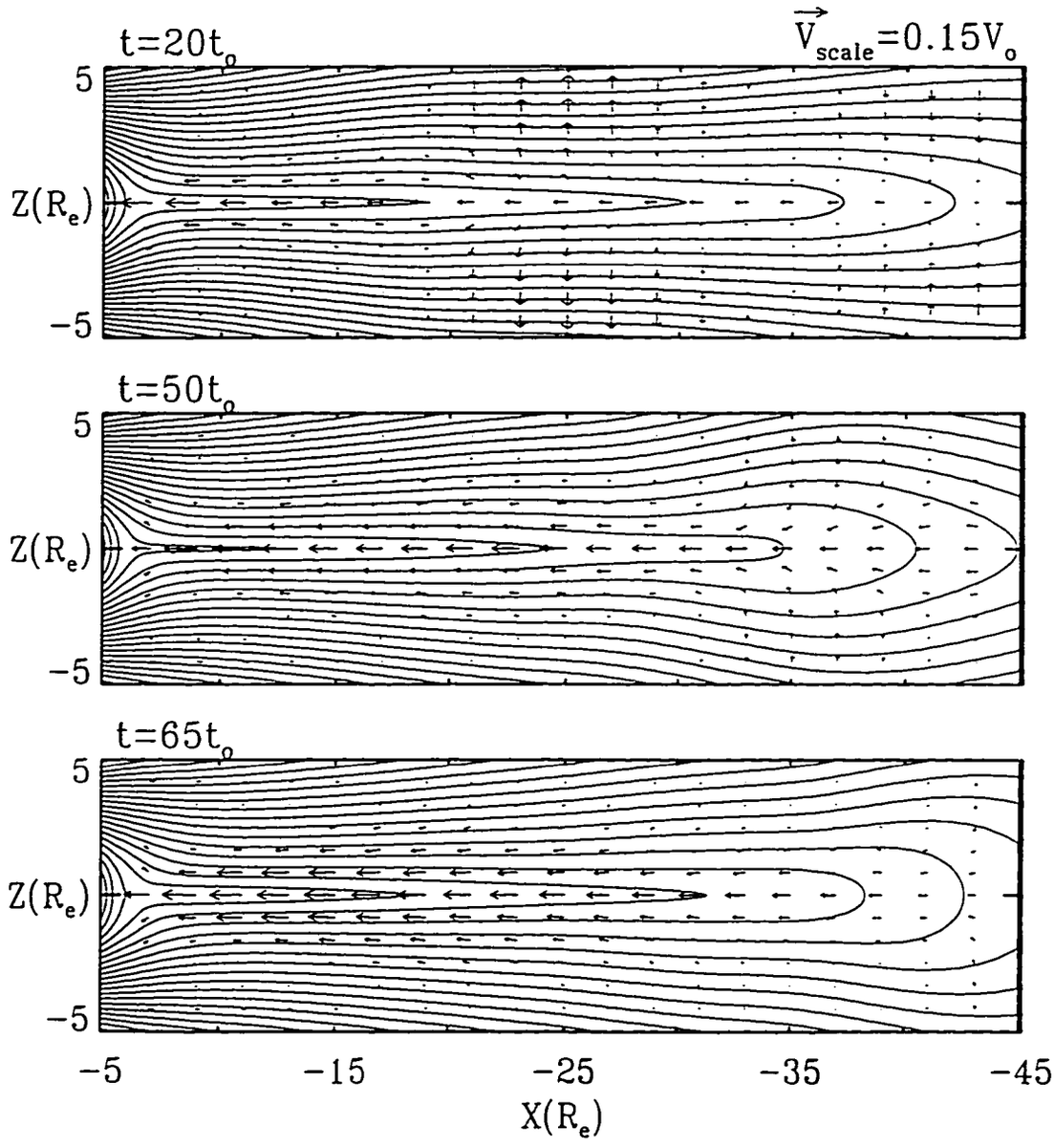

Figure 4.8 Plasma flow patterns at t=20, 50, and 65t_o for Case D. Earthward flows are present in the central part of plasma sheet.

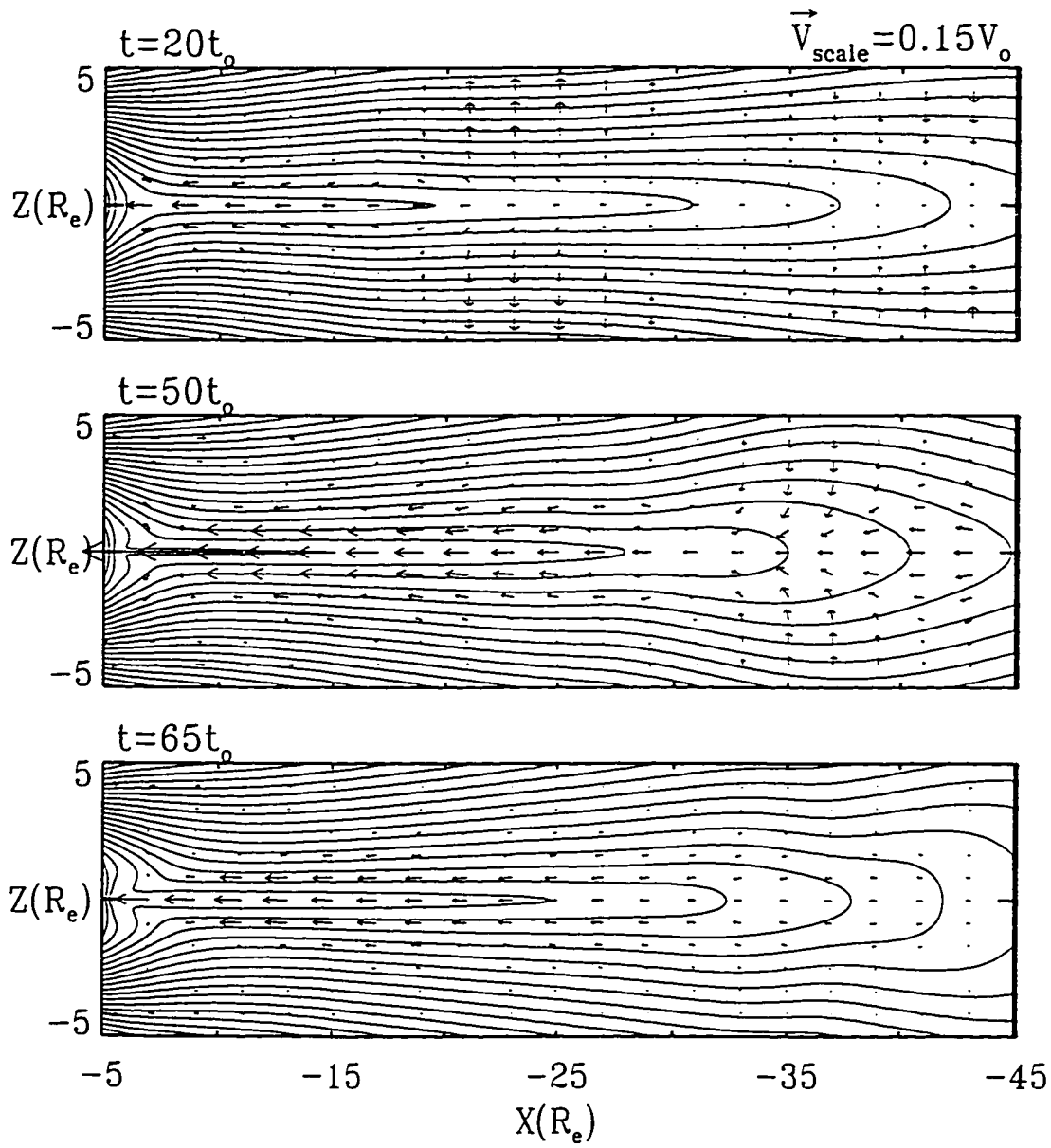

Figure 4.9 Plasma flow patterns at t=20, 50, and 65t_o for Case E. Earthward flows are present in the central part of plasma sheet.

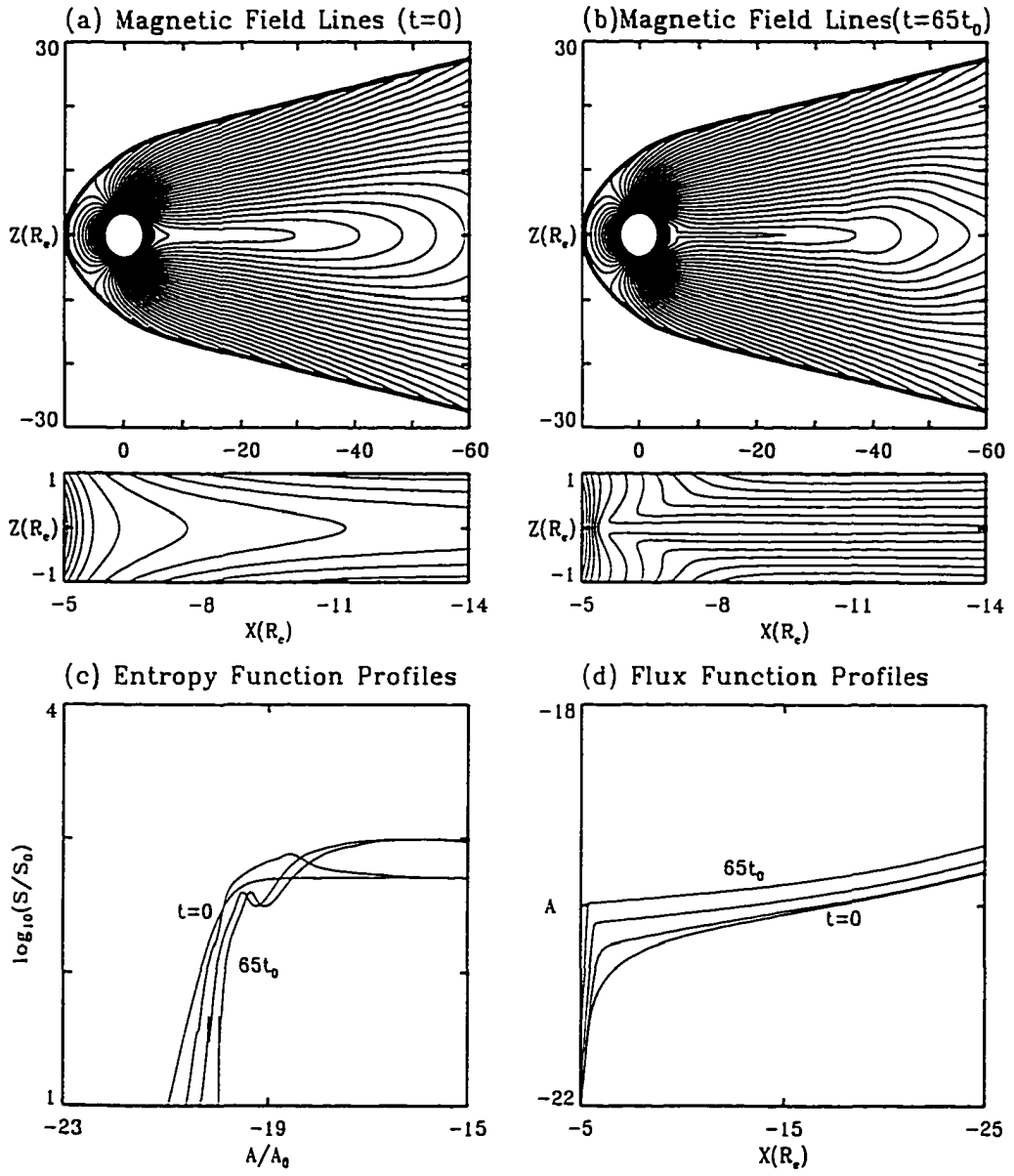

Figure 4.10 (a) The initial field configuration (t=0) and (b) the final configuration (t=65) for Case F ($\eta = 0$). (c) The entropy function S as a function of A, and (d) the flux function A as a function of x at different simulation times.

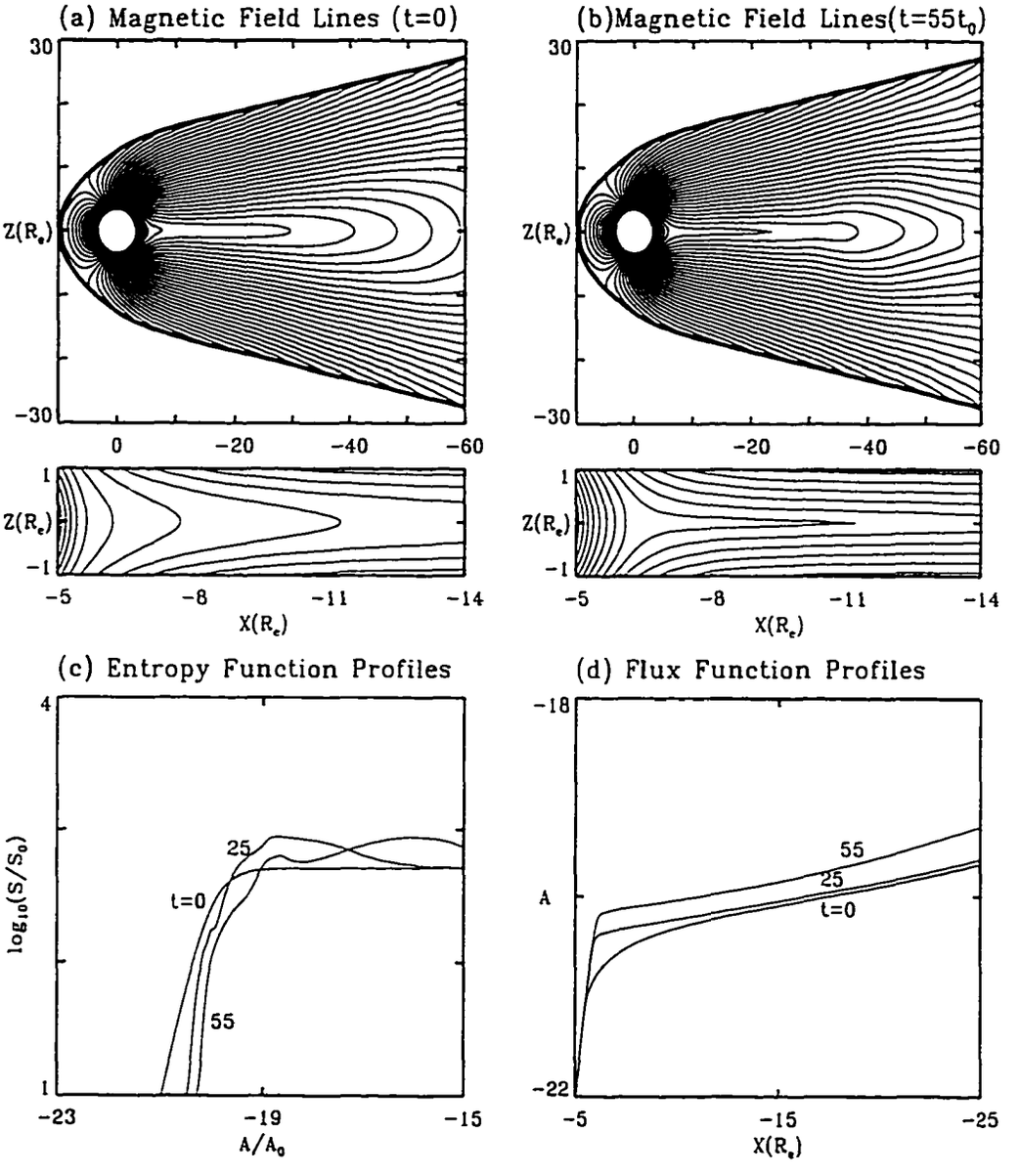

Figure 4.11 (a) The initial field configuration (t=0) and (b) the final configuration (t=55) for Case G ($D = 0$). (c) The entropy function S as a function of A, and (d) the flux function A as a function of x at different simulation times.

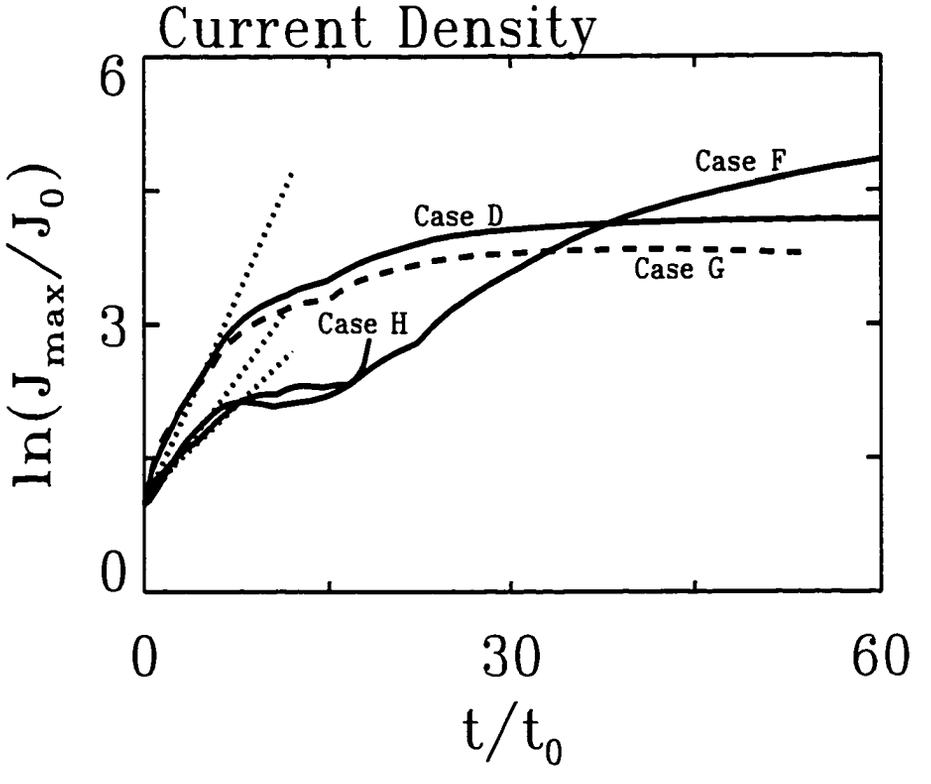

Figure 4.12 The maximum current density J_{max} in plasma sheet as a function of simulation time for Case D, case F ($\eta = 0$), case G ($D = 0$) and case H ($\alpha = 0.04$). In the case H, the magnetic reconnection occurs after $17t_0$.

than the value in (4.7). Therefore, the growth rate for an initially thick current sheet will be very small. The growth rate is larger for initially thinner current sheets. As shown in Figures 4.5a and 4.5b, the growth time for Case B is only $\sim 10t_o \sim 1$ minute. Ohtani et al. (1992) found an explosive growth phase of substorm before the full onset. In the explosive growth phase, the current sheet becomes thinner with a large current density for $\sim 1-2$ minutes. Therefore, the final stage of this entropy anti-diffusion instability may explain the occurrence of explosive phase.

As mentioned earlier, both MHD simulations [*Lee et al.*, 1995] and particle simulations [*Pritchett and Coroniti*, 1995; *Hesse et al.*, 1996] showed that a driving electric field imposed at simulation boundary leads to the thinning of plasma sheet. Global 3-D MHD simulations [e.g., *Usadi et al.*, 1993; *Ogino et al.*, 1994; *Fedder et al.*, 1995] also showed that the plasma sheet thinning and subsequent reconnection can occur in the near-earth magnetotail. On the other hand, my study of equilibrium configuration in Chapter 2 showed that the current sheet thickness depends mainly on the entropy content in flux tubes and entropy transition width. If the entropy content in flux tubes change and steepen the entropy gradient in the entropy profile, a thin current sheet can been formed from an initially thick current sheet. In order to change the entropy content in flux tubes, a plasma diffusion or some other non-adiabatic processes must occur. I suggest that the plasma sheet thinning observed in MHD or particle simulations is associated with the pressure/density diffusion and hence the entropy anti-diffusion instability. Note that the density/plasma diffusion is present in some MHD or particle simulations. In order to test this suggestion, we have studied the dynamic evolution of global 2-D

magnetotail with an imposed electric field at the boundary. It is found that the thinning of plasma sheet can occur in the presence of a finite diffusion coefficient. Without pressure diffusion, the current sheet thinning is relatively small with an imposed uniform E field [*Birn and Schindler*, 1985]. thick even with the imposed electric field. The result has been presented in Chapter 3. I have demonstrated that this pressure diffusion leads to an unstabile evolution (with decreasing current sheet width) independent of the precise diffusion mechanism. In case of resistive diffusion thinner current sheet develop if magnetic reconnection can not operate, i.e., if the resistivity is zero at the center of the current sheet.

In summary, I have examined the entropy anti-diffusion instability, which occurs in the near-earth plasma sheet with the presence of pressure diffusion. The instability leads to an earthward plasma flow and collapse of lobe fields to form a very thin current sheet. The growth time at the final stage of formation of a very thin current sheet is $\sim 1-2$ minutes, which may correspond to the explosive growth phase as reported by Ohtani et al. (1992).

Chapter 5

Summary and Discussion

Observations and modeling of the near tail region [e.g., *McPherron et al.*, 1987; *Mitchell et al.*, 1990; *Sergeev et al.*, 1993] have shown that a crucial feature of the substorm growth phase is the development of a thin current sheet in the tail region between geosynchronous distance and approximately $15 \sim 20R_e$. The thickness of such a current sheet is observed as small as $800km$. The increase in the local current density and the corresponding decrease of the current sheet thickness and of the magnetic field component B_z normal to the current sheet are presumably crucial to expansion phase onset [e.g., *McPherron et al.*, 1987; *Schindler and Birn*, 1993].

The evolution of these thin current sheets and their crucial role in the evolution of geomagnetic substorms gave motivated this thesis. Based upon my MHD simulations, the results of this theses are presented as follows.

5.1 Conditions For The Formation Of A Very Thin Current Sheet

A magnetofrictional method is used to construct two-dimensional MHD equilibria of the Earth's magnetosphere for a given distribution of entropy ($S = pV^{\gamma}$) on magnetic flux tubes, where p is the plasma pressure and V is the flux tube volume per unit magnetic flux. The purpose of this thesis is to determine typical properties of the earth's magnetospheric configurations during the growth phase and their dependence on the entropy function $S(A)$ and on the distribution of the lobe magnetic flux. Favorable conditions to form a very thin current sheet are (1) the entropy function S is enhanced, in the near-earth region ($-15R_e < x < -6R_e$), (2) the entropy gradient is steepened in A-space and (3) the lobe flux enhances.

It is found that a very thin current sheet with $B_z < 0.5nT$ and thickness $< 1000km$ can be formed in the near-earth magnetotail ($x \sim -8$ to $-20R_e$) during the growth phase of substorm. The formation of the thin current sheet can explain the observed explosive growth phase of substorms. The profile of the magnetic field strength B_z component in the equatorial plane is mainly determined by the entropy function $S(A)$. I obtain self-consistent equilibria of the Earth's magnetosphere with very strong lobe fields and a monotonically increasing B_z component towards the Earth. It is also confirmed that an enhancement of the lobe flux favors the formation of a current sheet during the early substorm growth phase. I show that the shape of magnetic field lines in the near-earth region are mainly determined by the location (A_c) of the transition point of the entropy function.

5.2 Dynamic Evolution of Magnetotail

During the substorm growth phase, satellite observations show that the plasma pressure in the region $-6R_e > x > -10R_e$ increases to about ten times the value in the quiet time [*Kistler et al.*, 1992]. At the same time, the magnetic field in the equatorial plane (B_z) may decrease to about 1/7 of the dipole field strength [*Lui et al.*, 1992]. As a rough estimate, the differential flux volume thus increases to seven times and the entropy function to about 250 times the quiet time value at a fixed point. During this period, geomagnetic field lines in the near-earth region are highly stretched tailward. The observations also demonstrate that the electric field is enhanced in the auroral oval region during the growth phase. This enhanced electric field can be transmitted by Alfven waves from the ionosphere to the closed field region of magnetotail along magnetic field lines. This would contribute to a dawn-to-dusk electrostatic component E_s of electric field in the plasma sheet. My simulation results show that the enhanced convection electric field E_s in the growth phase enhances the entropy in the near-earth region. Simultaneously, the entropy transition region (A_c) shifts toward the earth and magnetic field lines in the near-earth region are highly stretched tailward. It is implied that the enhanced ionospheric convection electric field is the main driving force of enhancing the entropy and highly stretching magnetic field lines in the near-earth magnetotail during the substorm growth phase.

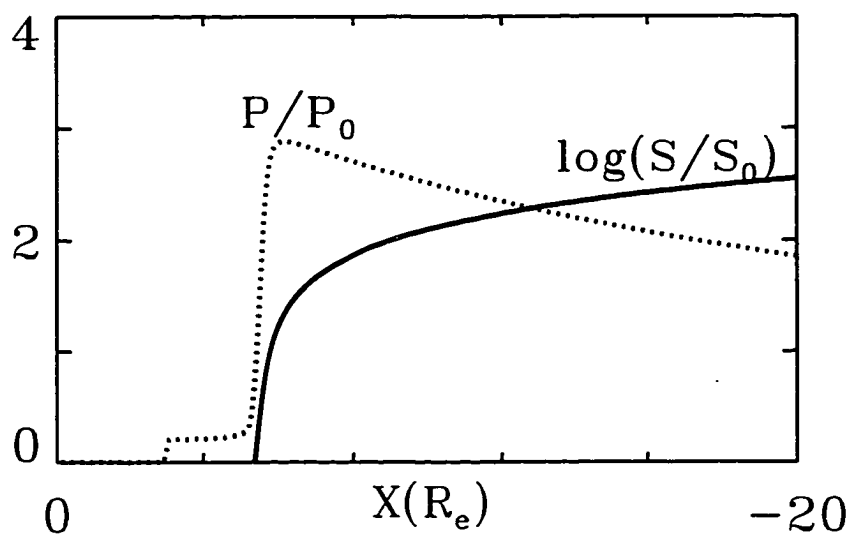

Figure 5.1 General distributions of entropy function $S = S = pV^{\gamma}$ and pressure p in the equatorial plane as a function of x .

5.3 Formation of a Thin Current Sheet

The formation and thinning of the tail current sheet is a crucial for the magnetotail dynamic evolution. In this thesis, I have identified a new instability called as "entropy anti-diffusion instability" which can lead to the formation of a very thin current sheet during the substorm growth phase. In chapter 2, it is found that a steeper profile of entropy function S leads to the formation of a thinner current sheet. In the presence of a density gradient at edges of a current sheet, the lower-hybrid-drift instability may lead to pressure diffusion. Since the pressure generally decreases and the entropy function S increases tailward, as shown in Figure 5.1, the diffusion of plasma pressure results in a steepening ,or anti-diffusion, of the entropy profile. This, in turn, leads to a thinner current sheet, which enhances the pressure diffusion. This positive feedback process is called the "entropy anti-diffusion instability". Based on MHD simulations with a pressure diffusion, I find that the entropy anti-diffusion instability leads to a further thinning of the near-earth current sheet and the onset of dipolarization of near-earth geomagnetic field lines. The growth rate of the instability is linearly proportional to the diffusion coefficient. The growth time at the final stage for the formation of a very thin current sheet is $\sim$ 1 minute. This instability may explain the observed explosive growth phase of substorms and the onset of dipolarization of geomagnetic field lines.

5.4 Future Studies

Possible topics for future studies are listed below. They include (a) aspects involved with the global equilibrium structure and the current sheet formation, and (b) the kinetic description of the study the entropy anti-diffusion instability.

5.4.1 Three-Dimensional Aspects

The magnetosphere is a three-dimensional configuration. To fully understand the interaction between the solar wind and the dynamic processes in the magnetotail, 3-D studies are desirable. Here a 3-D equilibrium study can be the first step for a 3-D global simulation.

Based on the results of this thesis, a thin current sheet could be formed in the near-earth region if the magnetotail is driven by a nonuniform dawn-to-dusk electric field. For my results, the dawn-to-dusk electric field E_y at the boundary of the simulation is constant, which is consistent with $\frac{\partial \mathbf{B}}{\partial t}|_{bound} = 0$. In three dimensions, the dawn-to-dusk E_y at the boundaries is in general nonuniform. Jaggi and Wolf [1973, 1975] suggested that there is 'the Alfven layer' at $\sim -7R_e$ region. The electric field becomes much weaker in the near-earth region $x > -7R_e$ and entropic equation (2.6) becomes a nonlinear convection equation. In the 'Alfven layer', the convection velocity is almost zero. The nonuniform convection of the plasma sheet allows a steepening of the entropy function such that a thin current sheet could formed in the near-earth region $x \simeq -7R_e$.

Three-dimensional convection to replace dayside magnetic flux (which is removed from the dayside by magnetic reconnection) with flux from the tail region

is subject to certain constraints. One of these is again entropic conservation such that only flux tubes consistent with this constraint can be convected to the dayside. This is also a potential source for the formation of a thin current sheet.

5.4.2 Kinetic Effects

There are two main kinetic aspects to be considered for future investigations. First, I have assumed particularly the lower hybrid drift instability in a phenomenological manner. It would be desirable to include this and other instabilities in a more self-consistent kinetic treatment of the entropy anti-diffusion instability. Second, the strong thinning of the current sheet can involve length scale of the order of the ion Larmor radius or the ion inertia length. Here, one would have to include finite ion gryoradus effects, the Hall term, and possibly the electron pressure gradient in a suitable fashion. Such an approach can yield insight into a transition to an instability for a sufficiently thin current sheet and therefore might provide an answer to the open problem of the expansion phase onset.

References

Akasofu, S. -I., Physics of Magnetospheric Substorms, D. Reidel Publishing Company, Dordrecht, 1977.

Akasofu, S. -I., ICS-2 summary session, in *Proceedings of International Conference on Substorms, 2,* ed. by J. R. Kan, J. D. Graven, and S. -I. Akasofu, p. 401, 1994.

Birk, G. T. and A. Otto, The resistive tearing instability for generalized resistivity models: Applications, *Phys. Fluids B, 3*, 1746, 1991.

Birn, J., R. Sommer, and K. Schindler, Open and closed magnetospheric tail configurations and their stability, *Astrophys. Space Sci., 35*, 389, 1975.

Birn, J., Self-consistent magnetotail theory: General solution for the quiet tail with vanishing field-aligned currents, *J. Geophys. Res., 84*, 5143, 1979.

Birn, J., K. Schindler, Computer modeling of magnetotail convection, *J. Geophys. Res., 90*, 3441-3447, 1985.

Birn, J., K. Schindler, On the influence of an external electric field on magnetotail reconnection, *J. Geophys. Res., 91*, 8817-8826, 1986.

Birn, J. and M. Hesse, The substorm current wedge and field-aligned currents in MHD simulations of magnetotail reconnection, *J. Geophys. Res., 96*, 1611, 1991.

Birn, J, The boundary value problem of magnetotail equilibrium, *J. Geophys. Res., 96*, 19,441, 1991.

Birn, J., K. Schindler, L. Janicke, and M. Hesse, Magnetotail dynamics under isobaric constraints, *J. Geophys. Res., 99*, 14863, 1994.

Birn, J., K. Schindler, M. Hesse, Magnetotail dynamics: MHD simulations of driven and spontaneous dynamic changes, in *Proceedings of International Conference on Substorms, 2*, ed. by J. R. Kan, J. D. Graven, and S. -I. Akasofu, p.135, 1994.

Brackbill, J. U., D. W. Forslund, K. B. Quest and D. Winske, Nonlinear evolution of the lower-hybrid drift instability, *Phys. Fluids, 27*, 2682, 1984.

Burkhart, G. R., J. R. Drake, P. B. Dusenbery, and T. W. Speiser, A particle model for magnetotail neutral sheet equilibria, *J. Geophys. Res., 97*, 13,799, 1992.

Cai, H. J., L. C. Lee, and L. Zhang, Tailward stretching of geomagnetic field lines in the presence of an enhanced ionospheric convection electric field, *Geophys. Res. Lett., 22*, 3449, 1995.

Ca, F., and V. M. Vasyliunas, Allowable Amount of Open Magnetic Flux in the Tail and the Earthward Displacement of Cross-tail Current Sheets, It is not published.

Chodura, R., and A. Schlüter, A 3-D code for MHD equilibrium and stability, *J. Comput. Phys., 41*, 68, 1981.

Choe, G. S. and L. C. Lee, Formation of solar prominences by photospheric shearing motions, *Solar Physics 138*, 291, 1992.

Coroniti, F. V., and C. F. Kennel, Changes in magnetospheric configuration during the substorm growth phase, *J. Geophys. Res., 77*, 3361, 1972.

Erickson, G. M., R. A. Wolf, Is steady convection possible in two dimensions, *Geophys. Res. Lett., 7*, 897, 1980.

Erickson, G. M., A quasi-static magnetospheric convection model in two dimensions, *J. Geophys. Res., 97*, 6505, 1992.

Fairfield, D. H., L. J. Zanetti, and T. A. Potemra, The magnetic field of the equatorial magnetotail: AMPTE/CCE observation at $R = 8.8R_E$, *J. Geophys. Res., 92*, 7432, 1987.

Fedder, J. A., S. P. Slinker, J. G. Lyon, and R. D. Elphinstone, Global numerical simulation of the growth phase and the expansion onset for a substorm observed by Viking, *J. Geophys. Res., 100*, 19083, 1995.

Francfort, Ph., and R. Pellat, Magnetic merging in collisionless plasmas, *Geophys. Res. Lett., 3*, 433, 1976.

Fuchs, K., and G.-H. Voigt, Self-consistent theory of a magnetospheric B-field model, in *Quantitative Modeling of Magnetospheric Process, Geophys. Monogr. Ser.*, vol. 21, edited by W. P. Olson, p. 86, AGU, Washington D. C., 1979.

Gary, S. P. and A. G. Sgro, The lower hybrid drift instability at the magnetopause, *Geophys. Res. Lett., 17*, 909, 1990.

Harel, M., R. A. Wolf, P. H. Reiff, R. W. Spiro, W. J. Burke, F. J. Rich, and M. Smiddy, Quantitative simulation of a magnetospheric substorm, 1, Model logic and overview, *J. Geophys. Res., 86*, 2217, 1981.

Harned, D. S. and D. D. Schnack, Semi-implicit Method for long time scale magnetohydrodynamic computations in three dimensions, *J. Comput. Phys. 65*, 57, 1986.

Hau, L.-N., R. A. Wolf, G.-H. Voigt, and C. C. Wu, Steady state magnetic field configurations for the Earth's magnetotail, *J. Geophys. Res., 94*, 1303, 1989.

Hesse, M., and J. Birn, Three-dimensional MHD modeling of magnetotail dynamics for different polytropic indices, *J. Geophys. Res., 97*, 3965, 1992a.

Hesse, M., and J. Birn, MHD modeling of magnetotail instability for anisotropic pressure. *J. Geophys. Res., 97*, 10,643, 1992b.

Hesse, M., D. Winske, M. Kuznetsova, J. Birn and K. Schindler, Hybrid modeling of the formation of thin current sheets in magnetotail configurations, *J. Geomag. Geoelectr., 48*, 749, 1996.

Hill, T. W., Magnetic merging in a collisionless plasma, *J. Geophys. Res., 80*, 4689, 1975.

Hones, E. W., Jr., Transient phenomena in the magnetotail and their relationship to substorms, *Space Sci. Rev., 23*, 393, 1979.

Hones, E. W., Jr., Plasma sheet behavior during substorms, in *Magnetic Reconnection in Space and Laboratory Plasmas, Geophys. Monogr. Ser., vol. 30*, edited by E. W. Hones, Jr., p. 178, AGU, Washington D. C., 1984.

Horton, W., L. Cheung, J.-Y. Kim, and Tajima, Self-consistent plasma pressure tensors from the Tsyganenko magnetic field models, *J. Geophys. Res., 98*, 17,327, 1993.

Huba, J. D., N. T. Gladd, and K. Papadopoulos, The lower-hybrid-drift instability as a source of anomalous resistivity for magnetic field line reconnection, *Geophys. Res. Lett., 4*, 125, 1977.

Jaggi, R. K. and R. A. Wolf, Self-Consistent Calculation of the Motion of a Sheet of Ions in the Magnetosphere, *J. Geophys. Res., 78*, 2852, 1973.

Kan, J., L. Zhu, and S.-I. Akasofu, A theory of substorms: onset and subsidence, *J. Geophys. Res., 93*, 5624, 1988.

Kaufmann, R. L., Substorm currents: Growth phase and onset, *J. Geophys. Res., 92*, 7471, 1987.

Kokubun, S. and R. L. McPherron, Substorm signatures at synchronous altitude, *J. Geophys. Res., 86*, 11,265, 1981.

Kistler, L. M., E. Mobius, W. Baumjohann and G. Paschmann, Pressure changes in the plasma sheet during substorm injections, *J. Geophys. Res., 97*, 2973, 1992.

Kokubun, S., and R. L. McPherron, Substorm signatures at synchronous altitude, *J. Geophys. Res., 86*, 11,265, 1981.

Lee, L.C., Z. F. Fu and S.-I. Akasofu, A simulation study of forced reconnection processes and magnetospheric storms and substorms, *J. Geophys. Res., 90*, 10,896, 1985.

Lee, L. C., The magnetopause: a tutorial review, in *Physics of Space Plasma (1990), SPI Conference Proceedings and Preprint Series, Number 10*, T. Chang, G. B. Crew, and J. P. Jaspers, eds., Scientific Publisher Inc., Cambridge, MA, p33, 1991.

Lee, L.C., L. Zhang, G. S. Choe, and H. J. Cai, Formation of a very thin current sheet in the near-earth magnetotail and the explosive growth phase of substorms, *Geophys. Res. Lett., 22*, 1137, 1995.

Lee, L.C., L. Zhang, H. J. Cai, and G. S. Choe, Entropy anti-diffusion instability and

dipolarization of geomagnetic field lines during substorms, AGU Fall Meeting, San Franciso, December 1995.

Lui, A. T. Y., R. E. Lopez, B. J. Anderson, K. Takahashi L. J. Zanetti, R. W. McEntire, T. A. Potemra, D. M. Klumpar, E. M. Greene, and R. Strangeway, Current disruptions in the near-earth neutral sheet region, *J. Geophys. Res., 97*, 1461, 1992.

Lyons, J., S. H. Brecht, J. D. Huba, J. A. Fedder, and P. J. Palmadesso, Computer simulation of a geomagnetic substorm, *Phys. Rev. Lett., 46*, 1038, 1981.

Lyons, L. R., A new theory for magnetospheric substorms, *J. Geophys. Res., 100*, 19,069, 1995.

Ma, Z. W., Xiaogang Wang, and A. Bhattacharjee, Growth, sudden enhancement, and relaxation of current sheets in the magnetotail: two-dimensional substorm dynamics, *Geophys. Res. Lett., 22*, 2985, 1995.

McPherron, R. L., C. T. Russell and M. P. Aubry, Satellite studies of magnetospheric substorms on August 15, 1968, 9, Phenomenological model of substorms, *J. Geophys. Res., 78*, 3782, 1973.

Mitchell, D. G., D. J. Williams, C. Y. Huang, L. A. Frank and C. T. Russell, Current carriers in the near-earth cross-tail current sheet during substorm growth phase, *Geophys. Res. Lett., 17*, 583, 1990.

Notzel, A., and K. Schindler, On the cause of approximate pressure isotropy in the quiet near-Earth plasma sheet, *J. Geophys. Res., 90*, 8293, 1985.

Ogino, T., R. J. Walker, M. Ashour-Abdalla, and J. M. Dawson, An MHD simulation of the effects of the interplanetary magnetic field b_y component on the interaction of the solar wind with the Earth's magnetosphere during southward interplanetary magnetic field, *J. Geophys. Res., 91*, 10,029, 1986.

Ogino, T., R. J. Walker, and M. Ashour-Abdalla, A global magnetohydrodynamic simulation of the response of the magnetosphere to a northward turning of the interplanetary magnetic field, *J. Geophys. Res., 99*, 11,027, 1994.

Ohtani, S., K. Takahashi, L. J. Zanetti, T. A. Potemra, and R. W. McEntire, Initial signatures of magnetic field and energetic particle fluxes at tail reconfiguration: explosive growth phase, *J. Geophys. Res., 97*, 19,311, 1992.

Olson, W. P., and K. Pfitzer, A quantitative model of the magnetospheric magnetic field, *J. Geophys. Res., 79*, 3739, 1974.

Pritchett, P. L. and F. V. Coroniti, Formation and stability of the self-consistent one-dimensional tail current sheet, *J. Geophys. Res., 97*, 16,773, 1992.

Pritchett, P. L. and F. V. Coroniti, Formation of thin current sheets during plasma sheet convection *J. Geophys. Res., 100*, 23551, 1995.

Pudovkin, M. I., and N. A. Tsyganenko, Particle motion and currents in the neutral

sheet of magnetospheric tail, *Plane Space Sci., 21*, 2027, 1973.

Reiff, P. H., R. W. Spiro, and T. W. Hill, Dependence of polar cap potential drop on interplanetary parameters, *J. Geophys. Res., 86*, 7639, 1981.

Roux, A., S. Perraut, P. Robert, A. Morane, A. Pedersen, A. Korth, G. Kremser, B. Aparicio, D. Rodgers, and R. Pellinen, Plasma sheet instability related to the westward traveling surge, *J. Geophys. Res., 96*, 17697, 1991.

Russell, C. T., and R. L. McPherron, The magnetotail and substorms, *Space Sci. Rev., 15*, 205, 1973.

Schindler, K., A theory of the substorm mechanism *J. Geophys. Res., 79*, 2803, 1974.

Schindler, K., and J. Birn, Self-consistent theory of time-dependent convection in the Earth's magnetotail, *J. Geophys. Res., 87*, 2263, 1982.

Schindler, K., and J. Birn, On the cause of thin current sheets in the near-Earth magnetotail and theor possible significance for magnetospheric substorms, *J. Geophys. Res., 98*, 15,477, 1993.

Sergeev, V. A., P. Tanskanen, K. Mursula, A. Korth and C. Elphic, Current sheet thickness in the near-earth plasma sheet during substorm growth phase, *J. Geophys. Res., 95*, 3819, 1990.

Smith, R. A., C. K. Goertz, and W. Grossman, Thermal catastrophe in the plasma sheet boundary layer, *Geophys. Res. Lett., 13*, 1380, 1986.

Siscoe, G. L., and W. D. Cummings, On the cause of geomagnetic bays, *J. Planet. Space Sci., 17*, 1795, 1969.

Speiser, T. W., Particle trajectories in model current sheets, *J. Geophys. Res., 70*, 4219, 1965.

Spence, H. E., M. G. Kivelson, and R. J. Walker, Magnetospheric plasma pressures in the midnight meridian: observations from 2.5 to 35 R_e, *J. Geophys. Res., 94*, 5264, 1989.

Stern, D. P., Parabolic harmonics in magnetospheric modeling: The main dipole and the ring current, *J. Geophys. Res., 90*, 10,851, 1985.

Swift, D. W., Possible consequences of the asymmetric development of the ring current belt, *J. Planet. Space Sci., 15*, 835, 1967.

Swift, D., Use of a hybrid code for global-scale plasma simulation, submitted to *Journal Computational Physics*, 1994.

Tsyganenko, N. A., and A. V. Usmanov, Determination of the magnetospheric current system parameters and development of experimental geomagnetic field models based on data from IMP and HEOS satellites, *J. Planet. Space Sci., 30*, 985, 1982.

Tsyganenko, N. A., Pitch-angle scattering of energetic particles in the current sheet of the magnetospheric tail and stationary distribution functions, *J. Planet. Space Sci.,*

30, 433, 1982.

Usadi, A., A. Kageyama, K. Watanabe, and T. Sato, A global simulation of the magnetosphere with a long tail: southward and northward interplanetary magnetic field, *J. Geophys. Res.*, *98*, 7503, 1993.

Vasyliunas, V. M., Mathematical models of magnetospheric convection and its coupling to the ionosphere, in *J. Particles and fields in the magnetosphere*, ed. by M. McCormac, p. 60, D. Reidel, Dordrecht, Netherlands, 1970.

Vasyliunas, V. M., Summary, in *Proceedings of International Conference on Substorms*, *2*, ed. by J. R. Kan, J. D. Graven, and S. -I. Akasofu, p. 403, 1994.

Wiegelmann, T. and K. Schindler, Formation of thin current sheets in a quasistatic magnetotail model, *Geophys. Res. Lett.*, *22*, 2,057, 1995.

Wolf, R. A., Effects of ionospheric conductivity on convective flow of plasma in the magnetosphere, *J. Geophys. Res.*, *75*, 4677, 1970.

Wolf, R. A., Ionosphere-Magnetosphere Coupling, *Space Sci. Rev.*, *17*, 537, 1975.

Wu, C. C., Shape of the magnetopause, *Geophys. Res. Lett.*, *10*, 545, 1983.

Zhang, L., L. C. Lee and H. J. Cai, Enhancement of Specific Entropy (pV^{γ}) in the Near-Earth Magnetotail During Substorm Growth Phase, AGU Fall Meeting, San Franciso, December 1994.